The Thesis Committee for Fernando Matías Rey Certifies that this is the approved version of the following Thesis:

Anatomy of Deltaic Compound Clinoforms; Colorado Delta in Baja California, Mexico, Pliocene Colorado Delta in Fish Creek-Vallecito Basin, California, USA, and a Review of Modern Examples

Committee:

Cornel Olariu, Supervisor

Ronald J. Steel

Brian K. Horton

Anatomy of Deltaic Compound Clinoforms; Colorado Delta in Baja California, Mexico, Pliocene Colorado Delta in Fish Creek-Vallecito Basin, California, USA, and a Review of Modern Examples

by

Fernando Matias Rey

Thesis

Presented to the Faculty of the Graduate School of

The University of Texas at Austin

in Partial Fulfillment

of the Requirements

for the Degree of

Master of Science in Geological Sciences

The University of Texas at Austin

May 2021

Dedication

To my wife, Veronica L Chertcoff.

Acknowledgments

I would like to thank my committee members Cornel Olariu, Ronald Steel, and Brian Horton for the advice and expertise they provided during this project. Ron and Cornel first introduced and then guided me through the amazing stratigraphy of the Fish Creek-Vallecito Basin. Thank you, Cornel, for helping me under the scorching sun of August on the Sonora desert to measure most of my sections. Thank you to Brian for the candid and constructive comments which help me to improve the quality of this manuscript.

Thanks to the Argentinian Presidential Fellowship, the Instituto Argentino del Petroleo y Gas Houston, and RioMar consortium for the funding that allowed me to pursue this project.

Thanks to Elaine Tulving and Jim Dice from UC, Irvine Steele/Burnand Anza-Borrego Desert Research Center for providing a place to stay near the field during the COVID-19 pandemic. Thank you to Lynn Murray and the California State Park Rangers for your comments and the park permit to carry out this project.

Many thanks to the Dynamic Stratigraphy Workgroup of the JSG for helping me to polish my ideas. Thanks to Rawan Al-Assad and Logan West for the discussions about the formation of the Gulf of California and to better understand the tectonic setting of the basin. Thank you to Sarp Karakaya for the discussions about the direction of the manuscript and for giving me quite a few ideas to think on. Thank you, Harry Hull, John Franey, Jake Burstein, Michelle Tebolt, and Britney Davis, for sharing their photos from the field class that we took in 2019 on the Fish Creek-Vallecito Basin.

Thank my parents Gustavo and Maria del Carmen, my brother Pablo and my sister Mayra for always supporting me in the pursuit of my ambitions. Thank you to my godfather Juan Carlos, for sharing with me his love for knowledge.

Finally, I would like to thank my wife Veronica for being part of the amazing adventure of living in the US these 2 years. You are my rock!

Abstract

Anatomy of Deltaic Compound Clinoforms; Colorado Delta in Baja California, Mexico, Pliocene Colorado Delta in Fish Creek-Vallecito Basin, California, USA, and a Review of Modern Examples

Fernando Matias Rey, M.S.GEO.SCI

The University of Texas at Austin, 2021

Supervisor: Cornel Olariu

Modern Delta systems commonly exhibit compound clinoforms that consist of two elements, a shoreline clinoform, and a separate subaqueous clinoform, both with a topset–foreset–bottomset morphology, with a wide low-gradient area called subaqueous platform (30-150 km wide) in between. Recent datasets on modern tidal Deltas suggest that a compound-clinoform model is characteristic for tide-dominated Deltas but there are few good examples from ancient deposits. The modern Colorado River Delta, in Baja California, Mexico, is tide-dominated and exhibits a compound clinoform. The 20 km-long outcrops of the Yuha and Camel Head members of the Deguynos Formation, located in Fish Creek-Vallecito Basin, California, are the ancient (mid-Pliocene) deposits of the paleo-Colorado Delta. These outcrops were measured, producing 4 stratigraphic sections through the Yuha and Camel Head members. From these measured sections 7 facies associations were recognized. These facies associations were assembled into 3 depositional environments: subaqueous foreset to bottomset, subaqueous topset, and

platform, and shoreline clinoform, using as an analogy the modern Colorado Delta deposit.

The Yuha and Camel Head Members exhibit multiple at least 22 high-frequency regressive-transgressive (R-T) cycles in which thickness changes laterally along the outcrops. R-T sequences, with an upward-coarsening lower part and a sandy to silty upward-fining upper part are interpreted as 5^{th} order sequence related to autogenic changes within the environment, as suggested by variations in thickness and approximate time duration of each cycle. The 5^{th} order R-T sequences are further organized in four sequences interpreted as 4^{th} order sequence, mapped by vertical changes in thickness and environment along the outcrop, and probably controlled by eustatic processes.

The exceptional setting of the basin (strongly dominated by tidal processes and the uncommonly high accommodation rate) probably was the key to the preservation of the compound clinoform morphology in the rock record of the Fish Creek-Vallecito basin.

To better understand sediment dispersal in tidal influenced Deltas, 138 bathymetry maps near River mouth were examined, finding 54 compound clinoform morphologies. The annual sediment flux (Mt/y) appears to be the most important factor in the preservation of the compound clinoform morphology. All River mouths with an annual measured sediment flux higher than 100 Mt/yr have a compound clinoform. In contrast, in River mouths with less than 15 Mt/yr, the compound clinoforms are rare. The 39 systems were divided into tide-dominated, wave-dominated, and mixed, following the averages measured values of tidal ranges and wave height from public databases. In these systems, the subaqueous platform area has a direct relationship with the annual sediment influx.

Table of Contents

List of tables

List of figures

Chapter 1

Introduction

Modern Delta systems commonly exhibit compound clinoforms that consist of two elements, a shoreline clinoform, and a separate subaqueous clinoform, both with a topset–foreset–bottomset morphology (Nittrouer et al., 1986; Kuehl et al., 1997; Pirmez et al., 1998; Ta et al., 2002; Walsh et al., 2004; Peng et al., 2018). The recent high-resolution datasets on modern tidal Deltas describe the compound-clinoform model as typical for tidal Deltas but there are only a few examples from the ancient deposits (e.g., Hampson 2010; Vakarelov et al. 2012; Patruno et al. 2015; Rossi and Steel 2016; Hampson and Premwichein 2017; Peng et al., 2018).

The modern Colorado Delta in Baja California, Mexico, also shows a compound clinoform geometry, emphasized by its wide subaqueous platform (6000 km^2), with a subaqueous clinoform rollover into a water depth of 40 m and 80 km seaward from the coastline. The River mouth/Delta position in the northernmost end of the Gulf of California shows tidal-current velocities and the macrotidal range (over 6 m) makes it the dominant process in the Deltaic/shallow marine environment (Thompson, 1968). Satellite images and bathymetry maps reveal several classic tidal morphological features on the subaqueous platform, such as tidal bars and tidal channels (Alvarez et al. 2009), and the existence of a large-scale (80 km wide and 30-40 m high) compound clinoform associated with the progradation of the Delta.

The 20 km-long outcrops of the Yuha and Camel Head members of the Deguynos Formation (Dibblee, 1954, 1984; Woodard, 1963, 1974; Kerr, 1982; Winker 1987; Dorsey et al., 2011), located in Fish Creek-Vallecito Basin, California, are the ancient (mid-Pliocene) (Dorsey et al., 2011) deposits of the Paleo-Colorado Delta. Therefore, an analogy

can be built between the modern and Pliocene Colorado River Delta, and the implication of its compound clinoform morphology, to explain the characteristics of the Deguynos Formation deposits.

In Chapter 2, this analogy is wielded to analyze Deguynos Formation stratigraphy and architecture that has been barely studied in previous papers and could serve as a compelling tool to better understand ancient compound clinoform deposits.

In Chapter 3, a review of 138 River mouth bathymetries around the world was compiled to illustrate in which places and under which conditions is possible to find compound clinoforms. The focus of this review has been to analyze the energy of the systems in which the compound clinoform is formed and how the components of the compound clinoform change with a differing mix of shallow marine processes and annual sediment flux.

Chapter 2

Anatomy of Deltaic compound clinoforms; Colorado Delta in Baja California, Mexico, and Pliocene Colorado Delta in Fish Creek-Vallecito Basin, California, USA

Introduction:

Clinoforms, defined as inclined stratal surfaces (Rich 1951), occur over various spatial scales ranging from Delta-front foresets (usually less than 150m) to continental margin slopes (over 200 m to few km) (Steel & Olsen, 2002; Pirmez et al., 1998, Patruno et al., 2015a). The breaks at the top and bottom of these inclined stratal surfaces are called rollovers and separate low-gradient topsets and bottomsets from a steeper foreset zone (Sangree & Widmier, 1977; Pirmez et al., 1998; Adams & Schlager, 2000; Patruno et al., 2015). Modern Delta systems commonly exhibit compound clinoforms that consist of two elements, a shoreline clinoform, and a separate subaqueous clinoform, both with a topset–foreset–bottomset morphology (figure 1.1.a) (Nittrouer et al., 1986; Kuehl et al., 1997; Ta et al., 2002; Walsh et al., 2004; Peng et al., 2018). These compound clinoforms are genetically and morphologically linked, and they are separated by a broad subaqueous topset platform (e.g., Cattaneo et al. 2003; Swenson et al. 2005; Helland-Hansen and Hampson 2009; Walsh and Nittrouer 2009; Patruno et al. 2015; Peng et al. 2018). Patruno et a. (2015) refer to the two distinct clinoforms as “subaerial” and “subaqueous” clinoforms, we prefer to use “shoreline” and “subaqueous” because the shallower clinoform deposits are not “subaerial” but rather linked with the shoreline progradation. The *double clinoform* or *compound clinoform* morphologies have been described in Deltas with strong tidal and wave energy in front of the distributaries. In tide-dominated Deltas, the shoreline clinoform comprises mainly the supratidal and intertidal portion of the Delta, including the coastal plain (e.g., Ta et al. 2002; Correggiari et al. 2005). The subaqueous

platform is in the subtidal zone until the subaqueous rollover is reached, the limit between the platform and the subaqueous foreset. This foreset encompasses two parts: an upper part that is essentially the active Delta-front and a lower part that is finer and transitions to bottomsets that are contiguous with the shelf (figure 1.1a). The shoreline clinoform extension depends on the tidal range of the area, commonly occurring at water depths between 10-30 m (Peng et al., 2020), whereas the subaqueous clinoform rollover lies at a variable distance (kilometers to tens of kilometers) offshore from the shoreline (Pirmez et al. 1998; Swenson et al. 2005) at water depths of 25 to 100 m (Patruno et al. 2015). The energy distribution along the clinoform profile is controlled by the position of the two clinoform rollovers. Along the shoreline, the fluvial influx combines with the ebb-tide currents to form a high-energy zone. Likewise, the subaqueous rollover enhances the energy by the expected increase in current velocity when the current is moving toward shallower depths (figure 1.1b) (Fleming et al, 1939). As the gradient in the subaqueous platform tends to be very low (Peng et al., 2020), the flow energy tends to generally decrease across the platform (figure 1.1b), boosting the sedimentation of finer deposits at times (Peng et al., 2020), though there can also be higher energy zones of tidal scour and sediment bypass to the Delta front (Goodbred and Saito, 2011).

The interaction of fluvial-derived water and sediments with shallow marine processes controls the sediment dispersal and spatial separation of the shoreline and subaqueous clinoforms (Swenson et al. 2005; Walsh and Nittrouer 2009). Shoreline clinoforms are controlled by fluvial discharge, while subaqueous clinoforms are mainly affected by tides, waves, and other currents (Pirmez et al. 1998; Driscoll and Karner 1999; Swenson et al. 2005; Rossi et al. 2016; Peng et al., 2018). Swenson et al., (2005) proposed that to be able to preserve the compound clinoform, the system must be able to compensate the high sedimentary influx from the fluvial system with similarly strong shallow marine

processes (figure 1.1c). The compound clinoforms are well developed in modern tide-dominated Deltas situated in energetic marine environments, such as the Amazon (Kuehl et al. 1986; Nittrouer et al. 1986), the Ganges–Brahmaputra (Kuehl et al. 1997; Michels et al. 1998; Kuehl et al. 2005), the Yangtze (Hori et al. 2001; Liu et al. 2006; 2007), the Fly River Delta (Walsh et al. 2004) and the Orinoco River (Peng et al., 2018) River Deltas.

The modern Colorado Delta in Baja California, Mexico, also shows a compound clinoform geometry, emphasized by its wide subaqueous platform (6000 km^2), with a subaqueous clinoform rollover into water depths of 40 m and 80 km seaward from the coast (figure 1.2b). The River mouth/Delta position in the northernmost end of the Gulf of California shows tidal-current velocities and the macrotidal range (over 6 m) (Thompsom 1968; Alvarez et al., 2009) makes it the dominant process in the Deltaic/shallow marine environment (Thompson, 1968). Until 1935 the Colorado River was the main source of terrigenous sediments that formed extensive Delta deposits, but the Delta is now in a destructive stage caused by the construction of multiple dams along the course of the River and decreased water and sediment flux to the Delta (Thompson, 1969; Carriquiry and Sánchez, 1999). Satellite images and bathymetry maps reveal several classic tidal morphological features on the subaqueous platform, such as tidal bars and tidal channels (Alvarez et al; 2009), and the existence of a large-scale compound clinoform associated with the progradation of the Delta (figure 1.2b).

Despite the ubiquity of compound clinoforms in modern tidal Deltas, there are only a limited number of examples in the ancient deposits (e.g., Hampson 2010; Vakarelov et al. 2012; Patruno et al. 2015; Rossi and Steel 2016; Hampson and Premwichein 2017; Peng et al., 2018). In this study, we link the compound clinoform of the tide-dominated, modern Colorado Delta with the deposits of the ancestral (Mio-Pliocene) Colorado River Delta in Fish Creek-Vallecito Basin, in Southern California. The Fish Creek – Vallecito Basin

outcrops show a well-developed progradation reflected in a vertical succession from outer-shelf deposits to proDelta to Delta front to fluvial (Arroyo Diablo Formation and Deguynos Formation respectively) (Winker, 1986; Dorsey et al., 2007; 2011). The Deguynos Formation outcrops have deposited such as coquina ridges, heterolithic deposits, and sand-rich channels with architectures that resemble the key geomorphological features in the modern Colorado Delta and demonstrates high-resolution and high-frequency variations of tide-generated facies at both large (tens of meters), medium (meter), and small (dm to cm) scales.

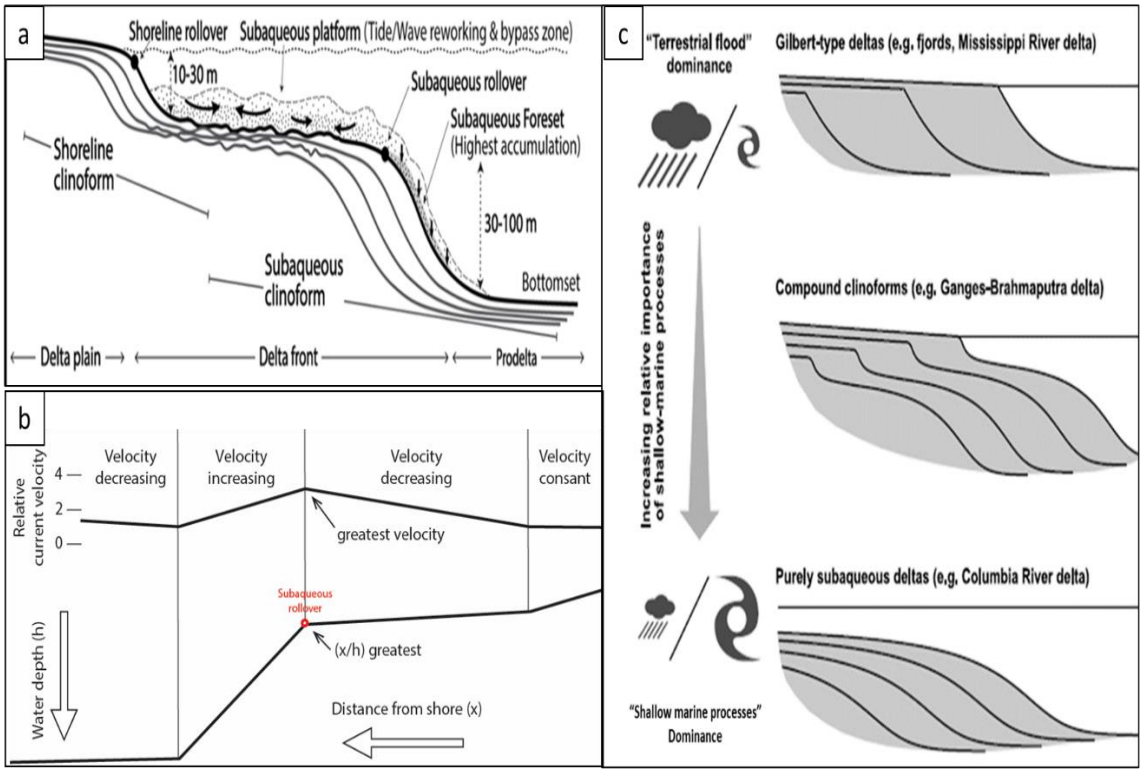

Figure 1.1. Introduction to compound clinoforms.
(a) Theoretical sketch of a compound-clinoform geometry showing the shoreline and subaqueous clinoforms (modified from Helland-Hansen and Hampson 2009; Patruno et al. 2015a; Peng et al., 2020) and the associated sub-environments. The subaqueous platform is represented as a bypass surface

where the shallow marine processes reworked the sediments coming from the River mouth. Most of these sediments are finally deposited in the subaqueous foreset. (b) Distribution of maximum tidal current velocities over the continental shelf, where there is transport across the shelf. The point of expected greatest velocity coincides with the subaqueous rollover (modified from Fleming et al., 1939). (c) Phase diagram for a fluvio-deltaic clinoform showing the range of clinoform geometries to the dominant process; modified from Swenson et al. (2005).

Geological Context:

The rationale of the workflow in the thesis below, alternating descriptions of the modern Colorado Delta and the paleo-Colorado Delta rather the keeping the two entirely separate, is deliberate. The reason to do it this way is to highlight the remarkable similarity in facies, architectural features, and compound clinoform geometry between the modern and the Pliocene Colorado Deltas.

The Modern Colorado River Delta

The Colorado River has one of the largest catchment areas in North America, covering an area of 246,000 sq mi (640,000 km^2) (Kammerer, 1990). The Colorado River trunk is fed by six tributaries which drain 78% of the total drainage basin area (figure 1.2.a) (e.g., Andrews, 1991).

The modern Gulf of California is a receiving basin characterized by a narrow N-S elongated structural trough into which the Colorado River supplied sediments from the northward end of the trough (figure 1.2.b) (Coleman and Wright, 1975). The region of the River mouth shows estuarine (brackish to marine salinity) conditions and fast tidal currents due to large amplitude (>6m) semidiurnal tides (Alvarez et al., 2009).

The Upper Gulf of California is surrounded by arid alluvial plains, piedmont deposits, and the Colorado River Delta/estuary to the north (Thompson, 1968; Alvarez et al 2009). Its seaward limit is roughly defined by the 40 m isobaths, where the Gulf is ~70

km wide, forming a wide subaqueous platform (6000 km^2), near the edge of the 200 m deep Wagner Basin (figure 1.2.b). The origin of the tidal ridges of the subaqueous Delta front in the Upper Gulf of California, (as well as their unlikely link to tectonic process, despite fault control on gulf elongated morphology), has been a matter of conjecture (Gorsline, 1967; Geehan, 1978; Huthnance, 1982; Carbajal and Montaño, 2001). However, they are likely to be subaqueous tidal-bar formed by strong tidal currents, such as otherwise well shown by modern tide-dominated Deltas (e.g. Han Delta, Korea, Cummings et al., 2016). Bathymetric surveys made between 1994 and 1998 in the Upper Gulf of California revealed narrow (1 to 3 km), up to 50 km long, and 2 to 7 m high, ridges of and intervening troughs interpreted as tidal bars and channels (Lavin et al, 1998; Alvarez et al., 2009). These sedimentary linear features are oriented NW-SE and run across the subaqueous Delta to the edge of Wagner Basin (figure 1.2b). Superposition of seismic swarm epicenters and a seismic reflection section on bathymetric features have suggested that two of the 10 major ridge-troughs structures may be fault-controlled, which may explain their height (10 to 15 m) compare to the rest (figure 1.2.b) (Alvarez et al., 2009).

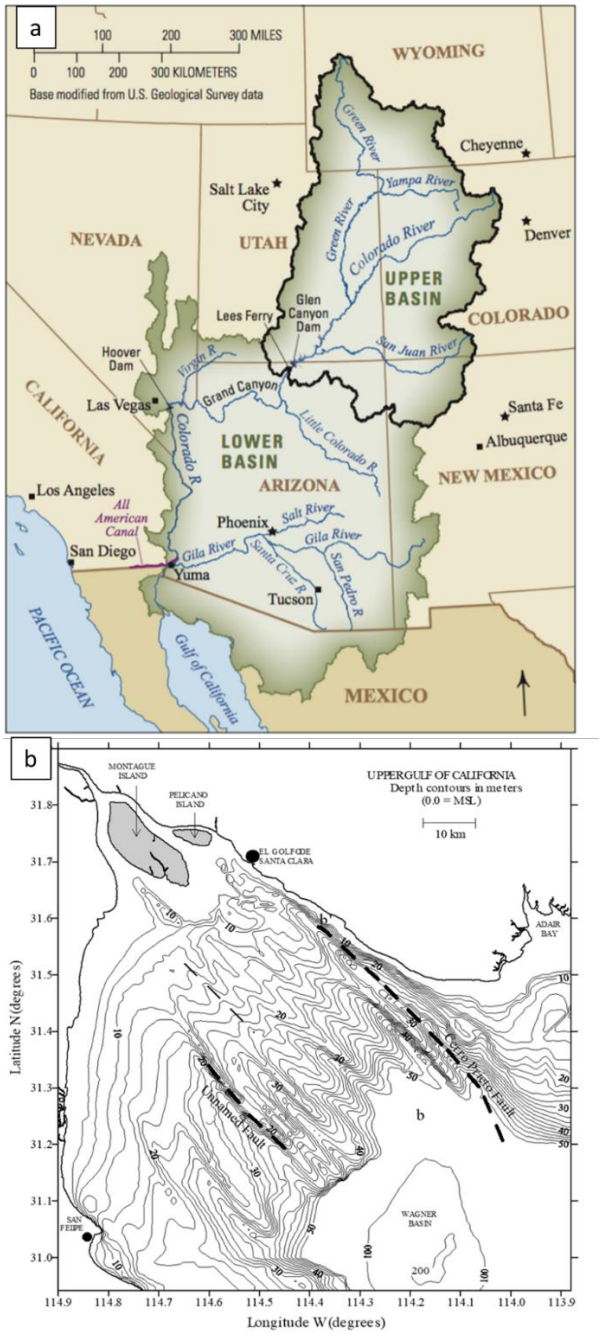

Figure 1.2. Modern Colorado River.

(a) The catchment area of the Modern Colorado River (taken from https://www.usgs.gov/media/images/colorado-River-basin-map). (b) Bathymetry map from the upper portion of the Gulf of California. In this map is possible to notice the positive relief features that were interpreted by Alvarez et

al. (2009) as tidal bars. The two dashed lines represent seismic active faults (Cerro Prieto and unnamed faults). Modified from Alvarez et al. (2009).

The Salton Trough and the Fish Creek-Vallecito Basin

The Salton Trough is a large continental depression in southern California that lies in the boundary zone between the North American and Pacific tectonic plates (figure 1.3.a). It is thought to have formed during the Miocene as a result of transtension along this interplate boundary and mostly accommodated along with the southern San Andreas Fault system to the east and the West Salton detachment fault system to the west (Winker, 1987, Axen and Fletcher, 1998; Dorsey et al., 2011; Waresak, 2016). The Fish Creek–Vallecito Basin is a westerly extension associated with this depression and was formed along the hanging wall of the West Salton Detachment Fault, bounded on the northeast side of the Salton Trough by the San Andreas fault (Dibblee, 1954, 1984; Axen and Fletcher, 1998; Dorsey, 2006;2011) (figure 1.3.b). The Fish Creek-Vallecito Basin is bounded to the north by the Vallecito Mountains, to the east by the Fish Creek Mountains, and the south by the Coyote Mountains (figure 1.3.b). The basin covers an area of approximately 373 km^2, a large part of which is enclosed within the Anza-Borrego Desert State Park of southern California (Remeika, 1995). Since the late Miocene, slip along the San Andreas fault system translated the Pacific plate (and hence the western Salton Trough and Fish Creek-Vallecito Basin) an estimated 200 km to the northwest relative to the North American plate (and the Colorado River Delta) (Dorsey, 2006). Subsequently, the region was uplifted due to transpression, and part of the Fish Creek-Vallecito Basin section was exhumed (Dorsey et al., 2011).

The accommodation in the Fish Creek-Vallecito Basin was generated by low-angle displacement along the West Salton Detachment Fault during the Miocene (Axen and Fletcher, 1998; Dorsey et al 2007). The basin was filled by approximately 5.5 km of

Miocene to Pleistocene sediments (figures 1.3.c,1.4) (Gibson et al., 1984; Peryam, 2012). Dorsey et al (2007, 2011) constructed a magnetostratigraphic calibrated correlation (Opdyke et al., 1977; Johnson et al., 1983; Dorsey et al., 2011) to date the deposits filling the Fish Creek-Vallecito Basin using also radiometric ages acquired from tuff in the Palm Spring Group, suggesting that the Colorado River arrived at the basin at 5.3 Ma. However, recent studies (Crow et al., 2021) performed mainly in basins upstream along the paleo-Colorado River suggested that the arrival of the Colorado River in the Fish Creek-Vallecito Basin occurred at least 0.5 My later(at 5.8 Ma) (figure 1.4). Therefore, the age of most of the succession formed by the paleo-Colorado after its arrival to the basin needs to be further refined (Crow et al., 2021).

The oldest sediments in the basin are coarse clastic alluvial deposits from the Miocene (figures 1.3c,1.4) (Elephant Trees Formation, Split Mountain Group) (Dibblee, 1954, 1984; Woodard, 1963, 1974; Kerr, 1982; Winker, 1987; Dorsey, 2007; 2011). These continental sediments are overlain by gypsum deposits, then by marine turbidites and two episodes of collapse and mass transport deposition (below and above the turbidites) from locally high topography (figures 1.3c,1.4) (Lycium Member., Latrania Formation, Imperial Group), deposited during the early Pliocene (Dibblee, 1954, 1984; Woodard, 1963, 1974; Kerr, 1982; Winker, 1987; Dorsey, 2007;2011). At about 4.8 – 4.63 Ma (Crow et al., 2021) the Colorado River entered the Fish Creek region and started to build a large Delta that prograded southwards into the marine rift basin at the north end of the Gulf of California during the Pliocene (figures 1.3.c,1.4) (Winker and Kidwell, 1986). The earliest evidence of this influx occurs in the Upper Pliocene (upper Latrania Formation) as submarine fan turbidites (Wind Cave Member) accumulating at the base of the new deep-water slope (figures 1.3.c,1.4) (Winker and Kidwell, 1996; Cloos 2000). Overlying these deposits are the muddy slope deposits themselves (Mud Hills member.) and then the shelf-building

Deguynos Formation, which records the progradation of the ancestral Colorado River Delta and the transition into the distributary channel deposits of the predominantly non-marine Palm Spring Group (Winker and Kidwell, 1996). The Fish Creek-Vallecito Basin is capped by Plio-Pleistocene lacustrine and locally derived stream sediments and then overlain by Quaternary deposits (figures 1.3.c,1.4) (Winker, 1987).

Deguynos Formation

The Deguynos Formation is composed of three members: Mud Hills, Yuha, and Camel Head members (Winker, 1987; Winker and Kidwell, 1996) (figures 1.3.c,1.4). Mud Hills member contains a 400 m-thick interval of muddy sediments. The lower part of Mud Hills member overlies and interfingers with the sandy turbidite fan of the Wind Cave Member with approximately 100 meters of marine mudstone and claystone. The claystone in the upper part of Wind Cave Member is a regionally extensive marine unit also known as "Coyote Clay" (Hanna, 1926; Jefferson and Lindsay, 2006) that records the deepwater base-of-slope mudstones. It is in turn gradationally overlain by rhythmitic mudstones and siltstones of the upper Mud Hills member (Winker, 1987). The deepwater rhythmites are gradually overlain by the shallow-water fossiliferous sandstones and mudstones of the Yuha Member, which is related to the development of a shallow marine shelf atop the underlying deepwater slope. This shelf was built by the prograding Colorado River Delta lobes (Winker, 1987; Winker and Kidwell, 1996). Yuha member is a 250 meters thick succession containing fossil-rich sandstone units (each a few meters thick) intercalated with or coarsening upward from tens of meters thick grey mudstone units. Coquina beds associate with the sandstones, consisting primarily of *Ostrea vespertina, Anomia subcostata*, and pectinids (Woodard 1963). Overlying the Yuha Member is Camel Head Member (figures 1.3.c,1.4). This unit suggests a transition to a more proximal environment,

dominated by more sandy beds and extensive muddy and heterolithic stratification. We define the contact between Yuha and Camel Head members at the incoming of reddish mudstones (at least 2 m thick) as a convenient mapping criterion, following Winker (1987). The top of the Deguynos Formation is a conformable transition to fluvial deposits of the Arroyo Diablo Formation (figures 1.3.c,1.4) (Dorsey et al., 2011).

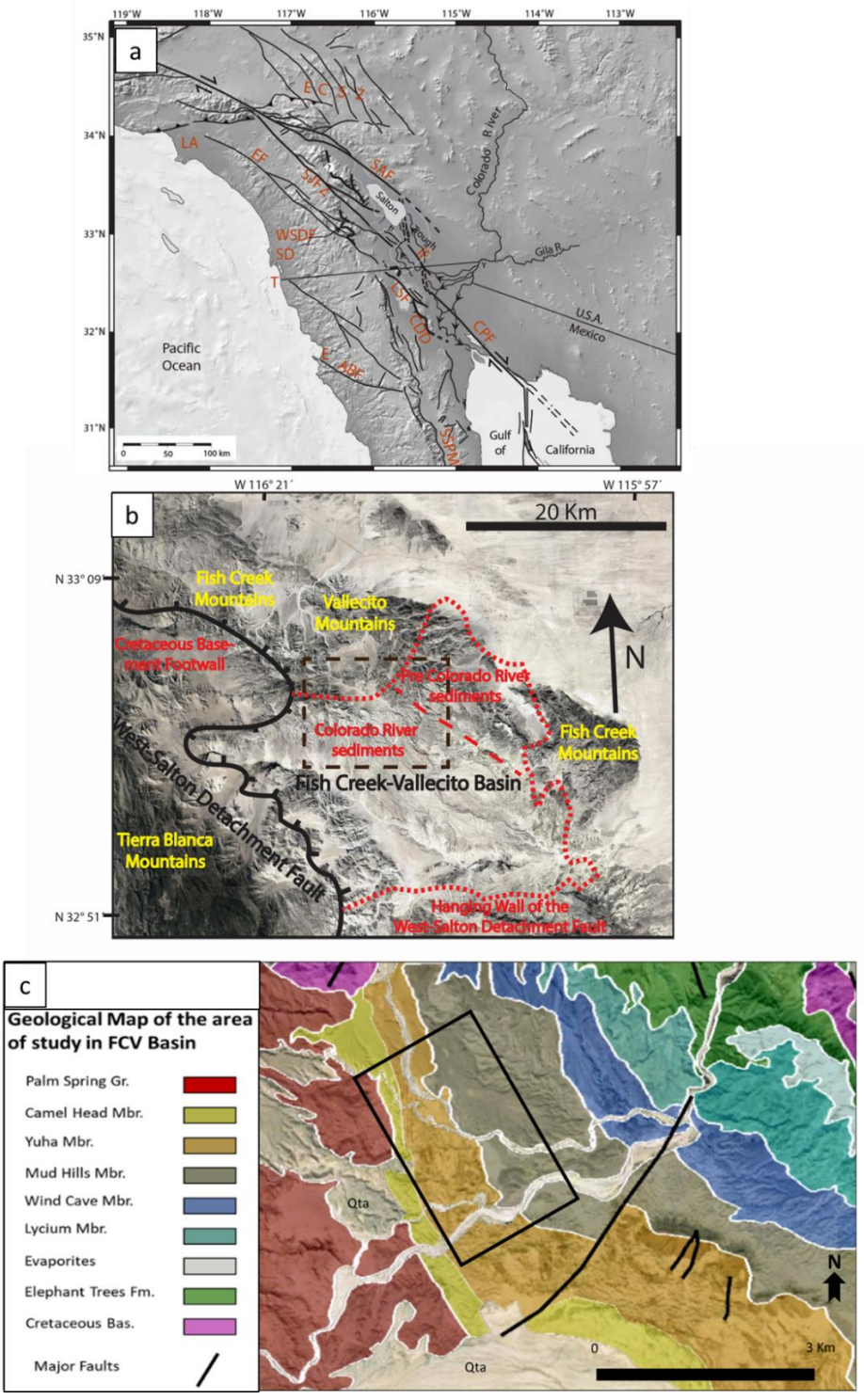

Figure 1.3. Location and Geology of Salton Trough and Fish Creek Vallecito Basin.

(a) Regional map of topography and main faults of the San Andreas fault system in the southwestern United States and northwestern Mexico. ABF—Agua Blanca fault; CDD—Canada David detachment; CPF—Cerro Prieto fault; E—Ensenada; ECSZ—eastern California shear zone; EF—Elsinore fault; IF—Imperial fault; LA—Los Angeles; LSF—Laguna Salada fault; SAF—San Andreas fault; SD—San Diego; SJFZ—San Jacinto fault zone; SSPMF—Sierra San Pedro Martir fault; T—Tijuana; WSDF—West Salton detachment fault; Y—Yuma. Modified from Dorsey et al., 2011. (b) Morphological and tectonic elements of the Fish Creek-Vallecito Basin (dotted in red) and the West Salton Detachment Fault (marked in black) (modified from Cloos, 2014). The dotted brown square map marked the position of figure (c). (c) Geological map of the study area in Fish Creek Vallecito Basin (modified from Dorsey et al., 2011 and Cloos, 2014). The square in black shows the position of the map in figure 1.4.

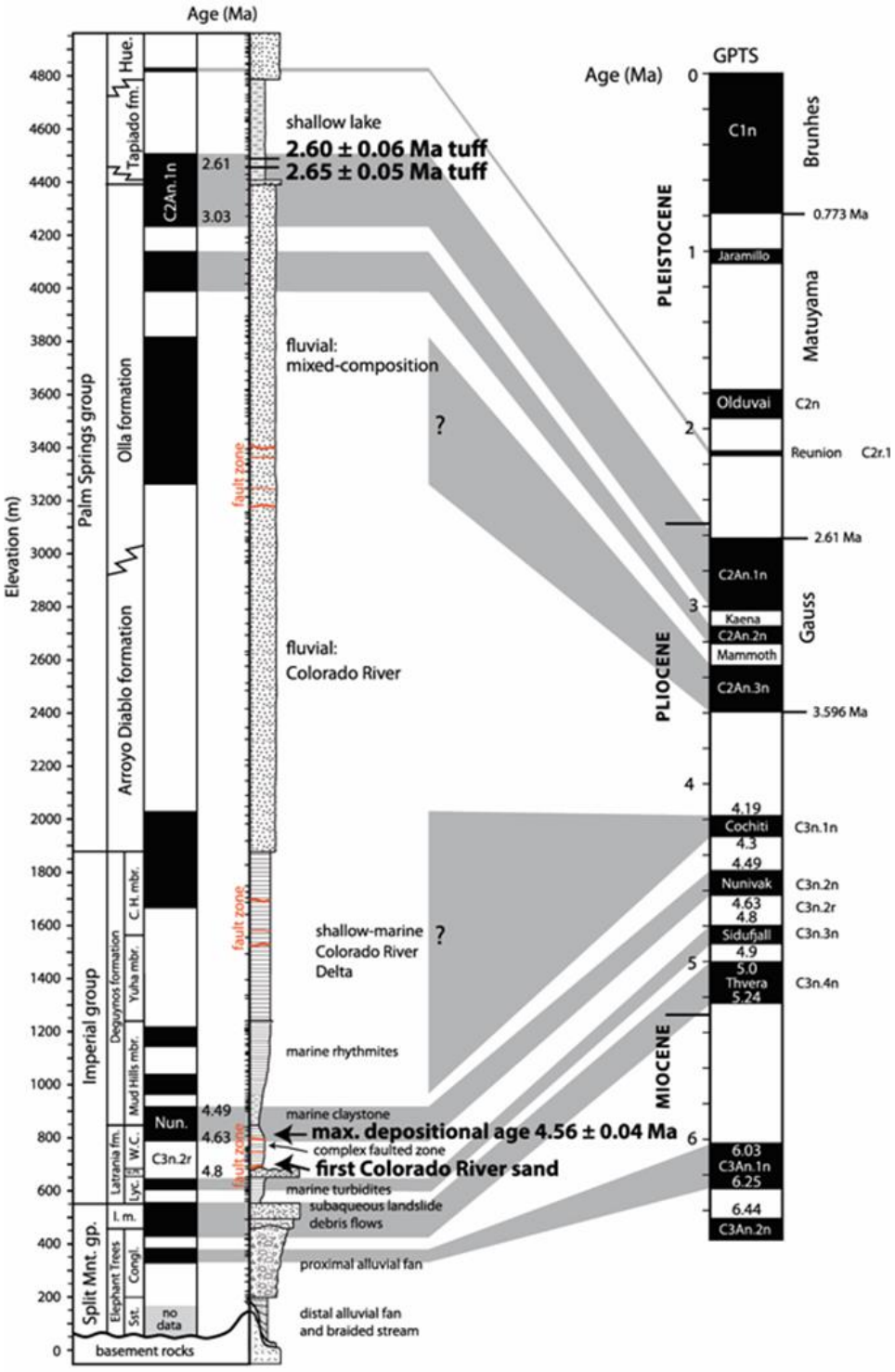

Figure 1.4. Composite section from the Fish Creek–Vallecito Basin proposed by Crow et al. (2021).

In this section, the correlation to the geomagnetic polarity time scale (GPTS) proposed by Dorsey et al. (2011) has been modified based on the new detrital sanidine ages from the upper part of the Wind Caves member and previous U-Pb results in the Tapiado formation. Also shown are positions of fault zones (red lines) suggested by Janecke et al. (2016). sst.—sandstone; congl.—conglomerate; l.m.—lower megabreccia; Lyc.—Lycium member; u.m.—upper megabreccia; W.C.—Wind Caves member; C.H.—Camels Head member; Hue.— Hueso formation; Nun.—Nunivak subchron.

Motivations and Methods

Motivation

The objective of this project is to use the analogy of the modern Colorado River, and the implication of its compound clinoform morphology, to explain the characteristics of the Deguynos Formation deposits, which has been proven to be linked to the ancient Pliocene Colorado River (Winker, 1987; Dorsey et al 2011; Cloos, 2014). Deguynos Formation stratigraphy and architecture have been barely studied in previous papers and could serve as a tool to better understand ancient compound clinoform deposits.

Field Work in Fish Creek-Vallecito Basin

The Fish Creek-Vallecito Basin outcrops provided data for four stratigraphic measured sections through the upper part of the Deguynos Formation (Yuha Member and Camel Head Member) (figure 1.5). All sections were then integrated into a large 2-D panel that is oriented NNE-SSW, aligned slightly oblique to depositional dip, and includes two short sections (FC 2 and 3) measured by Winker (1987). The muddy intervals were more difficult to measure because they were usually covered. The thickness of these sections was made by direct measurement on the outcrops, correcting for the angle to the dip of the strata measured and corroborated by a combination of satellite images and GPS points.

Logging included photography and description of grain size, bed thickness, sedimentary structures, the nature of bedding contacts, bioturbation, and erosional surfaces. The paleocurrents were measured, on asymmetric ripple and crossbedded structures on the side of the beds with a few exposed on bedding planes that allow the measurements of the lee face of the ripples (see appendix 1). Dip and strike stratal attitudes (with which we corrected the measured paleocurrents), were taken along each of the northwest to southeast transects within the Fish Creek-Vallecito Basin. After consideration of the variability of

lithological characteristics through the logged segments, a facies scheme was created for each of the units mapped and compared with analogous facies descriptions existing in the literature. The sedimentary logs were complemented with drone photos and satellite images to understand the lateral distribution of sequences and 3-D spatial relationships of the different facies.

The correlation between the different measured sections was possible because of the laterally continuous topographic ridges of Yuha Member and Camel Head Member, which allowed satellite image correlation and field ‘walk-out along the same bed for kilometers (figure 1.5). 17 of these ridges were measured.

For mapping the sequences and the sequence sets in the 2D architectural panel, the measured sections were divided first into facies and then clustered into associations of facies. Then, based on environmental interpretation of these associations of facies and the lateral changes of these deposits between measured sections, maximum flooding surfaces were interpreted that were also followed in the field. Using these surfaces 22 regressive-transgressive (R-T) were defined. These were further grouped into 4 sequence sets, based on identifying changes in thickness and trends up through the sequences R-T.

Colorado Delta Data

For the complementary work on the modern Colorado Delta, I used the available bibliography to gather a description of the modern environment before and after the construction of the dams and the irrigation system. Data from these studies provided information on the subaerial and subaqueous architecture of the Delta system.

The subaerial portion of the modern Colorado Delta was thoughtfully described by Thompson (1968), and from this report, it was possible to construct a facies

characterization that I could compare with the interpreted subaerial parts of the paleo-Colorado Delta facies recognized in the Fish Creek-Vallecito Basin.

For the extensive subaqueous portion of the Colorado Delta, I used existing bathymetry maps and satellite images to understand the geomorphology of the shallow marine environment below the water. The bathymetry map was obtained between 1994 and 1997 using an Ocean Data Equipment continuous depth recorder and GPS onboard the B/O Francisco de Ulloa of Centro de Investigación Científica y de Educación Superior de Ensenada, Baja California (CICESE), and the shallower waters were surveyed with a Raytheon DE-719 portable fathometer (Alvarez et al., 2009).

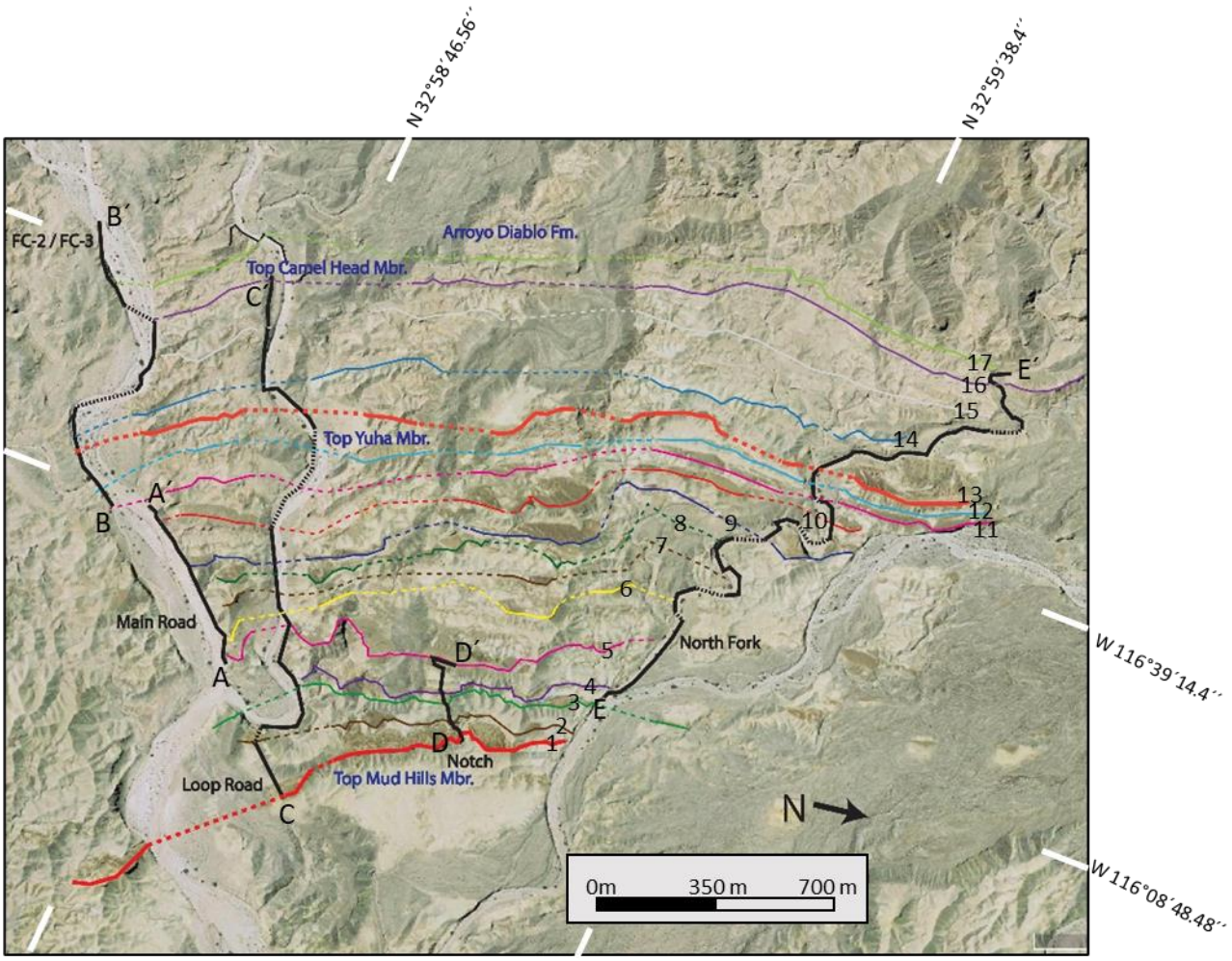

Figure 1.5. The satellite image is taken from Google Earth, where is shown the measured sections (in black) and the 17 correlated ridges (In colors) in the study area.

Modern Colorado River Delta

The modern Colorado River Delta in Baja California, Mexico shows a compound clinoform morphology in its bathymetry, with a steepened bathymetric gradient both in the shoreface area and in the front of the subaqueous Delta. Satellite images and bathymetry maps reveal several classic tidal morphological features, such as subaqueous tidal bars and tidal channels, and intertidal as well as supratidal flats around the shoreline zone. Thompson (1968) made a morphological subdivision (figure 1.6a) of the Deltaic deposits between high mudflat, intertidal and subtidal deposits.

High flats:

The high flats of Thompson (1968) (figure 1.6a) are located at the level of the extreme spring tides. They are placed along the Delta/estuary margins and represent a collection of sites of pronounced windows of driftwood supplied by the River when it was more active. Such accumulations form effective mud filters and have caused the formation of mud ridges. Some subbasins are filled with mud and formed in this zone because of persistent standing water after rare flooding.

Intertidal Zone:

The intertidal zone (figure 1.6a) has a very gentle gradient (0.1 to 0.2 degree) and extends from spring higher-high to spring lower-low tide level. It was divided into two zones:

- **Beach Ridges and Transition Zone** is occupied by a semi-continuous belt of subparallel beach ridges (figure 1.6b). These ridges of coarse material are incised by tidal channels (forming tidal inlets). Shell fragments are a dominant component of clasts forming these ridges (in some places up to 95%). The tidal inlets extend 3 to 6 km inland, forming a well-integrated drainage network (figures 1.6a,1.6b). The

channels are scoured 1 to 2 m below mean sea level, yielding relief of 4 to 5 m with the adjacent high flats. Gradients on the beach face average about 5 to 7 degrees and have 60 to 100 cm high dunes.

Seaward-dipping mud flats separate many of the subparallel beach ridges near the River mouth. Laminated silts constitute the predominant sediment on the mudflats. Gradients of these mudflats vary from 0.02 to 0.08 degrees, and the surfaces appear remarkably featureless except for occasional minor tidal gullies.

- **The lower Intertidal Zone** extends seaward from the toes of the modern beach ridges to the lower-low water level of spring tides. In some places, discontinuous longshore bars characterize the surface (figure 1.6c). Relief on the bars varies from 0.5 to 1 m between the crest and the adjacent seaward trough. The average crest-to-crest spacing is 150 to 200 m. Fine-to-medium sands comprise the bar crests. The bars are asymmetric in profile, the steep sides facing shoreward, and they are broken into segments by shallow ebb tide drainage gullies (figure 1.6c).

Subtidal Zone:

The subtidal zone starts below the lower-low water level of spring tides. The deposits in this zone begin with mudbanks similar to the mudflats present in the lower intertidal zone with a smooth, low-dipping plain. The dominant sediments are silty-clays with a shift in color from the intertidal zone (from moderate brown in the upper units to brownish-gray) probably relates to the lack of subaerial exposure and a slight increase in the organic material content.

The subtidal mudflats terminate at a depth of about 12 m, where the submarine terrace starts. At this depth, the bottom flattens out into an area is defined by a “submarine

terrace" (Thompson, 1968) of more than 70 km wide with a low gradient. Today we would term this terrace the subaqueous platform of the subaqueous Delta. This terrace is dominated by two morphological features: elongated positive relief sub-parallel with the River outflow from the Delta, covered by sands and skeletal parts, and a negative relief feature V-shaped in profile and have steeper eastern bank inclinations covered by mud and silt (figure 1.7).

The positive relief features were interpreted by Alvarez et al., (2009) as tidal bars (figure 1.7). The bars are 5 to 6 km wide, 2 to 5 meters in height, and have an asymmetrical flank slope (4°-6°), with the lee face toward the southwest. The bar axes are oblique oriented relative to the direction of peak tidal flow (3°-7°). The tidal bars are currently actively migrating into 15 meters of depth (with currents stronger than 0.5 m/s), and barely active in most of the subaqueous platforms between 15 to 40 meters of depth. From cores, we know that tidal bars are sandy though most of the skeletal material is concentrated in their top, ie an upward coarsening tendency. It has been argued that several of the bars have an orientation partially control by active faults in the gulf (Thompson, 1968; Alvarez et al., 2009).

The negative relief features were interpreted by Thompson (1968) as channels (figure 1.7) that are broadly V-shaped in profile and have steeper eastern bank inclinations ranging from 2 degrees to 3 degrees (the steepest measured in the subtidal zone). We interpret these features as tidal channels, perhaps originally built by tidal currents as they cut back from the edge of the subaqueous platform landward, but later became the channels into which the tidal bars laterally accreted. The channels are mostly filled at present by fine sediments (silts and clays) according to short cores and grab samples (Van Andel, 1964; Thompson, 1968) (figure 1.7). These channels have a key role in obliquely building the tidal bars forward and to the SW, as proved by the asymmetry of the bars (the steep side

on SW is the accreting the lee slope). Examples of this behavior (migration-accretion) between channels and bars can be recognized in the Han River (figure 1.8), South Korea, Cummings et al. (2016), or in the Gulf of Khambhat, India, (Saha et al., 2016), though the Han River case has a much bigger scale with tidal bars and channels extending the subaqueous Delta 100 km from the shoreline.

Beyond the "submarine terrace", across what we would term the subaqueous rollover is the subaqueous foreset that in Colorado case is close to shelf-break or shelf edge, and continue with a steep slope goes down ~150 meters until reach the Wagner Basin, a tectonically active depression with an area of 700 km^2 and a maximum depth of 225 m (Canet et al., 2010). The Sediments at this depression are mostly formed by very fine sands poured into the basin by the Colorado River via the subaqueous Delta channels and bars. (Hermoso-Salazar et al. ,2013).

Compound Clinoform Geometry, Facies, and Implications

A compound clinoform is easily recognized in the geomorphological profile of the modern Colorado Delta (figure 1.7) following the criteria proposed by Peng et al (2020).

The shoreline or intertidal zone of the Delta coarsens upwards with a lower part with mudflats and longshore bars, and a much coarser upper part defined by sandy and shelly beach belts. The gradient of the intertidal zone is relatively high (0.05°) for this setting (figure 1.7). The coarsening up and the dipping clinoformal geometry allow us to interpret this zone as the shoreline clinoform (figure 1.7).

The subtidal zone of the Delta is be divided into four different areas according to its depth and its gradient:

- An area comprised between the upper point of the mud banks (7 to 10 meters on average) to 15 meters deep. This area has a very gentle gradient (0.02°) (figure

1.7), and the tidal currents are strong enough to allow the active migration of sandy tidal bars. This migration of tidal bars allows the generation of coarsening upward tidal bars where the bar toe merges into mudflats deposits. This section has been interpreted as the inner subaqueous platform and gives way seawards to the muddy subaqueous Delta front (figure 1.7).

- An area consisting of the outermost portion of the subaqueous platform placed between 15 and 40 meters below sea level. This area currently has barely active tidal bar migration and it is mostly dominated by muddy deposits. The gradient in this area is 0.03° (figure 1.7), steeper than the upper portion due to the reduced influence of the shallow marine processes. This section has been interpreted as the outer subaqueous platform (figure 1.7).
- The area between 40- and 160-meters depth, which has an abrupt gradient (0.52°) (figure 1.7) and ends in the proDelta region. This zone has been interpreted as the subaqueous foreset (figure 1.7).
- Finally, the area in the Wagner basin has a very gentle gradient, and it has been filled with very fine sands poured by the Colorado River (Hermoso-Salazar et al., 2013), probably by turbidity flows. This area has been interpreted as the subaqueous bottomset merging onto the shelf (figure 1.7).

The compound clinoform morphology exhibit by the Colorado River Delta reflected the balance of energy that existed before the construction of the dam projects in its catchment area. The discharge of the River before the XX century was estimated to 20 km^3/y, and more importantly, the annual sediment flux to 120 Mt/y, an amount only surpassed by the Mississippi River in the North American continent (Curtis et al., 1973; Milligan et al., 2011). This strong sediment flux allowed the system to be molded to the tidal forces prevalent in the Gulf of California to form the compound clinoform

morphology now preserved in the modern Colorado Delta. The equilibrium shape of the Deltaic clinoform is reflected by the position and depth of the subaqueous rollover point (Thomsen and Gust, 2000; Walsh et al., 2004; Liu et al., 2013) which controlled the distribution of sediments out onto the shelf and Delta-front area but varied according to the oceanographic energy regime (Hori et al., 2002a). In the modern Colorado Delta, the rollover point occurs at about 40-50 m, deeper than in many other systems: e.g., 10 to 25 m in the Yellow River system (Liu et al., 2013), about 30 m in the Ganges–Brahmaputra River system (Kuehl et al., 1997), 30 to 40 m in the Amazon shelf (Nittrouer et al., 1996), and 25 to 40 m in the Gulf of Papua (New Guinea) (Walsh et al., 2004). The subaqueous rollover is predicted to be found in a deeper position as the sediment flux to the system decreased and the energy of shallow marine processes gets stronger (Friedrichs and Wright, 2004; Liu et al., 2013).

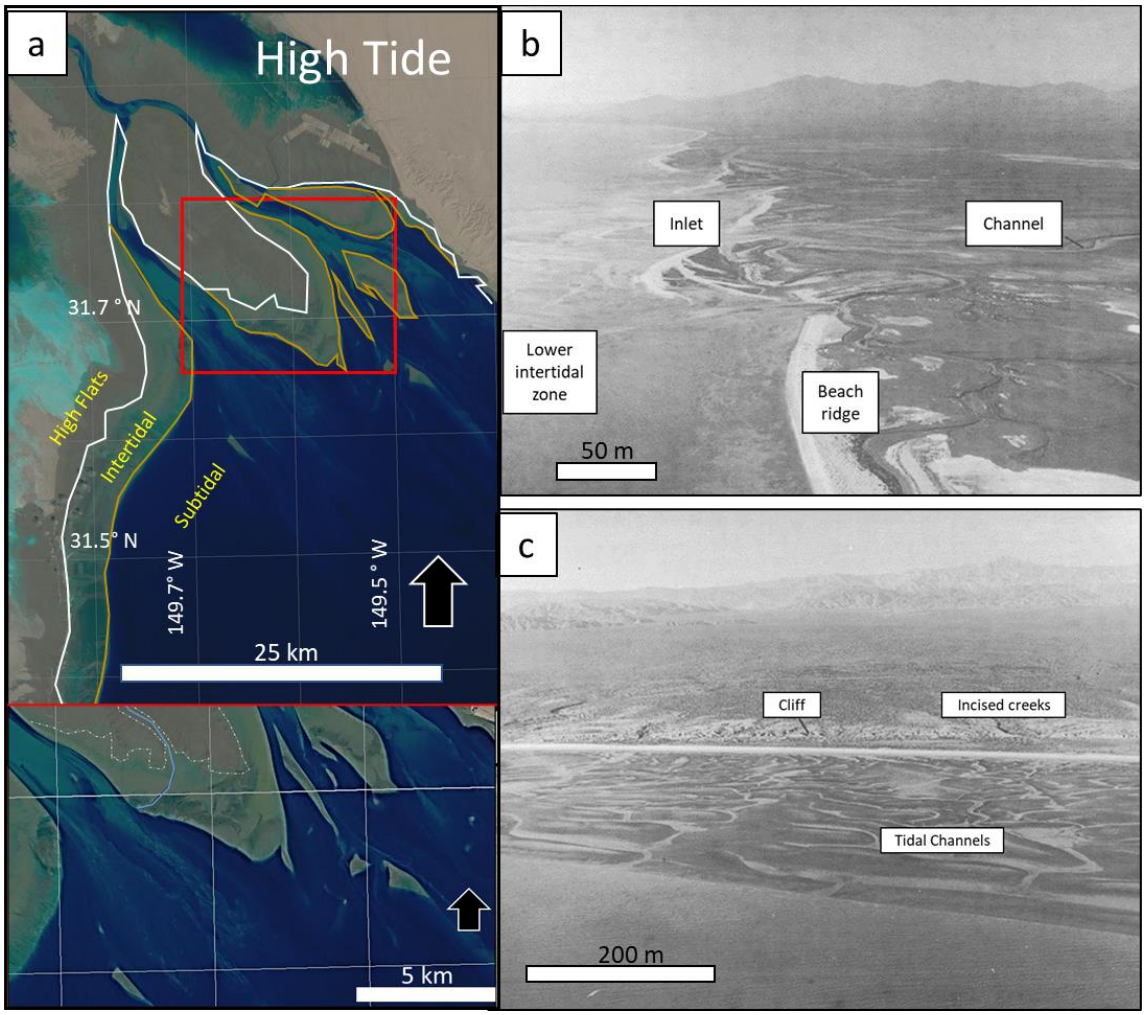

Figure 1.6. (a) Satellite images of the Mouth of the Colorado River in the northern portion of the Gulf of California. The images show the significant tidal range present in the area. The three morphological areas described by Thompson (1968) are indicated in the figures. During the low tides, the tidal channels on the coast remain flooded, and the sea can penetrate almost 5 km inland. During the high tides, there is a wide intertidal plain, displaying beach ridges, longshore bars, and drained tidal channels. (b) Aerial photos from the northern area of the western coast of the Delta, modified from Thompson (1968). (c). tidal channels covering much of the lower intertidal zone, modified from Thompson (1968).

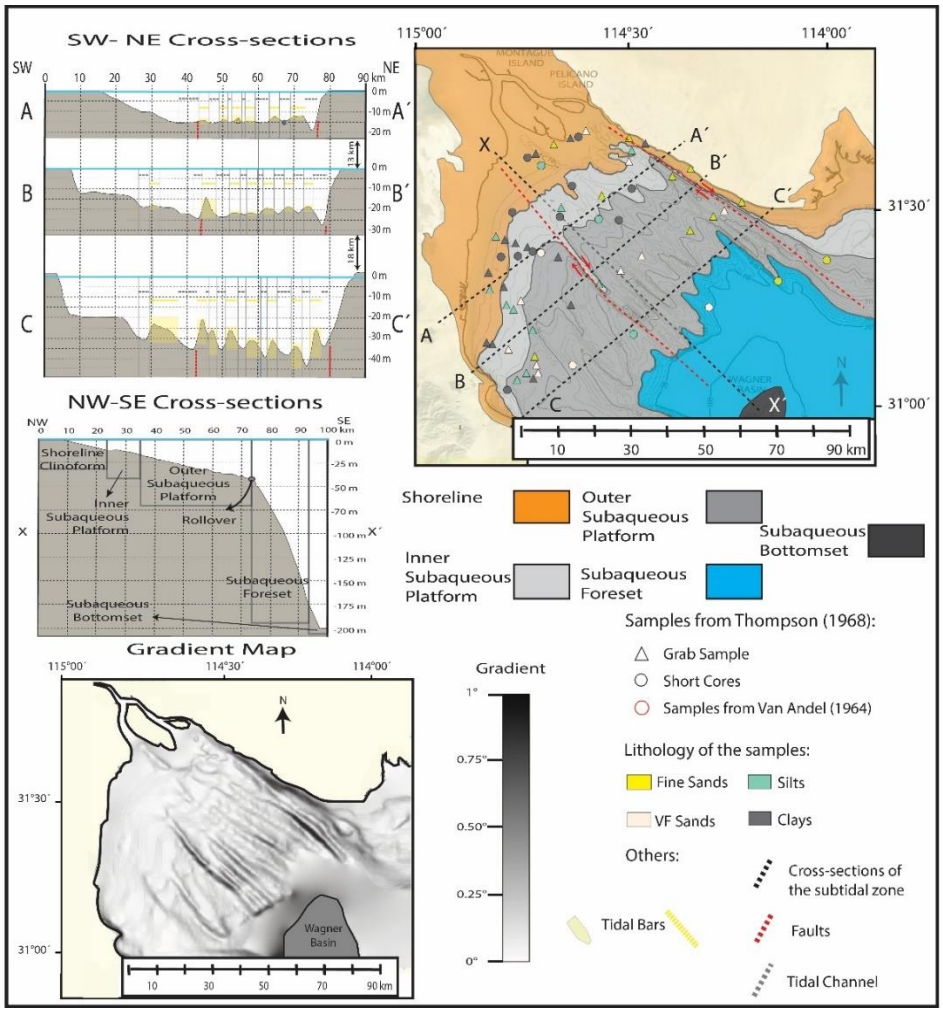

Figure 1.7. Modern Subaqueous Colorado Delta. In the upper section of the figure, a map modified from Alvarez et al., (2009) where the short core and samples acquired in the Colorado Delta seafloor (Van Andel (1964) and Thompson (1968)) were taken. These samples indicate a correlation between the positive relief features (tidal bars) and coarse-grained sediments. Note the interconnection of the tidal channels and tidal bars. Three SW-NE cross-sections through the Modern Colorado Delta are shown on the right.

These cross-sections display very well the positive relief of the tidal bars and the negative relief of the tidal channels, and their correlation with coarser and finer sediments (respectively). Also, the two faults that run NW-SE across the gulf can be seen. The location of the steeper foreset face of the bars allows the determination that the bars are migrating toward the SW. Also, the "relief" of the bars seems to increase with the water depth. In addition to that, the

clear bathymetric evidence of the compound clinoform identified in the Modern Colorado Delta, with the smaller subaerial clinoform at the landward end of each cross-section and the larger subaqueous clinoform highlighted by the Delta-front rollover at about 40m water depth. The NW-SE cross-sections display the five areas of the compound clinoform. In the lower section of the figure, the gradient map of the Colorado Delta is modified from Alvarez et al. (2009). The map shows the slope gradient of the subaqueous portion of the Delta. Note the remarkable change in the gradient due to the tidal bars in the subaqueous platform.

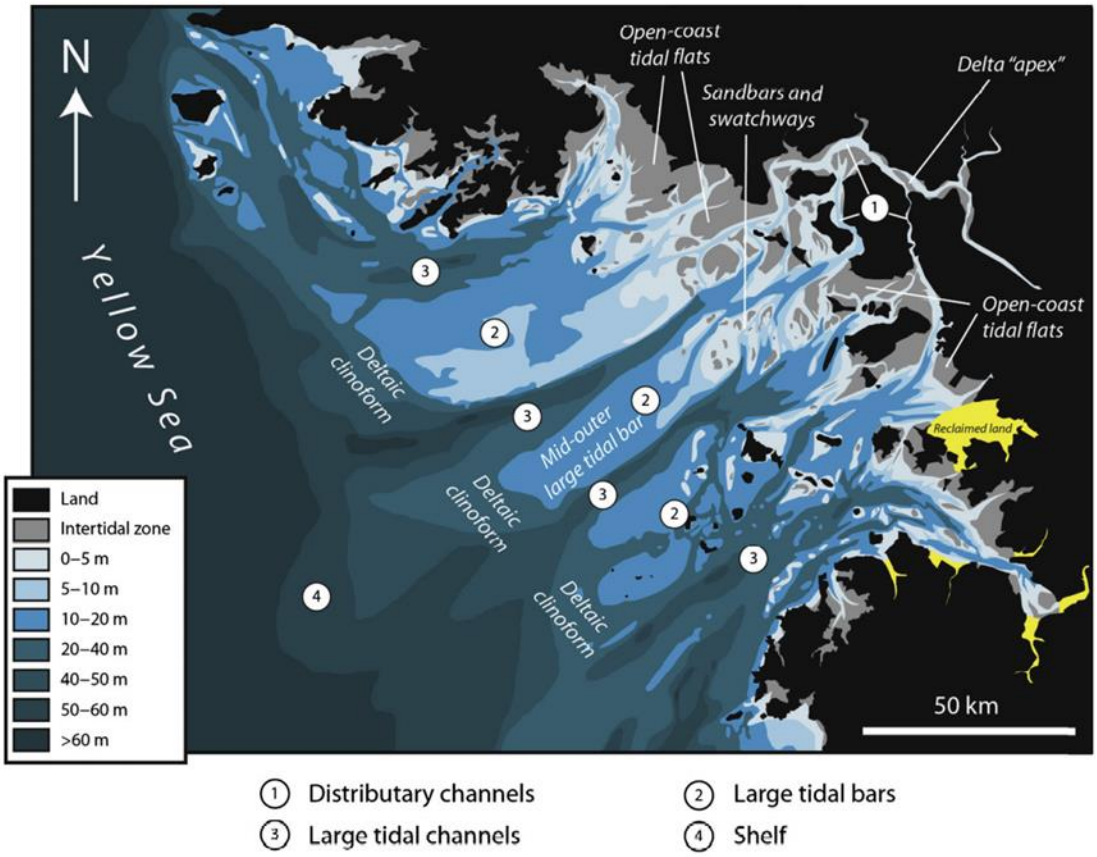

Figure 1.8. Major morphological elements in the Han River Delta. Note the relationship between tidal bars and tidal channels, as well as the great distance between the shoreline and subaqueous Delta front. Taken from Cummings et al., 2016.

The Pliocene Colorado Delta: Deguynos Formation

Measured sections of the Deguynos Formation (figures 1.5,1.18,1.19,1.20) describe in detail the sedimentary characteristics of the rocks. The description and data collected allowed recognition of distinct facies for which the paleo-environmental interpretation was made. The facies are grouped into facies associations for which a proposed depositional environment interpretation was proposed.

Facies:

The results of this facies analysis are summarized in Table 1.

Name	*Description*	*Code*	*Figure*	*Interpretation*
Structureless Mudstone	*Gray* structureless mudstone beds with Organic material (1-3%). Clay and silty clays. M to tens of m thick with a sharp base. Intense to moderate bioturbated (mostly *Teichichnus* or *Psilonichnus*).	Ms	1.9.a	Flocculation of mud in the distributary channels and channel mouth area due to a change of salinity of the water.
Gray Laminated Mudstone	Gray laminated mudstone. Clay and silty clays. Intercalation of thin lenses of very-fine sandstones. M to tens of m thick with sharp bases.	Ml1	1.9.c, 1.10.d	Suspension settling of the mud particles to the seafloor.
Red laminated Mudstone	*Red* laminated mudstone. Intercalation of thin lenses of gray silt and very fine sandstone. Clay and silty clays. 20 cm to m thick. Sandstone injected structures.	Ml2	1.9.d	Sediment suspension settling in an environment partially exposed to subaerial conditions.
Rhythmites	*A*lternation of light to moderate gray structureless clayey-silts which commonly grades to structureless or rippled silty-sandstones. Couples of 8 to 15 cm thick in packages of 5 to 15 m thick. Continuous tabular shape beds.	R	1.9.f, 1.9.g	Intercalation of suspension settling mudstones with density flows deposits, probably originated by hyperpycnal flows.
Gray laminated siltstone	*G*ray laminated siltstone and silty sandstones. M thick beds with sharp base. Rarely bioturbated.	Sll1	1.9.c,1.9.e, 1.10.d	formed under a weak unidirectional current.
Red laminated Siltstone	*Red* laminated siltstones. Mainly silt. 20 cm to 1 m thick with a sharp base. Occasionally petrified woods. Minor bioturbation (P*aleophycus*).	Sll2		formed under a weak unidirectional current partially exposed to subaerial conditions.
Structureless siltstone	Gray structureless siltstone and very fine sandstone. 10 to 60 cm thick with mostly sharp, rarely gradational base. Moderate to intense bioturbation, mostly vertical burrows. *Teichichnus*, *Arenicolites* and *Paleophycus*.	Sls		Decantation in low-energy areas with a stable seafloor. The frequency of bioturbation allows tying these deposits to a low level of stress conditions in the environment.
Bioturbated sandstone	*L*ight yellow to reddish structureless sandstones. Grain size silty to very fine. 20 to 60 cm thick with a sharp base. Intense bioturbation, mostly by vertical burrows, *Diplocraterion*, *Ophiomorpha*, *Thalassionides*, and *Teichichnus*. 20 to 40 % content of shells (*Ostrea Vespertina)*.	Sb	1.9.a	Low energy environment where organisms can thrive without much stress from the current. Probably related to tidal flats.
Laminated sandstones	Light yellow to reddish laminated sandstone with intercalation of lenses of laminated silt. Lower to upper very-fine. 10 to 80 cm thick with a sharp base. Moderate bioturbation, *Diplocraterion*, *Skolithos*, and *Ophiomorpha*. 10 to 40% of shells, mostly *Ostrea Vespertina*.	Sh	1.9.h	Low energy environment with a weak seafloor current. The abundance of bioturbation indicated a low level of stress conditions in the environment.

Table 1. Summary of the Deguynos Formation facies with proposed interpretations.

Name	*Description*	*Code*	*Figure*	*Interpretation*
Sandstone with wavy bedding	*Very*-fine light yellow to reddish sandstones and gray mudstone organized in wavy laminated beds. 10 cm to 1 m thick with a sharp base.	Sw	1.10.a, 1.10.b	Alternation (reversal) of tidal current and slack water conditions.
Sandstone with flaser bedding	Light yellow or reddish sandstone and gray mudstones with flaser lamination. Very-fine to fine. 5 to 8 cm and the packages 20 to 40 cm of thickness.	Sf	1.10.b	Alternation of current (slightly stronger than in Sw) and slack water conditions.
Ripple cross-laminated sandstone	Silty to fine, mostly very-fine light yellow or reddish sandstones. 10 to 50 cm with a sharp base. Moderate to intense bioturbation, *Planolites*, and *Paleophycus.* Frequently mud drapes with organic material. Commonly display mudclasts and pebbles at the base.	Sr	1.10.d	Migration of ripples due to a light to moderate energy current. The presence of mud drapes indicates that the tidal processes were dominant during the formation of the deposits.
Sandstones with shells	Very fine Light-yellow to reddish sandstones, with 40 to 60 % of shell content (mostly *Ostrea Vespertina*). 10 to 30 cm thick with a sharp base. At times, moderate to intense bioturbation, *Ophiomorpha*.	Ssh	1.10.c	Reworking of a weak current over shell beds. The presence of common bioturbation allows linking these deposits to a low level of stress conditions in the environment.
Sandstone with low angle cross stratification	Very-fine to coarse, mostly very-fine *l*ight-yellow sandstones. Low-angle cross-stratification with frequent accretional surfaces with abundant mudclasts. 30 to 50 cm thick with a sharp base.	Sl	1.10.e	Moderate unidirectional current forming dunes over the seafloor.
Sandstone with hummocky cross-stratification	Very fine Light-yellow sandstones. Packages of 20 to 50 cm thick with sharp bases. Hummocky cross-stratification. Occasionally, interfingered with thin lenses of shell-rich sandstones.	Shm	1.10.f	Formed by the reworking of the storm waves over the seafloor.
Deformed Sandstones	*D*eformed sandstone beds with a lenticular shape. Very fine to fine. Erosive or sharp base with frequent mudclasts and shells. 1 to 4 m thick. Moderate bioturbation, mostly *Paleophycus*. Petrified woods.	Sd	1.11.a, 1.11.c, 1.11.e	Migration of dunes due to a moderate to high energy current. The deformation occurs post-depositional as water escapes due to an overload of sediment. Maybe triggered by earthquakes.
bi-directional cross-bedded fine Sandstone	Light-yellow to reddish sandstone. Very fine to fine, sometimes medium. Cross bedded stratification sets of 8 to 20 cm, packages of 20 cm to 1 m thick. The base sharp and displays mudclasts and shells. Occasionally bi-directional (herringbone) structures. Abundant mud drapes, and rarely minor bioturbation (*Paleophycus* or *Ophiomorpha*).	Spf	1.11.d	Migration of dunes due to a moderate to high energy current. The evidence of bidirectionality (herringbone structures) and mud drapes indicate tidal processes.
Planar cross-bedded coarse Sandstone	Light-yellow to reddish sandstone. Coarse to very coarse. Cross-bedded stratification, with sets of 5 to 20 cm, packages of 20 cm to 50 m thick. The sharp base with shells, mudclasts, and pebbles. Occasionally petrified wood.	Spc		Migration of dunes due to a moderate to high energy current. The fragments of petrified wood and shells in the base of the dune sets allow linking these deposits with distributary channels.
Coquina with low angle cross-stratification	*Coquina* beds formed of broken skeletal parts on a matrix of very fine to fine sand grains jointed by a carbonate cement. parts have 1 to 5 cm of diameter, mostly bivalves *Ostrea Vespertina, also Pecten deserti* and *Anomia Subcostata* (described by Winker, 1987). 40 cm to 2 m thick, frequently low angle cross-stratification with multiple accretion surfaces.	C	1.11.b, 1.11.f, 1.11.g	Formed by the reworking of the current over shell beds. In the case of these deposits, the current allowed the migration of bars.

Table 1. Continued.

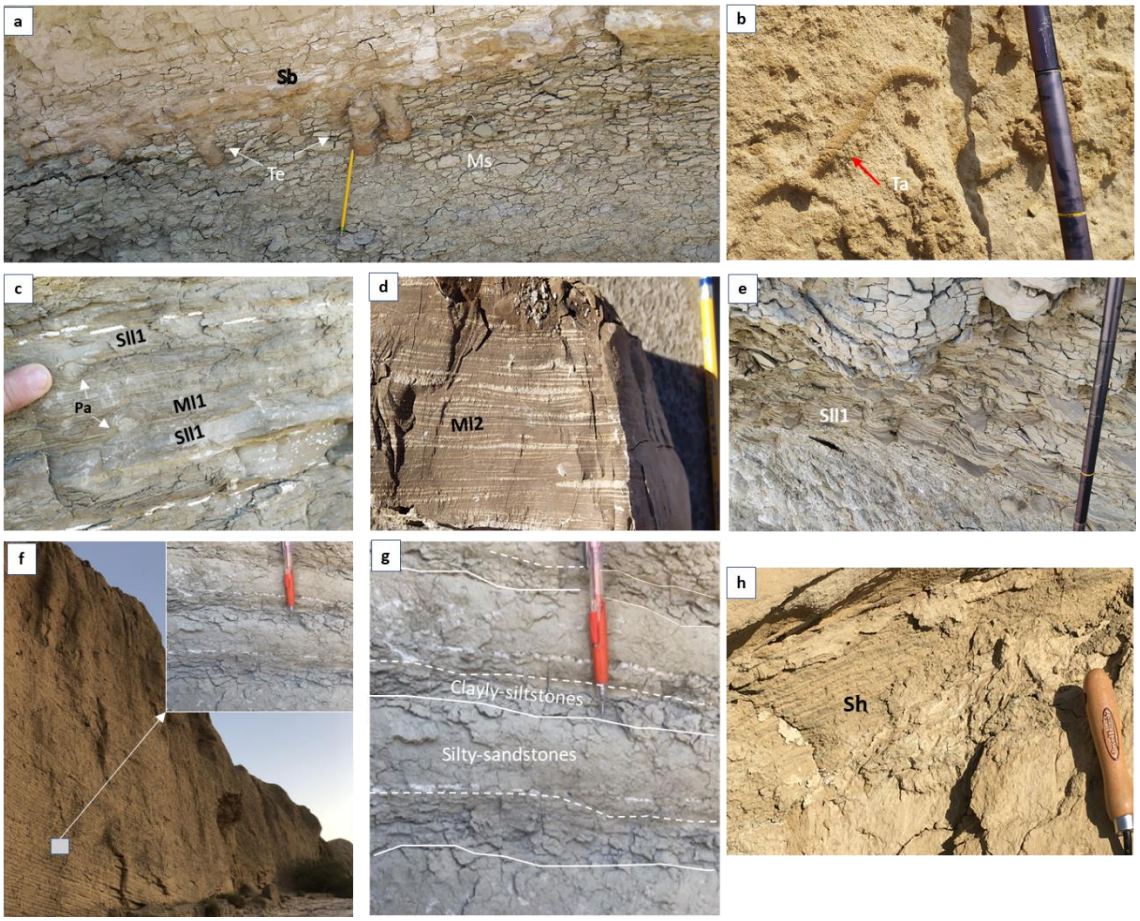

Figure 1.9. Facies photos of Deguynos Formation. (a) *Teichichnus* (Te) at the base of a bioturbated sandstone *(Sb)*. The bioturbation can be found up to 60 cm below the base of the sandstone into the structureless mudstone beds. (b) *Thalassinoides s.p* (Ta) at the top of a bioturbated sandstone facies (*Sb*). (c) Laminated gray mudstone with stripes of sandstone (*Ml1*). The bioturbation (*Paleophycus*) can be recognized both in the mudstone and the sandstone. (d) Red mudstone (*Ml2*) with the thin laminae of siltstone and very fine sandstone. (e). A 20 cm package of thin laminated siltstones from the gray laminated siltstone facies (*Sll1*). (f) Outcrop in the lowermost Yuha Member with the rhythmites facies (R). (g) Detail of the rhythmite beds (R) with cm thick intercalation of clayey-siltstones and the silty-sandstones. Note how the contact is sharp between the silty sandstones and the clayey-siltstones, and more transition when the order of the beds is inverted. (h) A 10 cm bed with thinly laminated sandstones (*Sh*) in the lower Yuha Member.

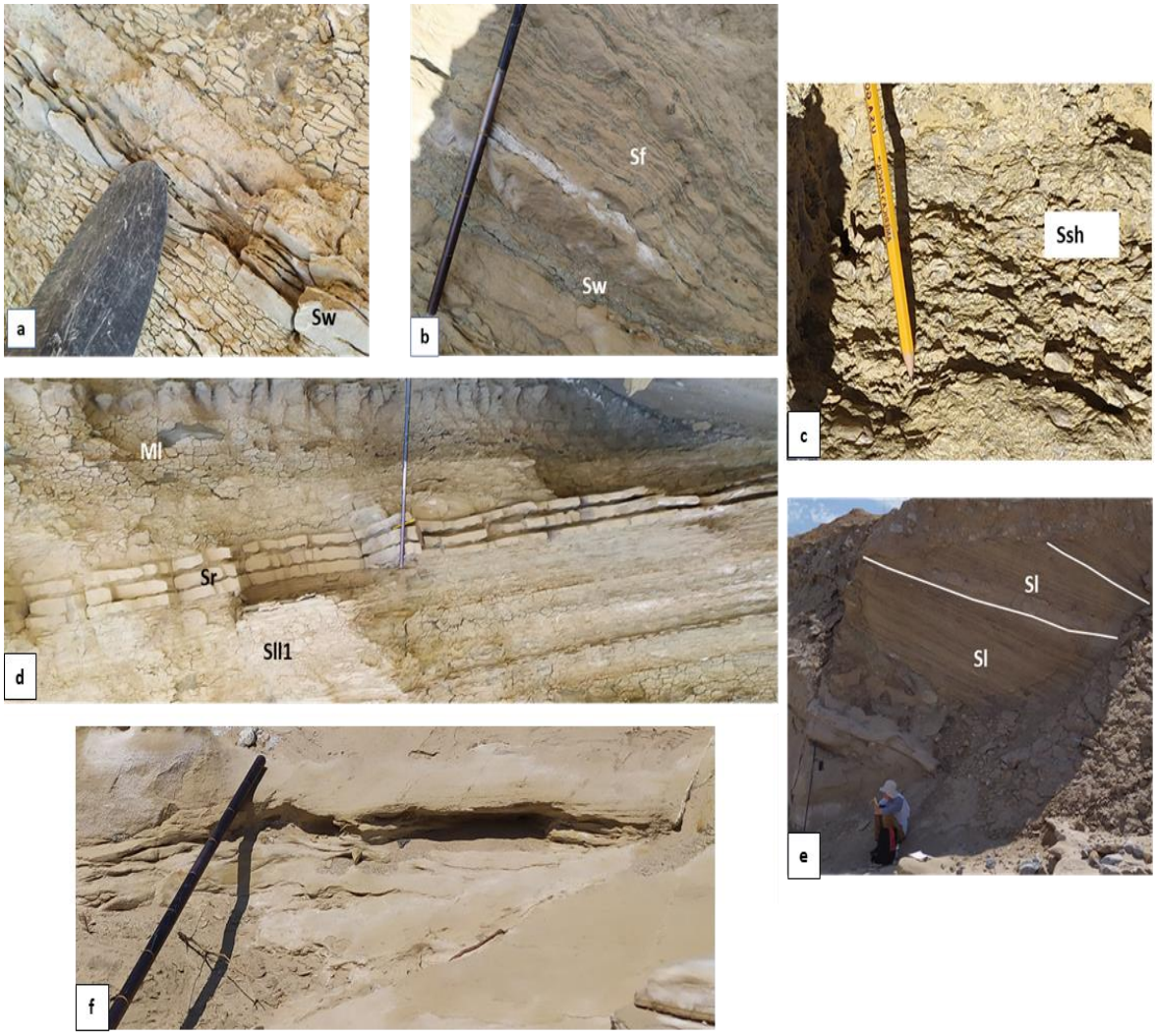

Figure 1.10. Facies of Deguynos Formation. (a) Cm-thick bed of sandstone with wavy lamination (Sw) interbedded within structureless mudstone (Ms). (b) A 30 cm thick intercalation of sandstones with flaser lamination (Sf) and sandstones with wavy bedding (Sw). (c) A 10 cm unit of sandstone with shell facies (Ssh). (d) A 50 cm intercalation of laminated mudstones (Ml1), gray laminated siltstones (Sll1), and well-defined rippled sandstone (Sr) beds in the lower Yuha Member. (e) 3 meters interval of inclined low-angle laminated sandstones (Sl) with multiple reactivation surfaces. (f) A 10 cm sandstone bed with a hummocky structure (Shm).

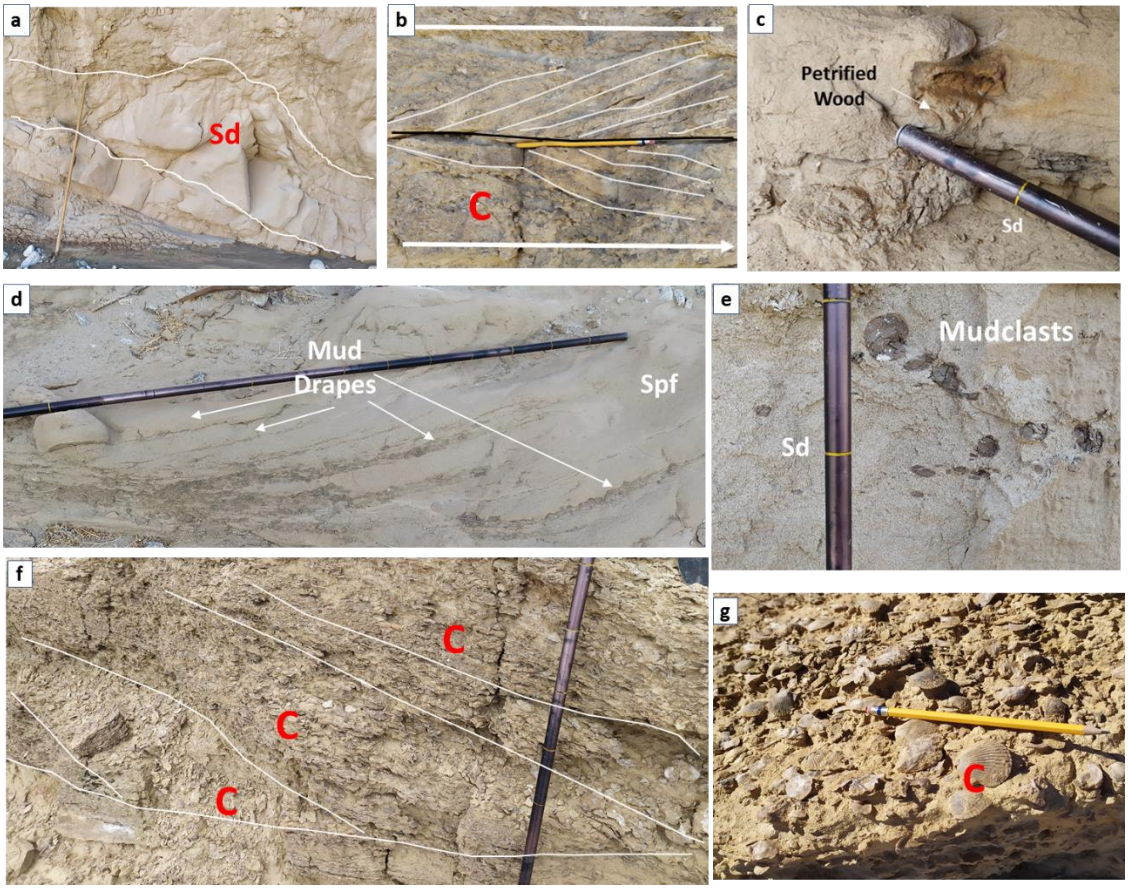

Figure 1.11. Facies of Deguynos Formation. (a) Deformed 40 cm thick intervals of deformed sandstone facies (Sd) in the lower Camel Head Member. (b) 20 cm bed with herringbone cross strata related to low-angle stratification in coquina facies (C). (c) Petrified wood fragment within a deformed sandstone (Sd) bed. (d) 50 cm package of cross-bedded, fine-grained sandstone (Sp1) with prominent mud drapes. (e) Mud clasts within a deformed sandstone (Sd) bed. (f) Multiple beds of low-angle cross-stratification coquina bed (C) showing an accretional surface at the base. (g) fossil concentrations commonly found in a low-angle accreting coquina bed (C). These fossils are mostly formed by *Ostrea vespertina* (Winker, 1987).

Paleocurrents:

Some 100 paleocurrents (see appendix 1) from ripples cross-stratification and crossbedded sandstones and coquinas were measured within the Deguynos Formation. The

paleocurrents exhibit a consistent direction towards the south with minor deviations towards the southeast and southwest (figure 1.12d). This direction is shared in both Yuha (n=26) and Camel Head Members (n=74) as well as with the paleocurrents reported in the underlying Wind Caves deposits (Cloos, 2014). The paleocurrents were measured in both rippled lamination (n=12) and cross-stratification (n=88). In the cross-bedded facies, the paleocurrents were strongly southward, while in the ripple laminated facies, the direction was more varied (figure 1.12.a).

In addition to the measurement of paleocurrents in sedimentary structures, multiple accretional surfaces were documented associated with the low-angle cross-bedded coquina beds (C) facies. These surfaces exhibit bi-directionality (200°-40°) and tend to be slightly oblique to the dominant direction exhibit in the cross-bedded facies (180°) (figures 1.12b,1.12c).

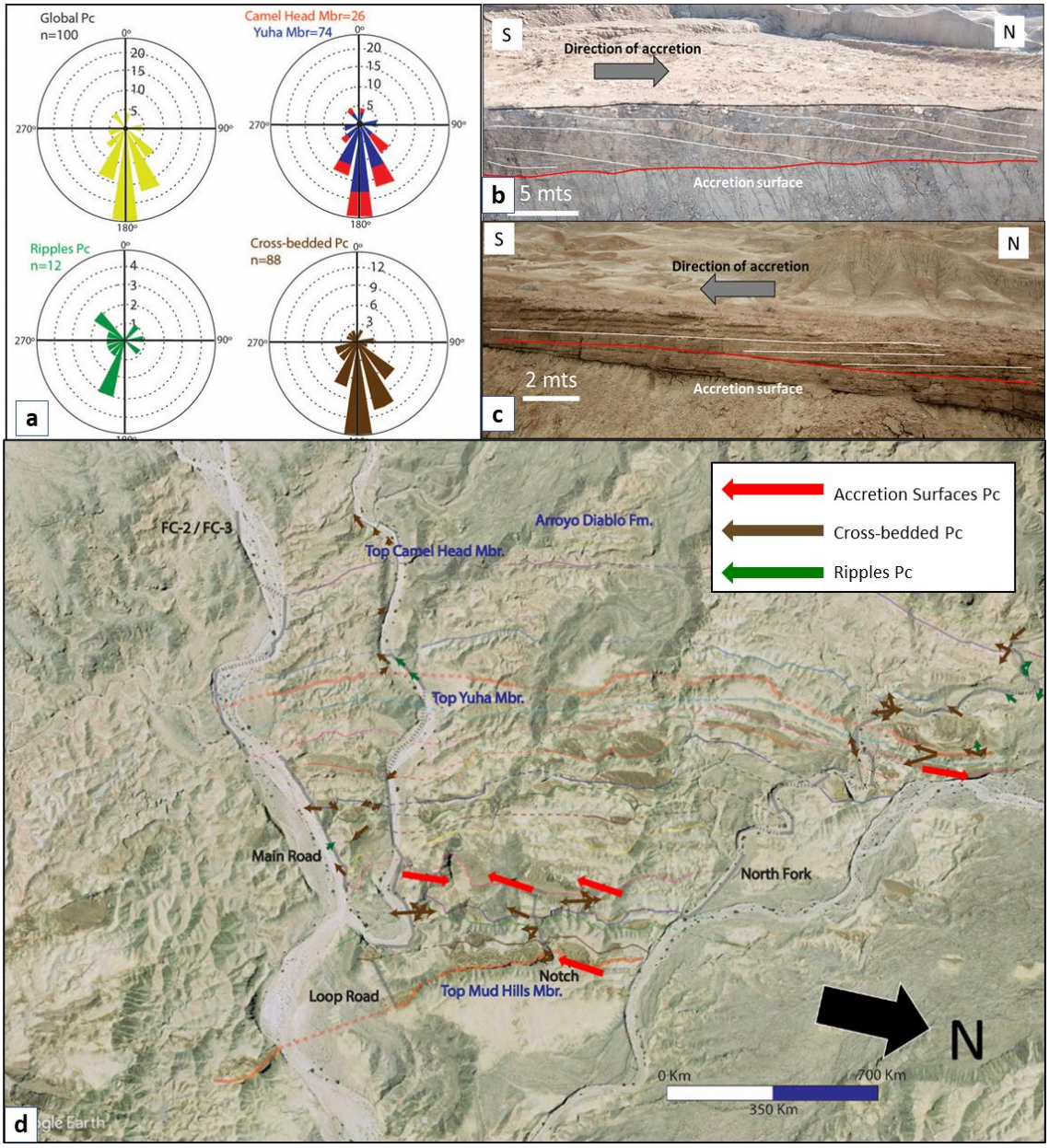

Figure 1.12. Location of paleocurrents on Deguynos Formation. (a) Four plots with the paleocurrents measured in the field. The plots are differentiated by Member and sedimentary structures. (b) (c) Photos of the coquina ridge (R4) which exhibits well-developed, low-angle accretion surfaces. The accretion surfaces exhibit opposite directions, presumably dominant and secondary tidal current directions. (d). This map presents a summary of the paleocurrents measured in the outcrops (north is on the right).

Facies Associations and their Environmental Significance:

Mudstones facies association (A1*)** is formed by 10 to 40 m thick intervals of structureless mudstones with cm-thick intercalations of siltstones and very fine-grained ripple cross-laminated sandstones (Sr***) beds. Mudstones are mostly structureless ***(Ms or Slm)*** or occasionally very thin laminated (***Ml1*** or ***Sll1***). Organic matter and shell fragments (*Ostrea Vespertina*). The bioturbation is commonly related to the thin-bedded sandstones, varies from moderate to intense, and is formed by vertical trace fossils (*Teichichnus* or *Psilonichnus*) (figure 1.13).

A1 denotes subaqueous flow conditions, and the fine grain size and ripples imply a low-energy with a unidirectional flow environment. The 10 to 40 m thickness (figure 1.13) and the frequent structureless and ripple-cross-strata beds strongly suggest a persistent and strong sediment supply. We interpret facies association ***A1*** as related to mud belts formed in the outer Delta front or the proDelta, similar to the ones described in the Amazon subaqueous Delta (Nittrouer et al., 1986; Allison et al., 1999). The strongly tide-dominated nature of the Delta and the confined conditions of the Gulf of California during the Pliocene probably hindered the dispersion of the mud sideways along the shelf.

Rhythmic beds facies association (A2) is composed of meters to tens of meter-thick units of alternating cm-thick siltstone and structureless or rippled very fine sandstones (***R*** facies). The ***A2*** facies association occurs in close relationship with the ***A1*** and ***A5*** facies association in the lower part of the Yuha Member. These deposits are mostly tabular in shape and can be followed laterally for a few km (figure 1.14,1.15a,b).

The deposits which formed the A2 facies association were probably formed by intercalation of suspension settling mudstones with density flows deposits, probably

originated by hyperpycnal flows. The stratigraphic position of the facies association A2 (above A1 and below A5 facies associations) indicates that they should be formed in the outer part of the Delta front.

Laminated siltstones and sandstones facies association (A3) accumulated as meters to tens of meters thick intercalation between gray mudstone and siltstone, mostly laminated (***Ml1*** *or* ***Sll1*** facies) though with some structureless intervals (***Ms*** *or* ***Sls*** facies), with thin (5 to 20 cm) beds of very-fine sandstones (***Sr***, ***Sw,*** and ***Sb*** facies). Bioturbation is moderate to intense in sandy intervals with *Teichichnus*, *Arenicolites*, *Planolites*, *Paleophycus*, or *Thalassinoides*. Organic matter and shell fragments are common. The deposits are usually in sharp or gradational contact above ***A5*** and below ***A1*** facies associations or above Sandstone intervals with mud drapes (***A6***) beds. Facies association ***A3*** is especially frequent in the upper part of Yuha Member and the lower part of Camel Head Member (figure 1.15.a).

The slight increase in the grain size in ***A3***, in contrast with ***A1*** and ***A2*** *facies association*, the common lamination of the beds suggests a slight increase in energy, possibly related to a shallower water depth. The increase in bioturbation intensity and the diversity of trace fossils is usually related to low environment stress (salinity, suspended sediment, turbidity), which allows fauna to thrive. ***A3*** facies association is interpreted as Silt and Heterolithic Belts located in the subtidal zone near the shoreline, similar to what has been described in the modern Colorado Delta (Thompson, 1968)

Laminated siltstones with petrified woods **facies association** ***(A4)*** accumulated as m to 10 m thick of reddish mudstone (***Ml2*** facies*)*, siltstone (***Sll2*** facies), and very fine sandstones (***Sr*** and ***Sb*** facies), with shells and petrified wood fragments. The facies association A4 units have a tabular shape, occasionally with an erosive base. The sandy intervals display minor to moderate bioturbation with *Paleophycus*. ***A4*** facies association

is found in sharp contact overlaying ***A6*** and ***A7*** and can be commonly observed throughout the Camel Head Member (figure 1.16.a).

The reddish color of the beds in ***A4*** strongly suggests subaerial exposure. The lack of bioturbation, in comparison with other similarly fine facies associations (***A1*** or ***A3***), may suggest variable paleoenvironmental conditions such as salinity variations, related to the proximity of the River mouth (e.g Stupples, 2002; Rossi et al 2019). The alternation of dm thick very fine sandstone, siltstone and mudstone beds in ***A4*** indicates periods of varying low flow velocity and slack water. ***A4*** facies association is therefore suggested to relate to mud flats in proximity to the River mouth or brackish conditions, in the intertidal or supratidal zone (Yang et al., 2005; Fan, 2012; van Cappelle et al., 2017).

Coarsening upward beds **facies association (*A5)*** is 2 to 10 m thick. A5 contains a meters-thick basal zone of interbedded meters-thick siltstones (***Sll1*** facies) and very fine sandstones with ripples, wavy or horizontal lamination (***Sr***, ***Sw,*** and ***Sh*** facies), then multiple sets of cross-beds (***Spf*** facies), and finally to 1 to 3 meters thick of low-angle crossbedded coquina beds (***C*** facies***)***, sometimes overlaid by 10 to 30 cm of bioturbated very fine sandstones (***Sb*** facies), heavily cemented. ***A5*** facies association intervals are very continuous and can be followed laterally for 100s of m, and in some units for the extension of the entire study area (1.5 km), allowing easy correlation of sequences along the outcrop belt. The individual beds within the units show low-angle accretion surfaces (figures 1.12.b,1.12c,1.14.d) and typically can be followed for less than 100m before downlapping to the basal surface. The accretion of the beds (dip direction of the surfaces) is oblique (lateral) to the paleocurrents direction measured in the cross-bedded sets associated with the accretion surfaces. Facies association ***A5*** is displayed in sharp contact above ***A1***, ***A2,*** and ***A3*** (figures 1.13, 1.14), and it is frequently found throughout Yuha Member.

A5 facies association show a clear upward coarsening grain size trend, with a vertical thickness of 5 to 15 m, and sedimentary structures which suggest the accretion of sand bodies in high energy conditions. Watkins (1990) interpreted this unit as lateral accretion deposits of meandering distributary channels on shallow marine portions of the Delta. However, this explanation conflicts with the abundant shell fragments, coarse sands, and the upward coarsening of the accretional unit. ***A5*** facies association rather resembles the modern elongated tidal bars where coarse shell material occurs along the crest of the bars, there is a coarsening upside trend (albeit rather abrupt), and where there is an oblique orientation between the prevalent tidal current and the orientation of the elongated axis of the bars. Moreover, the 10 to 30 cm thick bioturbated sandstone capping some of the intervals present shallow marine ichnofacies, reinforcing the idea of its shallow marine origin (figure 1.9b). Therefore, ***A5*** facies association is interpreted as tidal bars in a brackish or marine environment (Darlymple et al., 1992; Mellere and Steel, 1996; Willis, 2005; Olariu et al 2012). If we use as an analogy the dimension of tidal bars described by Alvarez et al (2009) for the modern Colorado Delta, the tidal bars of Deguynos Formation may have extended for 10s of km, explaining the lateral continuity of these facies association along the outcrops (figure 1.7). The coarser sediment with bioclasts that are heavily cemented forming beds that cap ***A5*** facies association may have resulted from extended physical reworking and sediment bypass across the top of the subaqueous Delta (Hampson and Premwichein, 2017).

Sandstones with mud drapes **facies association** ***(A6)*** is formed intervals of 0.5 to 5 meters thick units, made of sandstone beds deformed (Sd) cross-bedded (Spf), or laminated (Sh). The base of the A6 units is usually erosional and commonly shows mudclasts and pebbles. A6 sometimes presents a fining upward, with dm beds made of laminated (Sh), rippled (Sr), or heterolytic-bedded with flaser (Sf) or wavy (Sw)

laminations very fine sandstones, and overlain by laminated silts (Sll1). The A6 facies association displays multiple reactivation surfaces and mud drapes are frequent in the rippled and crossbedded sandstones. Some beds of 20 to 60 cm thick of hummocky beds (Shm) facies can be found within the A6 facies association. The units of the A6 facies association have lenticular geometries and are found in contact with facies association A2, A3, and A7, it is commonly through Camel Head Member (figure 1.15.a).

The fining upwards grain size trend, erosive base with mudclasts and pebbles, lenticular geometry, and multiple reactivation surfaces suggest A6 are deposits formed in channels. The abundant mud drapes facies in A6 suggest a tidal environment, and so A6 is interpreted as deposits of tidal channels, with some degree of reworking by waves (as it is suggested by the beds with hummocky cross-stratification) in the intertidal and subtidal zones (Terwindt, 1988; Dalrymple & Choi, 2007; Van den Berg et al., 2007; Longhitano et al., 2012).

Sandstones with shells and petrified wood facies association (A7) are composed of intervals of 1 to 5 meters thick, made of deformed ***(Sd)*** or crossbedded ***(Spf or Spc)*** very fine to coarse sandstones. The bed sets sometimes have a finning upward trend, with dm thin beds made of laminated (Sh) or rippled bedded (Sr) very fine sandstones and capped by red laminated siltstones (Sll2). A7 facies association displays multiple reactivation surfaces, shells, and petrified wood fragments. A7 facies association usually overlies A4 and is interbedded with A6 facies association in the upper part of Camel Head Member (figure 1.16.b).

A7 facies association shares with ***A6*** a similar grain size trend, erosional base, geometry, and multiple reactivation surfaces, suggesting ***A7*** deposits are also formed in channels. However, in ***A7***, the presence of both shells and petrified wood fragments point to an environment in which there is the influence of shallow marine and fluvial processes,

suggesting the channels might be Delta distributaries (Choi et al., 2004; Olariu et al.,2015). Modern analogs for this environment can be found in the Mahakam system in Indonesia (Lambert, 2003; Storms et al., 2005) or near the River mouth and in the lower reaches of the Colorado River where it is common to find sandy beds with driftwood and shells (Thompson, 1968).

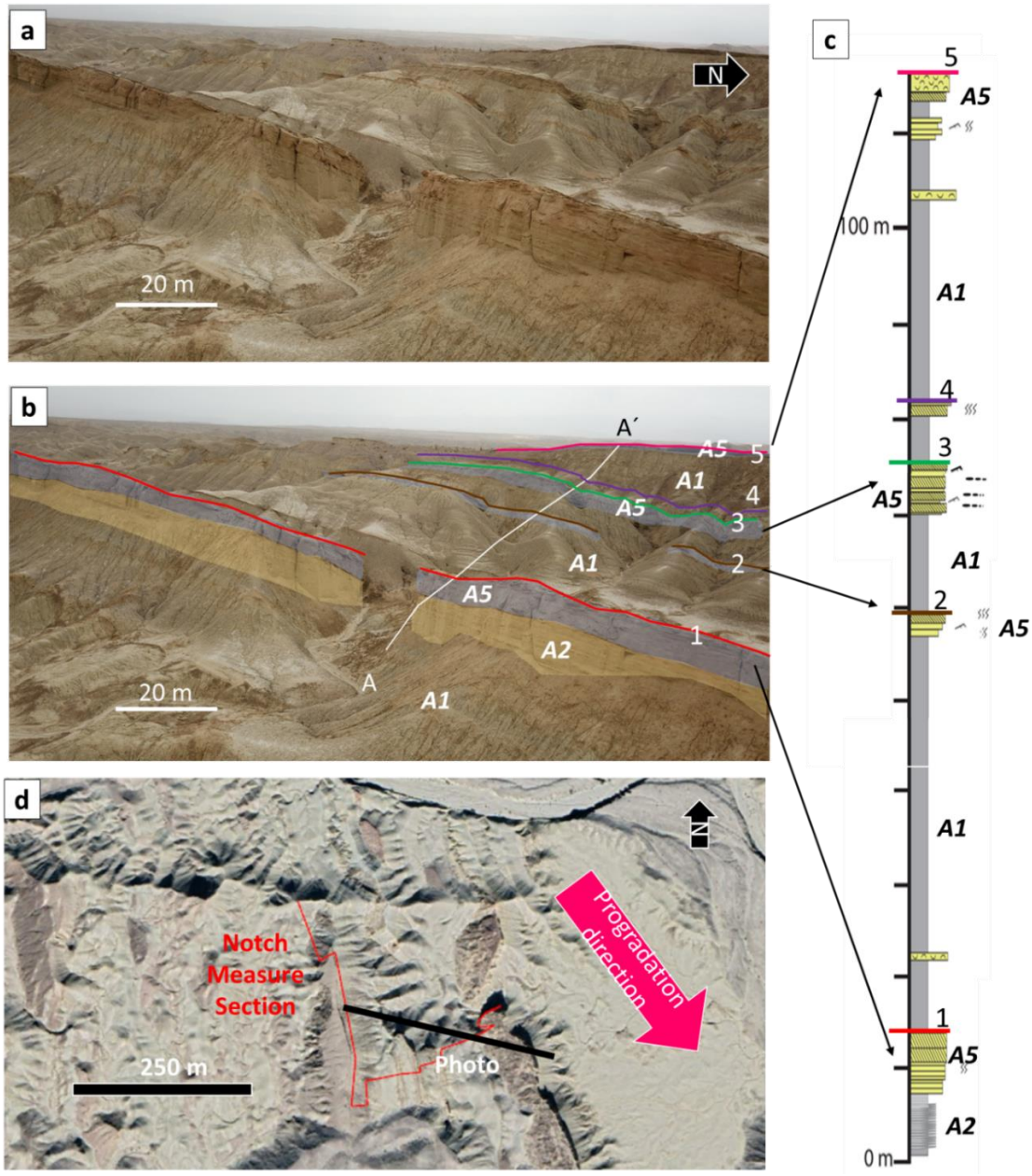

Figure 1.13. Facies association A1 (mudstones) and A2 (rhythmic beds).

(a) Drone photo showing the lower Yuha Member with repetitions of three facies associations: thick mudstone beds (*A1*), rhythmites beds (*A2*), and coarsening upwards beds (*A5*). (b) The interpretation of the photo. Facies association and ridge number are pointed out in the figure. Note that ridges and facies associations have great lateral continuity. (c) The measured log with an association of facies and ridge number and color. (d) Aerial photo with the

position of the photo from (a) and (b) and the direction of progradation of the paleo-Colorado Delta.

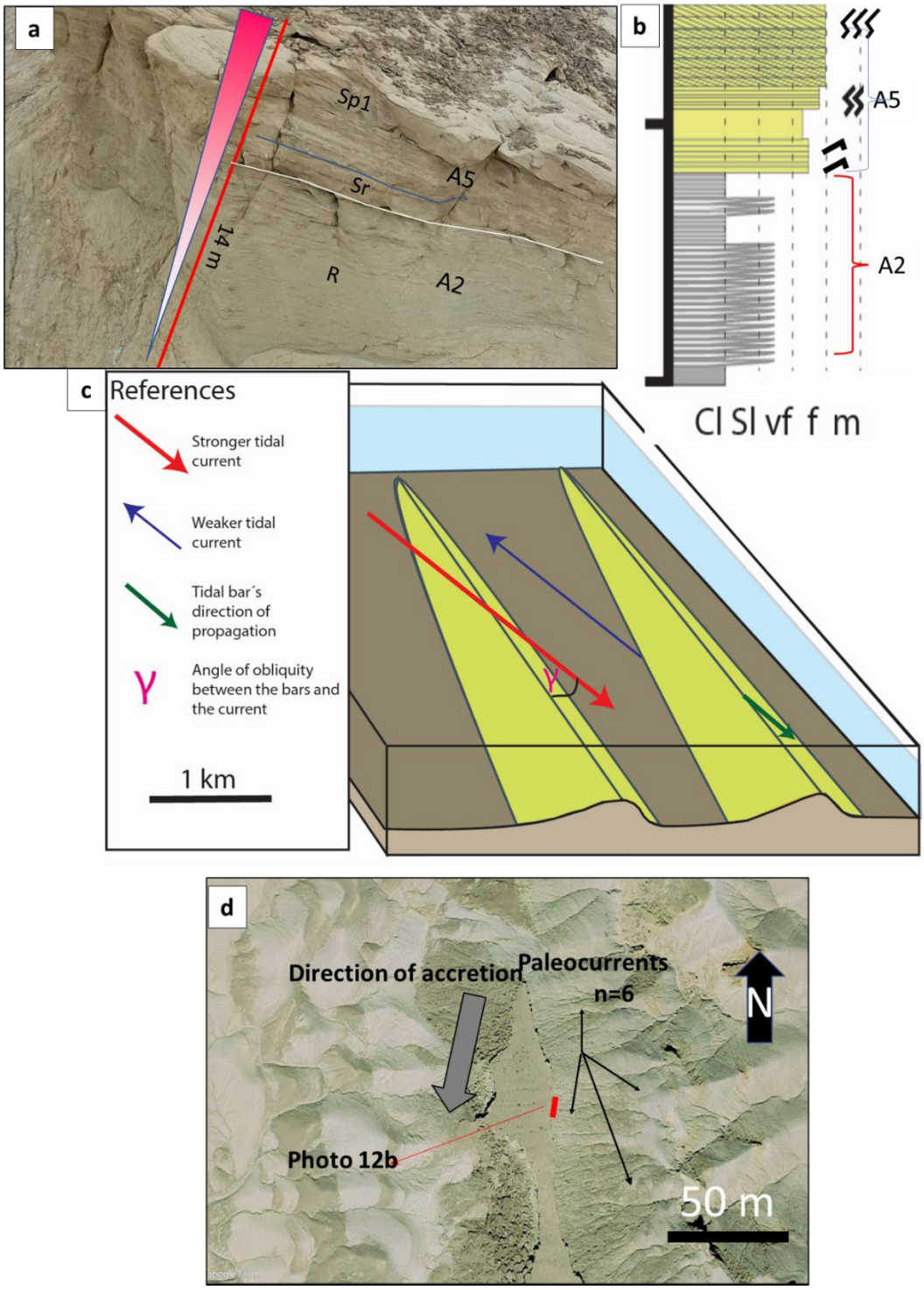

Figure 1.14. Association of Facies A5 (Coarsening upwards beds).

(a) Measure section of the coarsening upwards sequences interpreted as tidal bars, the association of facies A2 and A5 are marked in the figure. (b) Section measured on the outcrop showed on photo 1.14a (c) Theoretical model of the migration of tidal bars (modified from Stride et al., 1982, Olariu et al.,2012). In the model is shown that the direction of accretion of the tidal bars should be oblique to the direction of the flow. (d) Satellite image from the position of photo 12.b, which shows that the accretion direction of the beds may be oblique to most of the paleocurrents measured. This observation matches with the theoretical model of the tidal-bar geometry.

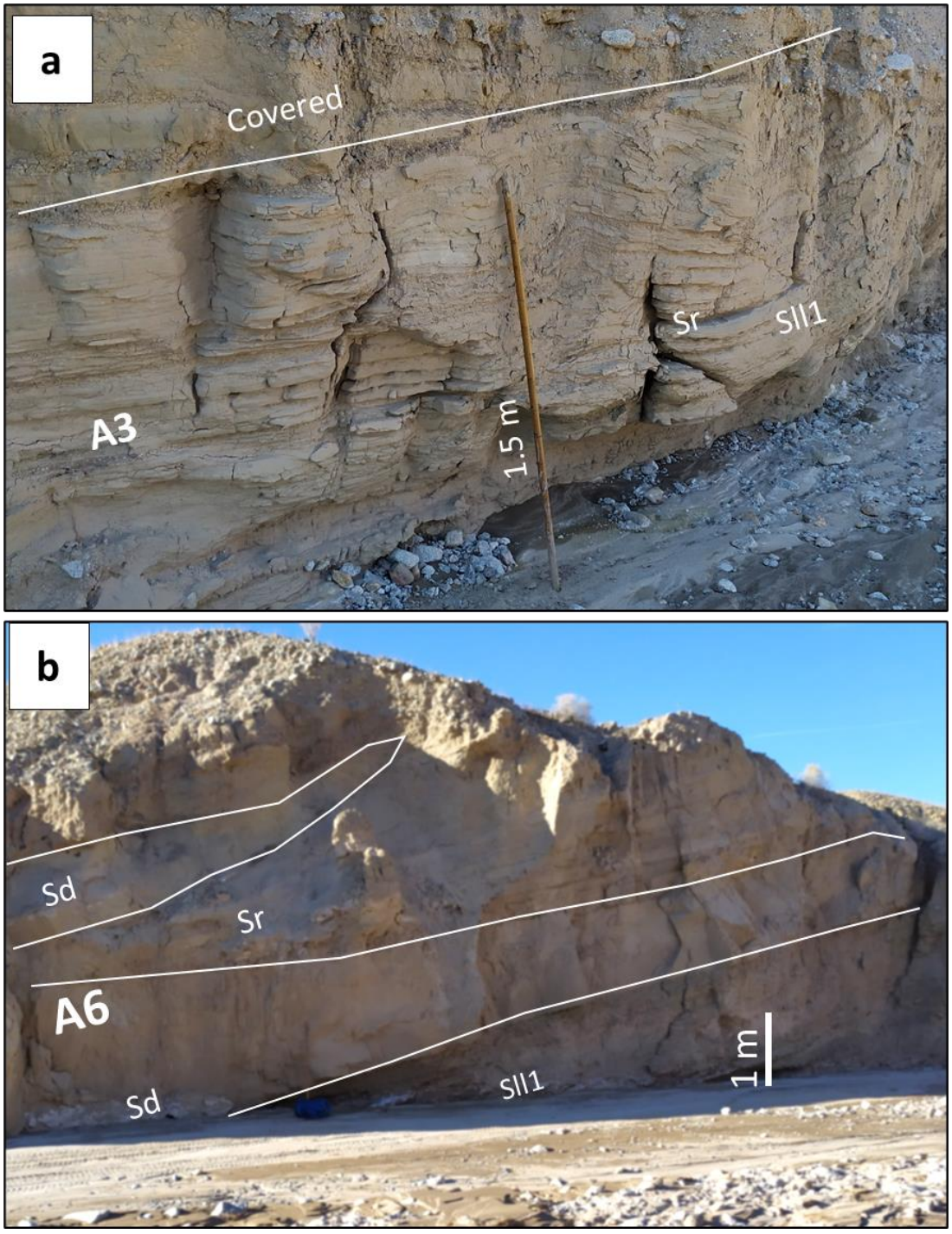

Figure 1.15. Association of Facies A3 (Laminated siltstones and Sandstones) and A6 (Sandstones with mud drapes).

(a) Tabular beds of laminated siltstone (Sll1) interbedded with laminated ripples sandstone (Sr), this section is interpreted as facies association A3 “laminated siltstones and sandstones”. (b) 1 to 2 m thick deformed sandstones (Sd) beds with lenticular geometry and sharp base. The bed's grades to sandstone with ripple lamination (Sr). This section is interpreted as facies association A6 “sandstones with mud drapes”.

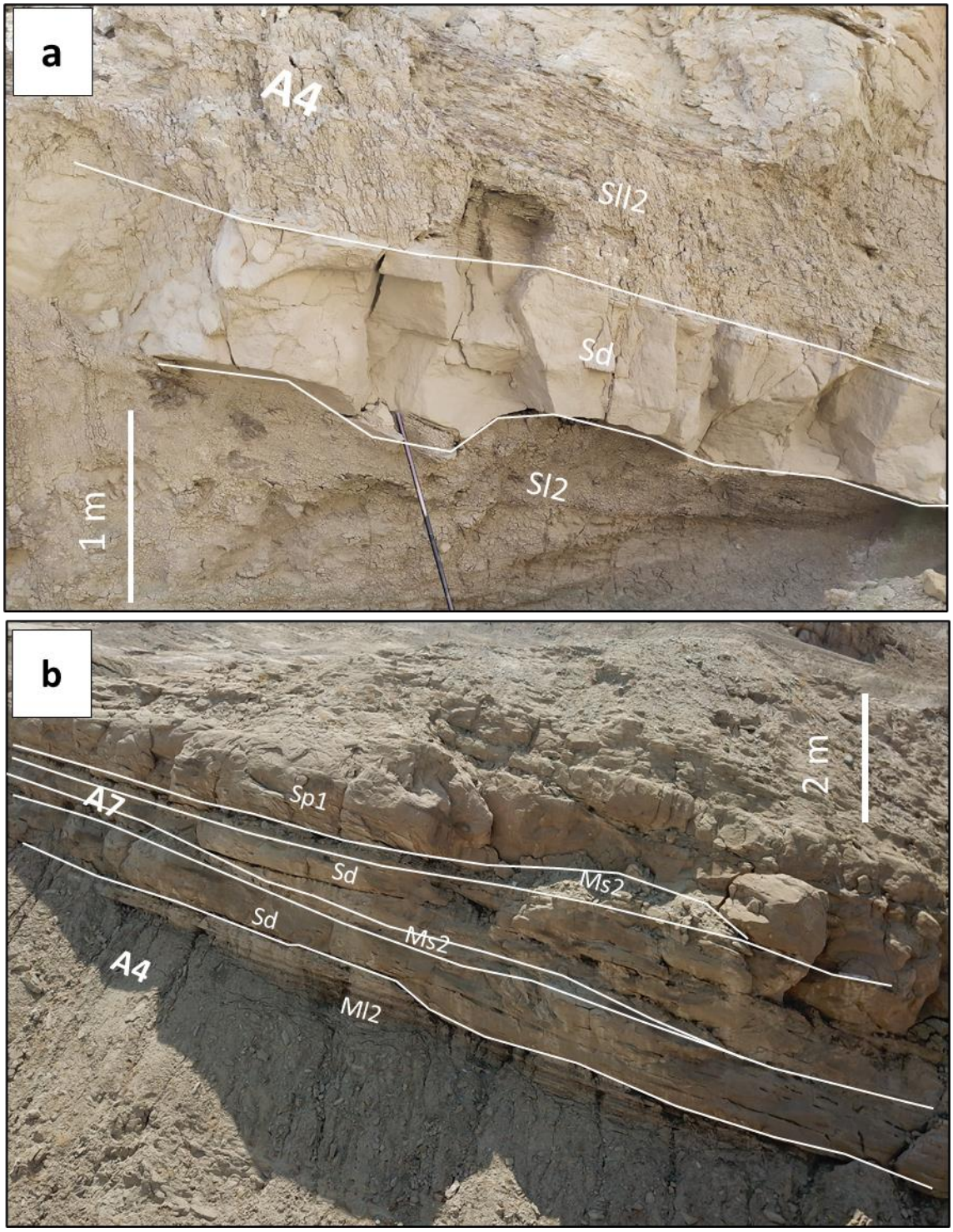

Figure 1.16. Association of Facies A4(laminated siltstones with petrified woods) and A7 (sandstones with shells and petrified wood).

(a) 1 m thick lenticular sandstone bed with erosive base encased within thin (cm) bedded reddish siltstone. This section is interpreted as facies association A4 "*laminated siltstones with petrified woods*". (b) Deformed (Sd) and cross-bedded (Sp1) sandstone with erosive base (lateral amalgamation) and lenticular geometry, interbedded with thin reddish laminated mudstone. This section is interpreted as facies association A7 "sandstones with shells and petrified wood"

Association of Facies	*Code*	*Description*	*Figures*	*Depositional environment*
Mudstones	**A1**	10 to 40 m thick of mostly structureless mudstones (*Ms*). Interbedded with cm ***Sr***. Bioturbation is moderate to intense, vertical burrows.	1.13	**Mud belts**
Rhythmitic beds	**A2**	Meters to tens of meters thick of rhythmites (***R***). Mostly tabular in shape and are laterally continuous for km.	1.13,1.14a,b	**ProDelta to Delta front**
Laminated siltstones and sandstones	**A3**	Meters to tens of meters ***Ml*** and ***Sll1*** interbedded with ***Sr***, ***Sw,*** and ***Sb***. Bioturbation is common, intense to moderate, and diverse.	1.15a	**Proximal subaqueous platform**
Laminated siltstones with petrified woods	**A4**	Meter to tens of meters thick of reddish ***Ml2***, ***Sll2***, ***Sr,*** and ***Sb***, with shells and petrified wood fragments. Tabular, and occasionally erosive base.	1.16a	**Tidal flats**
Coarsening upwards beds	**A5**	Coarsening upwards intervals of 2 to 10 m thick. First ***Sll1***, ***Sr***, ***Sw***, ***Ssh,*** and ***Sh***, then multiple sets of ***Sp1*** and finally1 to 3-meter-thick of ***C***, sometimes top by 10 to 30 cm of ***Sb***. Can be followed for km. Accretion surface oblique to the paleo flow direction discontinuous after tens of meters.	1.13,1.14	**Tidal Bars**
Sandstones with mud drapes	**A6**	0.5 to 5 meters thick, sets of ***Sd***, ***Spf***, ***Sl,*** and ***Ssh***. Erosional base with mudclasts and pebbles. Fining upward arrangement. Mud drapes are frequent. Deposits of ***Shm*** are sometimes interbedded within the cycles.	1.15b	**Tidal Channels**
Sandstones with shells and petrified wood	**A7**	Meter to 5 meters thick, made of sets of ***Sd***, ***Spf,*** and ***Spc***. Erosional base with mudclasts, shells, and pebbles. Finning upward arrangement. Multiple reactivation surfaces. Shells and petrified wood fragments are common.	1.16b	**Delta distributary channels**

Table.2. Summary of the interpreted Facies Associations.

The Broader Deltaic Environments

The facies association interpretations shown above are integrated into a model of the Deguynos Formation as subaerial and subaqueous Delta lobes, combined within a compound clinoform. A somewhat similar interpretation was suggested by Winker (1987), who argued that the Yuha and Camel Head were unusually thick compared to what was displayed in most other Deltaic sequences and suggested that the Delta front may have been considerably detached from the shoreline and nonmarine part of the Delta. Winker (1987) broadly suggested that the description of Nittrouer et al. (1986) on the continental shelf offshore from the Amazon River mouth could be an analog to the Deguynos Formation.

Although the extremely dry conditions in the Sonora desert allow us to have excellent access to the outcrops, the roughly 1.5 km wide research area makes it hard to identify directly the conformal geometry. The reason for the lack of direct observation of the geometry might be the relative fine (muddy) grain size of the proDelta and distal Delta front deposits that form subaqueous clinoform that likely attenuated (flatten) the geometry during burial and compaction. In addition, if we take the gradient measured in the modern Colorado River Delta as a reference, the shoreline clinoform will have 0.05°, the subaqueous platform 0.02°, and the much steeper subaqueous clinoform 0.50°. This will show a topographical drop in an uncompacted sequence of 1.31 m for the shoreline clinoform, 0.51 m for the subaqueous platform, and 13.1 m for the subaqueous clinoform along the extension of our study area parallel to the direction of progradation of the paleo-Colorado Delta (1.8 km). Though 13 meters is a thickness drop that it may be possible to measure, the muddy character of the subaqueous foresets makes it difficult to see internal geometries.

Our strategy to determine the presence of a compound clinoform morphology is not to directly measure the presence of clinoforms but to recognize the facies trends build by progradation. From other studies (e.g. Patruno et al., 2018 or Peng et al., 2020) we know that compound Delta clinoforms preserve two upward coarsening trends overlay one over the other, with the coarser grain sediments display at the proximity of the rollover point of each clinoforms (figure 1.17).

The facies associations A1 and A2 represent most of the deposits interpreted as foresets and bottomsets of the subaqueous clinoforms (figures 1.17, 1.18, 1.19, and 1.20). Peng et al. (2020) characterized this part of the subaqueous clinoform muddy foresets as having scours, rhythmites, and inclined heterolytic. The A1 muddy sequences, with their thick, mudstone beds are formed in the lower, more distal part of the subaqueous clinoform (bottomset). A2 rhythmites are interpreted as a transition to the outer subaqueous platform deposits. These intervals would have formed in seaward-dipping foresets (0.5°) of the subaqueous Delta, where deposition of clayey-silts and silty-sands occurred from intermittent hyperpycnal flows and suspension fallout (see analogies from Waresak, 2014; Hampson and Premwichein, 2017), and the lower and middle portion of the first coarsening upward trend associated to the progradation of the subaqueous clinoform (figure 1.17).

The facies association A5 (38%) and A3 (36%); and to a lesser degree facies association A1 (14%) and A6 (12%) formed in the upper part of the subaqueous clinoform (topset) and the subaqueous platform (figures 1.17, 1.18, 1.19, 1.20). The coarsening upwards sequences of facies association A5 interpreted as tidal bars imply a steady increase of by-passing current energy, similar to what was described by Peng et al., (2020) for the roll-over of one of the paleo-Orinoco subaqueous clinoforms. The heavily cemented and reworked surfaces which usually capped facies association A5 can be linked with the bypass surface described by Hampson and Premwichein (2017), as a representation of the

subaqueous platform, where the high energy of the shallow marine processes form multiple erosional surfaces. The thick mudstone beds of A1 are low energy deposits associated with the infill of the gullies in places near the outer edge of the platform, similar to the erosional morphologies in the subaqueous platform of the modern Colorado Delta (interpreted as tidal channels) that are filled by clays and silts (Van Andel, 1964; Thompson, 1968). The onset of facies association A5 also indicates the topset of the subaqueous clinoform, and hence the upper portion of the first coarsening upward trend (figure 1.17). The A3 intervals are mostly represented by silty and heterolithic laminated sequences with abundant mud drapes, which suggest a significant influence of tidal processes (Terwindt, 1988; Dalrymple & Choi, 2007; Van den Berg et al., 2007; Longhitano et al., 2012, Rossi et al., 2019). These intervals have intense and diverse bioturbation, implying a marine environment with normal salinity. Peng et al (2020) interpreted similar deposits as the inner subaqueous platform, where the shallow marine processes are still prevalent, but the energy in the system is reduced significantly in comparison with the outer platform. A6 facies association, interpreted partly as tidal channels on the outer Delta plain, is commonly related to A3 and extending subaqueously to associate with A5. A6 is formed by multi-episodic lenticular beds with common mud drapes. In the modern Colorado Delta, 10 s m wide and km long tidal channels extend from the upper shoreline clinoform to the subaqueous platform (figure 1.6), therefore the A6 facies association is interpreted as related both to the subaqueous platform and the shoreline clinoform. Facies association A3 and A6 indicate the lower portion of the second coarsening upward trend related to the progradation of the shoreline clinoform. Consequently, both the topset of the subaqueous clinoform (upper portion of the first coarsening upward trend) and the bottomset of the shoreline clinoform (lower portion of the second coarsening upward trend) are grouped into the subaqueous platform (figure 1.17).

Facies associations A7 (40%) and innermost A6 (36%), and to a lesser extent A4 (13%) and A3 (11%) (figures 1.17, 1.18, 1.19, 1.20) are the main deposits forming the shoreline clinoform (see also Peng et al., 2020). Facies association A7 represents channels with tidal facies and fluvial derived wood fragments and are therefore interpreted as fluvio-Deltaic distributary channels. These channels are interbedded with red laminated mud (A4) with frequent occurrences of wood fragments and only minor bioturbation. These are interpreted as tidal flat deposits in a brackish setting or in supratidal flats like the ones that are described by Thompson (1968) in the modern Colorado Delta. Facies association A6 deposits associated with this environment, are interpreted as the intertidal reaches of the Delta-plain tidal channels, as it has been recognized in the modern Colorado River (figures 1.6a, 1.6c). Facies association A3 is interpreted as mud banks formed in lower energy areas near these tidal channels in the lower subtidal to the intertidal zone. Facies association A4 and A7 indicate the upper portion of the second coarsening upward trend related to the progradation of the shoreline clinoform. The Deguynos Formation measured sections with their interpretation are displayed in figures 1.18, 1.19, and 1.20.

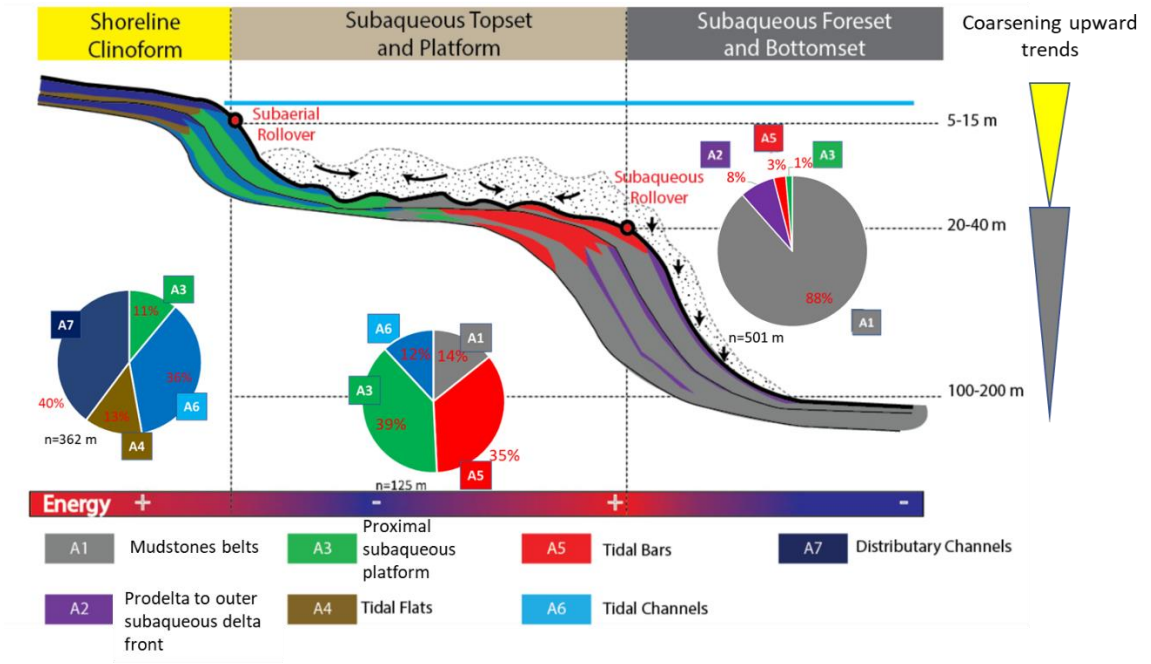

Figure 1.17. A 2-D diagram of a compound clinoform (Modified from Peng et al., 2020) indicating the percentages of facies associations for each depositional sub-environment.

The figure shows the composition and lateral variation of the three broader environments described for the Deguynos Formation. The proportion of the association of facies measured in each environment is shown in a pie chart (n is the number of m measured per environment). The Subaqueous Foreset and Bottomset are the thicker of the broader environments, and consist of mostly mudstones and outer Delta front deposits, with rare coarser material, and encompassed the lower portion of the first coarsening upward trend. The Subaqueous Topset and Platform preserved usually thinner deposits due to the common bypass and reworks of the sediments by the shallow marine processes. The coarser portion of the deposits (Tidal Bars and Tidal Channels) tends to be found in the limits of the environment, near both rollover points, due to the increase of energy-related to them. The finer deposits (mud belts, and mud and silt banks) then are focused in the center of this area, where the energy of the system is lower, and comprised the upper portion of the first trend and lower portion of the second. Finally, the Shoreline Clinoform is made mostly of coarse deposits delivered by Tidal Channels and Distributary channels alternating with thinner intervals of fine deposits (Tidal flats and Mud and Silt banks) and covered the upper portion of the second coarsening upward trend.

2-D Architectural Panel, R-T Sequences, and Sequence Sets:

The measured vertical sections through the Pliocene paleo-Colorado Delta system were correlated so that architectural changes along the outcrop and repeated vertical stacking and cyclicity could be identified. A 2-D architectural panel was built using the surface topographic ridges to aid in the correlation (figures 1.5, 1.21). At least 22 regressive-transgressive (R-T) sequences were identified in the stratigraphy, and these were further grouped into 4 sequence sets. The R-T sequences were defined using the maximum flooding surfaces, and the sequence sets were defined by identifying changes in thickness and trends up through the R-T sequences (figure 1.21b).

Sequence Set 1 is formed by the lower Yuha Member deposits and contains at least 6 R-T sequences (average thickness 30 m) which oscillate between the lower subaqueous foreset, the upper subaqueous foreset, and the subaqueous platform, and were dominated by shallow marine processes. In this sequence set, the muddy lower subaqueous foreset deposits are more frequent. The thickness of the stacking cycles decreases upward, as there is an increase in the thickness of the more proximal facies in each cycle upwards.

Sequence set 2 consists of the 7 R-T sequences (average thickness 18 m) of the upper-middle to upper Yuha Member and, as in Sequence set 1, shows intercalations between the lower subaqueous clinoform, the upper subaqueous clinoform, and the subaqueous platform that were dominated by shallow marine processes. In this sequence set, deposits of the upper subaqueous foreset and subaqueous platform deposits are more frequent. The same pattern as in sequence set 1 is repeated (decrease in the thickness of the sequences in parallel with an increase in the thickness of the more proximal facies).

Sequence set 3 is comprised of 4 R-T sequences (average thickness 32 m) and occupies the uppermost part of the Yuha and lower Camel Head Member. In this sequence

set, we have a transition between shallow marine and fluvial processes, and all the environments inside a compound clinoform are preserved. There is a decrease in the thickness of the sequence (from 45 to 25 m) toward the south.

Sequence set 4 is located on the upper part of the Camel Head Member and is formed by 5 R-T sequences (average thickness 23 m). In this sequence set, fluvial processes have more prominence. Its cycles involve an alternation of deposits associated with the inner subaqueous platform and shoreline clinoforms. These beds and cycles are highly amalgamated and reworked, making it harder to correlate them laterally. There is a notable increase in the thickness (from 15 to 30 m North to South) of the deposits basinward (towards the south). Some sequences seem too thin towards the north.

The paleocurrents in the outcrop are mainly toward the south, thus it was of interest and was expected to see changes southwards due to the proximal position of the North Fork log (figure 1.5 and 1.21). These changes are noticeable in sequences sets 1 (sequences 5 and 6), 2 (sequences 9, 12, and 13), and 3 (sequences 14 and 15), where it is possible to follow the change toward more distal environments and the progradation of the clinoforms toward the south. For sequence set 4, it is harder to identify a clear progradation of environments due to the prominence of the deposits associated with the shoreline clinoforms.

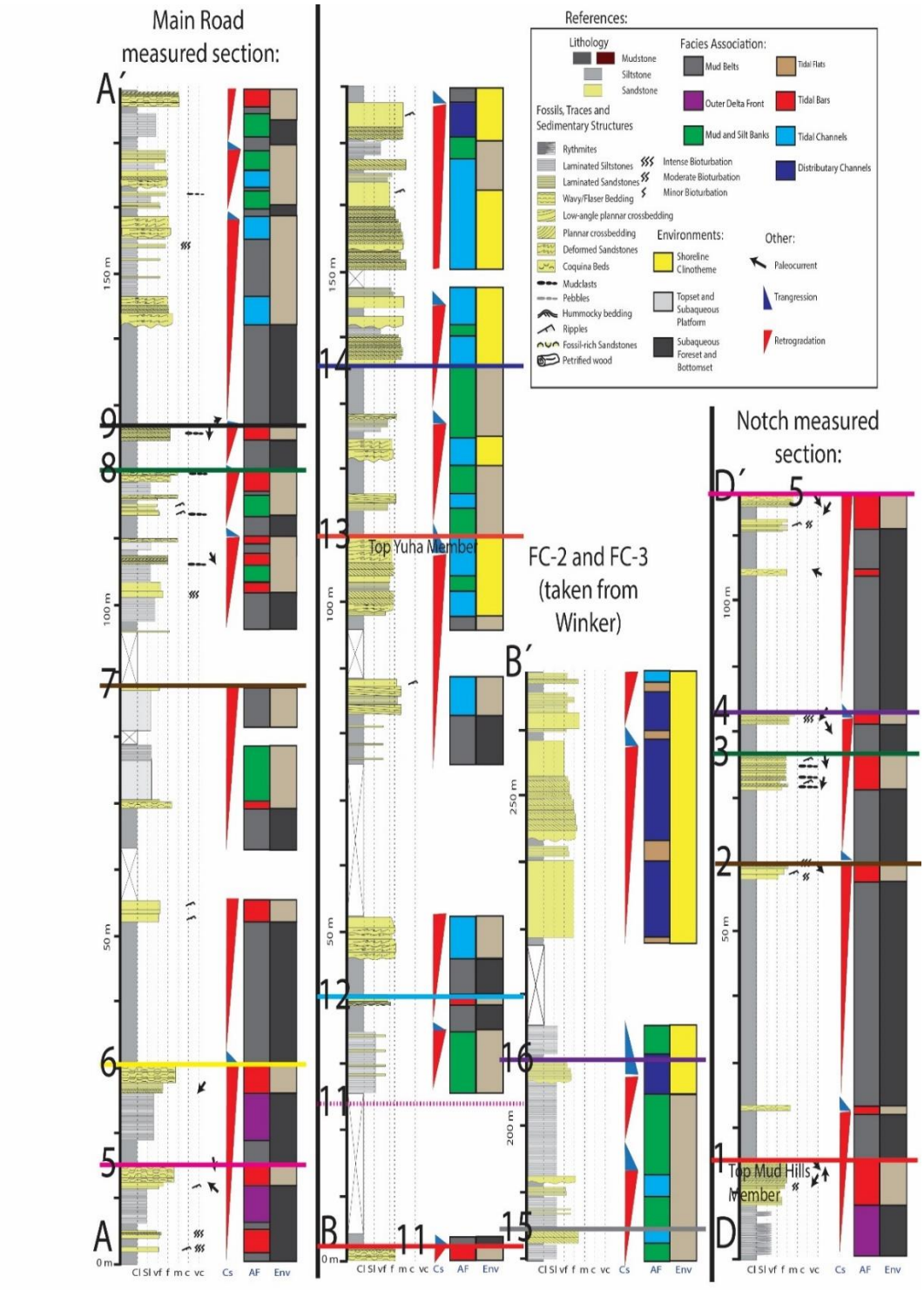

Figure 1.18. Main Road (A-A´), FC-2/FC-3(B-B´), and Notch(D-D´) measure sections, with the references for the measured sections.

The sections include the correlated ridges (colored line with numbers) shown on the map figures 1.5 and 1.13. . It also contains interpreted regressive-transgressive cycles inferred from the change in facies association.

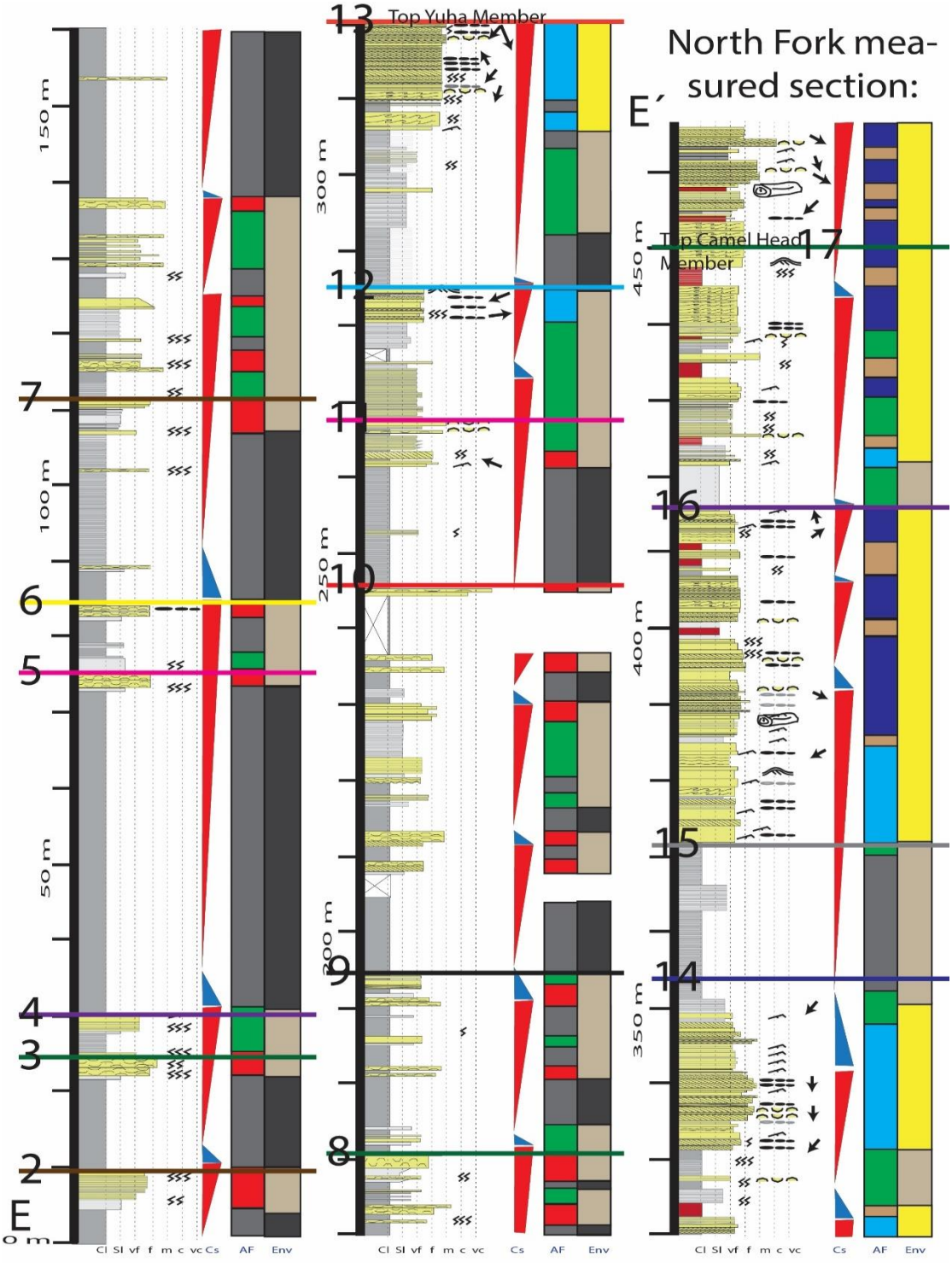

Figure 1.19. North Fork (E-E´) measure sections.

The sections include the correlated ridges (colored line with numbers) shown on the map figures 1.5 and 1.13. . It also contains interpreted regressive-transgressive cycles inferred from the change in facies association.

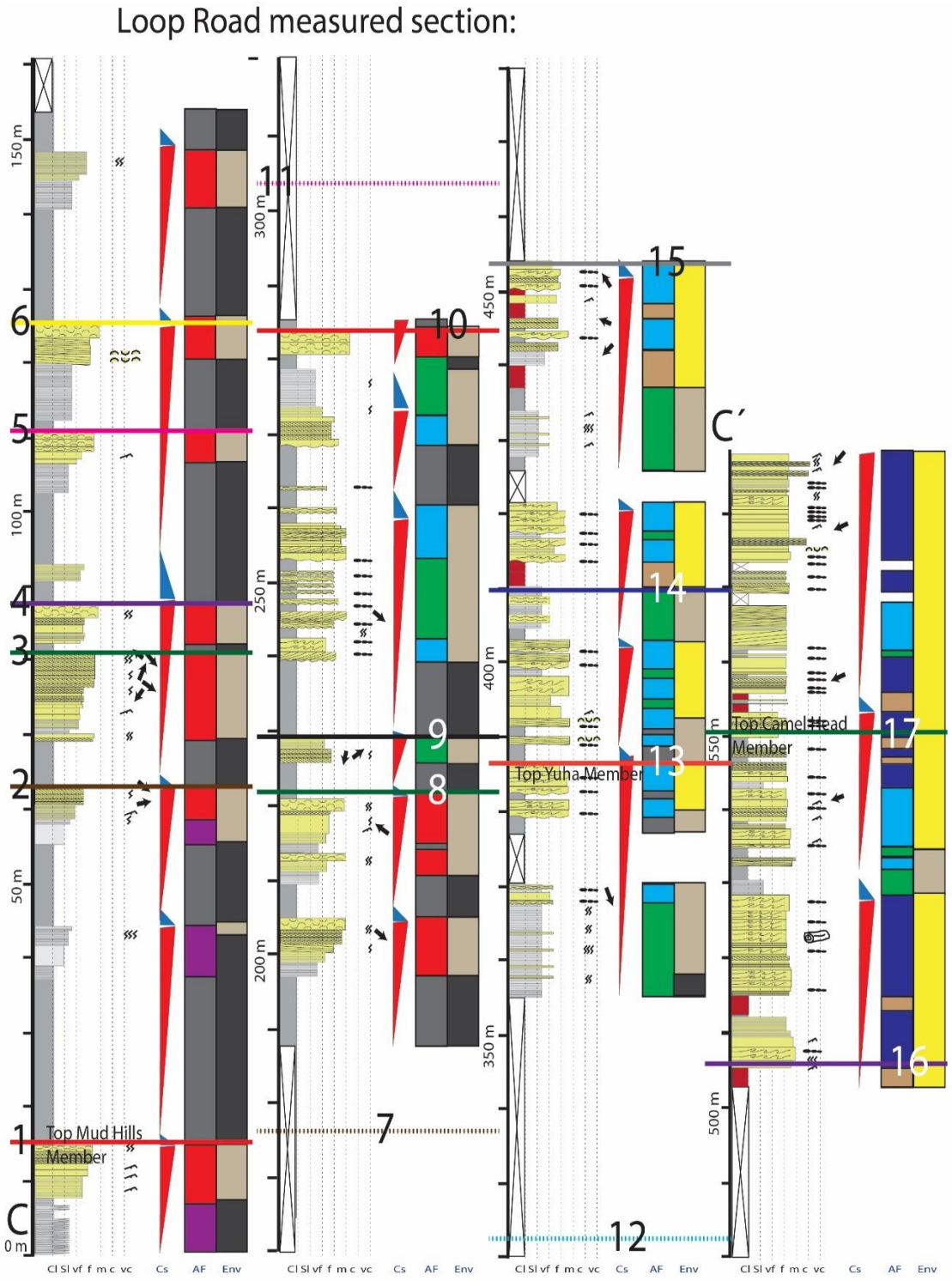

Figure 1.20. Loop Road (C-C´) measure sections.

The sections include the correlated ridges (colored line with numbers) shown on the map figures 1.5 and 1.13. It also contains interpreted regressive-transgressive cycles inferred from the change in facies association.

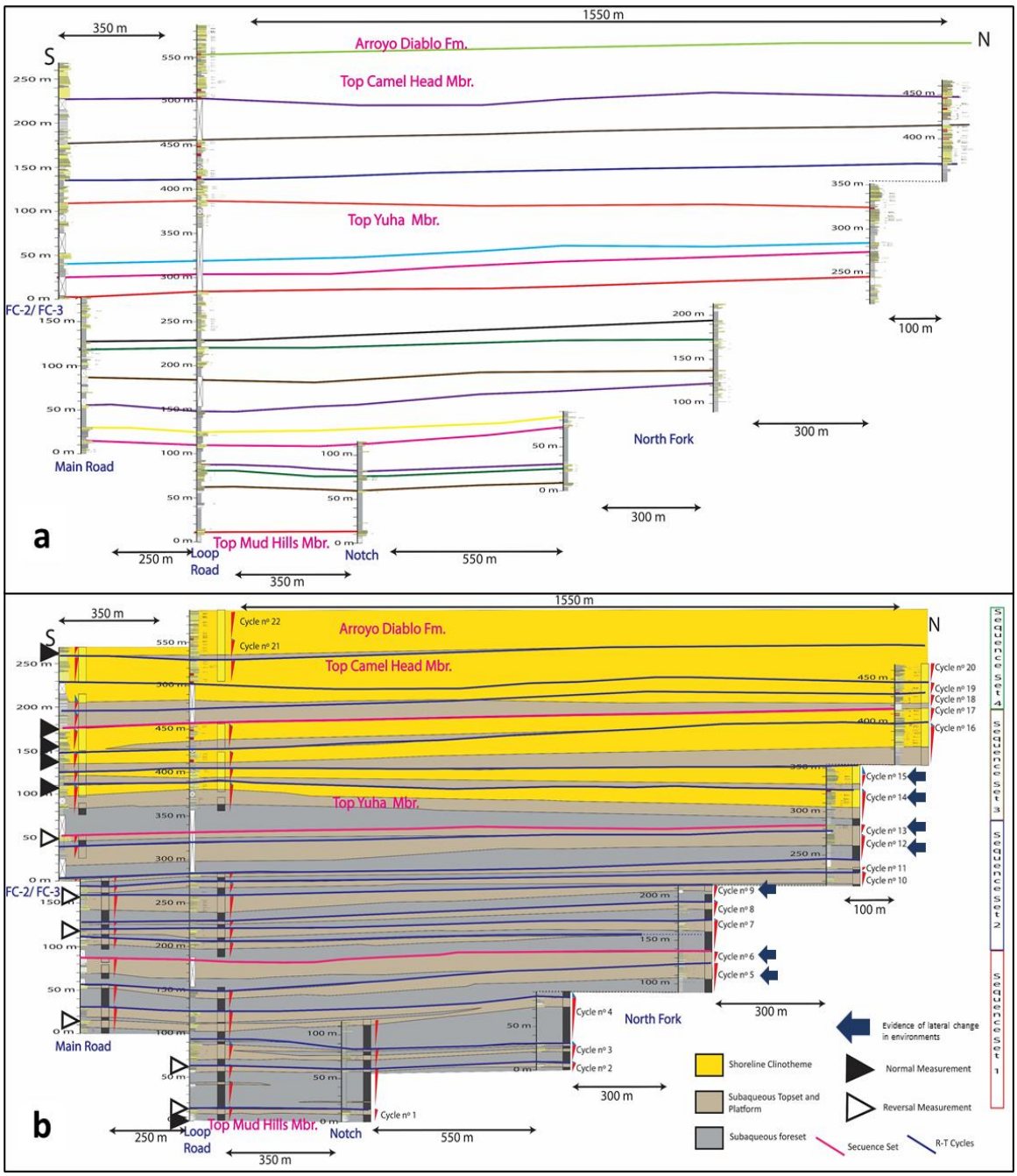

Figure 1.21. Close to depositional dip architectural panel.

(a) Correlation of the measured sections also aided by the field and aerial photography mapping (for measured sections location see figure 1.5; for a detailed measure, sections see figures 1.17, 1.18, 1.19) with the 17 correlated ridges. (b) Correlation of the measure sections with the environmental interpretation. The section also contains R-T sequences (blue lines) and sequence sets (pink lines) interpretation and the position of magnetic polarity measurements (in black and gray) from Opdyke et al, (1977) and Dorsey et al. (2011). Also, we indicate the southward progradation of clinoforms based on the overall orientation of the paleocurrent measurements.

Age of Deguynos Formation

The age of the deposits in the Deguynos Formation was established by magnetostratigraphic analyses made by Opdyke et al, (1977) and Dorsey et al. (2007; 2011) (figure 1.22). Dorsey used as correlation fixed points the reversals of 2 tuff beds in the Olla Formation and the estimated date of arrival of the Colorado River to the basin (5.3 Ma). The Yuha is almost completely contained within one of the reversals measured (figures 1.21.b, 1.22.a), which allows us to calculate an approximate sediment accumulation rate for the study area and speculate about the origin of the two-time scales of cyclicity exhibit on the outcrops. However, the age of the deposits of the Deguynos Formation is still debated after a recently published paper by Crow et al 2021, where it is proposed that the Colorado River arrived at the Fish Creek-Vallecito Basin at least half a million years later than earlier suggested by Dorsey et al (2011). This adjustment in the age of arrival of the Colorado River to the basin may change some of the assumptions earlier made about the basin. Crow et al., 2021 attribute this change to previously un-noticed major strands of the Earthquake Valley fault zone in the >5 km stratigraphic section (Janecke et al., 2016), which may have duplicated polarity intervals. The changes in dates (Crow et al., 2021) decrease the number of reversals to be correlated between this interval from five to three (figure 1.4).

We measured the Yuha and Camel Head intervals at four different locations, and found them undeformed, noticing only minor faults with no repetition of the stratigraphic section. It is still a possibility that we missed some faults in the areas with the most covered outcrops in the upper Yuha Member and the lower Camel Head Member in the southern portion of the study area. Nevertheless, we believe that the reversed magnetic interval recorded into the Yuha Member deposits is valid, and we will argue which of the three intervals should be the best fit for Yuha Member.

The thickness measured for the reversed interval is approximately 350 meters using as reference the Loop Road Log. The average thickness measured for the R-T sequences is 25 and for the Sequence, sets are 122 m (table 3). The three possible reversal intervals to be fit into the Yuha Member interval are C3n.1r (190 kyr), C2Ar (590kyr), and C2An.2r (120 kyr) (table 3). Therefore, depending on which interval we choose for the Yuha Member reversal, our average accommodation rate (by dividing the total thickness by total time) could change from 0.59 to 2.92 mm/yr (Table 3).

Polarity Chron	Base (Ma)	Duration (kyr)	Acc. Rate (mm/yr)	R-T Sequences (kyr)	Sequences Sets (kyr)
C2An.2r (Mammoth)	3.21	120	2.92	8.47	41.94
C2Ar (Gilbert)	3.6	590	0.59	41.66	206.22
C3n.1r	4.3	190	1.84	13.42	66.41

Table 3. Calculation of accumulation rate and estimate the duration of the R-T sequences and Sequence Sets according to the Polarity Chron interval, from the geomagnetic polarity time scale (GPTS) (Ogg, 2012; Channell et al., 2020), we choose the reverse interval identified by Opdyke, (1977) and Dorsey et al. (2007; 2011).

As an approach to determine which of the three possible accommodation rates is the correct one, we calculate the accommodation rate for all intervals between Wind Caves

Member and Tapiado Formation in each of the three options (figure 1.22.b, table 4). For this calculation, we used the thicknesses determined by Dorsey et al. (2011). Although some doubt about these thicknesses has been raised by Janecke et al. (2016) and Crow et al. (2021), there is no information available regarding the extension of the fault zone or the fault location, thus the only option available is to continue using the Dorsey et al (2011) ages. We also added to the plot (figure 1.22) the relative sea-level curve calculated by Miller et al, (2005, 2011), because the sea level controls the accommodation in the basin. Figure 1.22.b shows that the best match as a whole is option 3, which only has modest variations in sediment accumulation rate. Moreover, both option 1 and option 2 show large jumps in the accommodation rate which coincides with periods of steep decrease in the sea level. Thus, if we choose option 3, we could say that C3n.1r (190 kyr) will be the interval that it would fit Yuha Member (table 4). This assertion will leave the entire Camel Head Member fitting into one single normal paleomagnetic period (C3n.1n "Nunivak, 138 kyr), a proposal that may be proven with more work.

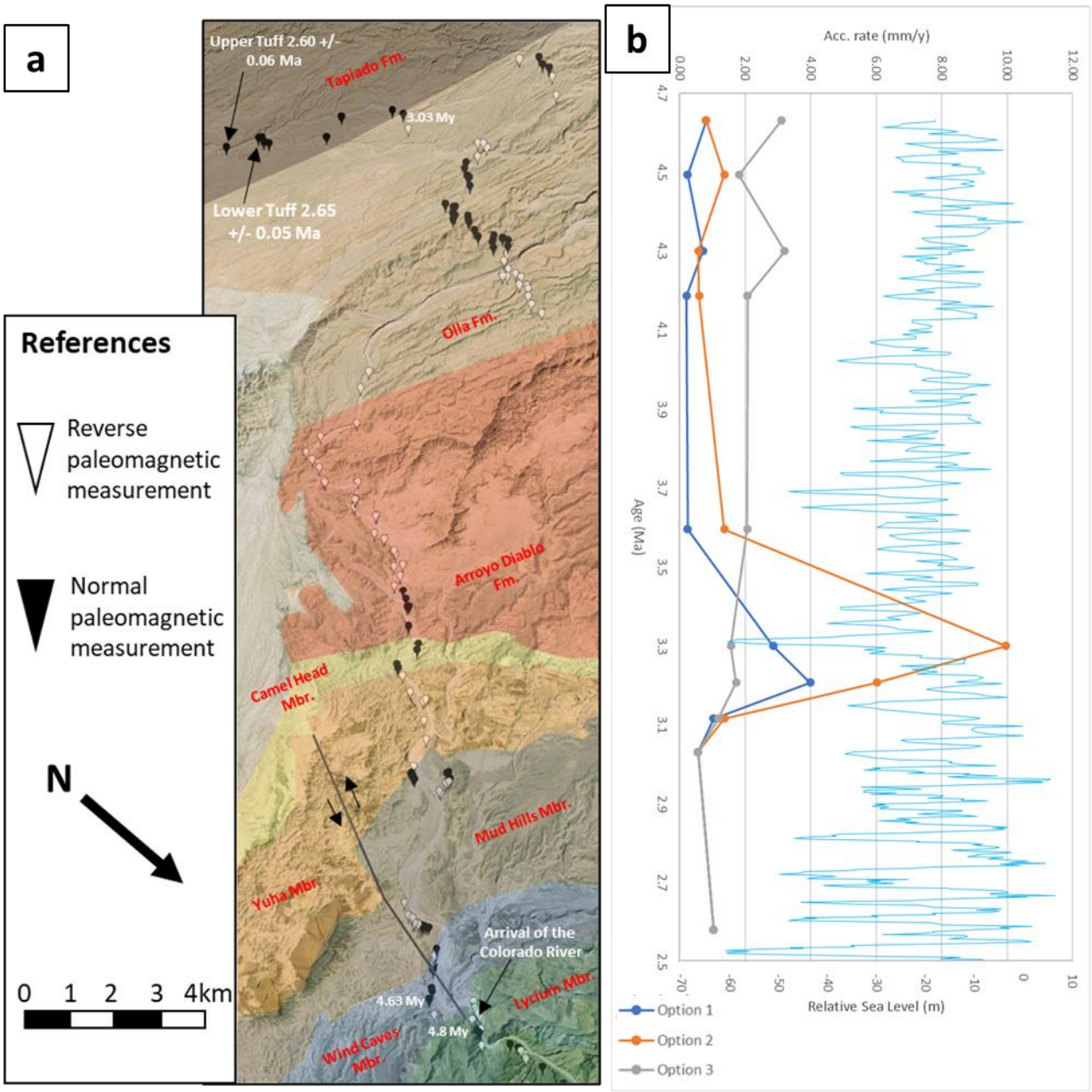

Figure 1.22. (a) Map of the Fish Creek-Vallecito Basin outcrops with unit names and paleomagnetic measurements (Opdyke et al.,1977; Dorsey et al.,2011). The interpretation of the dates of arrival of the Colorado River to the Fish Creek-Vallecito Basin (Crow et al., 2021) and the U-Pb results from the Tapiado Formation Dorsey et al. (2007;2011). (b) A plot of accommodation rate (mm/y) vs age (Ma) shows the three options stated in tables 3 and 4. Also,

it shows the relative sea-level curve calculated by Miller et al (2005,2011). The plot shows that the most robust option is the number 3 because it has modest variations and it doesn´t contradict the sea-level curve.

		Option 1			Option 2			Option 3		
Unit Name	**Thickness (m)**	**Polarity Chron**	**Base (Ma)**	**Acc. Rate (mm/yr)**	**Polarity Chron**	**Base (Ma)**	**Acc. Rate (mm/yr)**	**Polarity Chron**	**Base (Ma)**	**Acc. Rate (mm/yr)**
Hueso Fm.	102									
Tapiado Fm.	449.5	C2r.2r (Matuyama)	2.581	1.04	C2r.2r (Matuyama)	2.581	1.04	C2r.2r (Matuyama)	2.581	1.04
Olla Fm.	252.2	C2An.1n	3.032	0.56	C2An.1n	3.032	0.56	C2An.1n	3.032	0.56
	99.4	C2An.1r (Kaena)	3.116	1.04	C2An.1r (Kaena)	3.116	1.36	C2An.1r (Kaena)	3.116	1.18
	156.4							C2An.2n	3.207	1.72
	192.8							C2An.2r (Mammoth)	3.3	1.57
	547.4				C2An.2n	3.207	6.02	C2An.3n (Gauss)	3.596	2.06
Arroyo Diablo Fm.	1224.9				C2An.2r (Mammoth)	3.3	9.96	C2Ar	4.187	2.07
Camel Head Mbr	362	C2An.2n	3.207	3.98	C2An.3n (Gauss)	3.596	1.36	C3n.1n (Cochiti)	4.3	3.20
Yuha	448.9	C2An.2r (Mammoth)	3.3	3.65	C2Ar	4.187	0.76	C3n.1r	4.493	2.33
Mud Hills Mbr.	64	C2An.3n (Gauss)	3.596	0.24	C3n.1n (Cochiti)	4.3	0.57	C3n.2n (Nunivak)	4.631	3.10
	126	C2Ar	4.187	0.21	C3n.1r	4.493	1.36			
	80	C3n.1n (Cochiti)	4.3	0.71						
	46.5	C3n.1r	4.493	0.24						
Wind Caves Mbr.	112	C3n.2n (Nunivak)	4.631	**0.81**	C3n.2n (Nunivak)	4.631	**0.81**			

Table 4. Paleomagnetic intervals measured by Dorsey et al. (2011), with estimated thickness and polarity chron interval, fit following the geomagnetic polarity time scale (GPTS) (Ogg, 2012; Channell et al., 2020). Also, it is shown our three options for a fit of the reversal period display on figure 1.22.b.

Discussion:

The Analogy between Modern and Ancient Colorado Delta

The validity of the analogy between the modern and Pliocene Colorado Delta rests on the evidence of them being fed by the Colorado River, accumulating into a tectonically active, elongated basin, and on both Deltas exhibiting a dominance of tidal processes, although the water and sediment discharge were certainly greater in the ancient compared to the modern.

The paleo-Colorado River origin of the sediments in the Deguynos Formation has been proven by multiple studies (Winker, 1987; Dorsey et al., 2007, 2011). Winker (1987) described a "C" or "Colorado" Suite of Sandstones for the sediments of Imperial, Deguynos, and Palm Spring formations, where the difference in texture, color, and mineralogy separated them from the underlying sandstones (which he designated as "L" or "Local" Suite). The timing for the arrival of the Colorado River into the Gulf of California has recently been re-dated to 4.6 Ma (Crow et al., 2021).

The elongate and funnel-shaped configuration of the Gulf of California both protects from large ocean storm waves and produces a large tidal range with strong tidal currents in the Gulf of California. Tidal processes thus become the dominant shallow marine process impacting the Delta, though Riverine processes were also strong during the Pliocene Delta growth. During the Pliocene, the Gulf of California had a similar tectonic configuration (Stock & Hodges, 1989a; Oskin et al., 2001; Lizarralde et al., 2007; Darin et al., 2016), and so the Deltaic Yuha and Camel Head members also testify to the abundant evidence of tidal dominance, such as their heterolithic beds with wavy and flaser lamination (figures 1.10a, 1.10b), ripple cross-stratification with abundant mud drapes (figure 1.11d) and large sets of cross-bedded sandstones with bidirectional paleo flow

(figure 1.11c), as well as the characteristic cross-bedded sandstones and coquina beds within accretional bars in Yuha Member (figures 1.11f, 1.12b,1.12c,1.15). The final element of similarity between the two Deltaic systems is the compound character of the bathymetric clinoform of the two Delta systems, as demonstrated for the first time herein.

Regarding the first arrival of the Colorado River-derived sediment into the region, it should be noted that the Delta was not the first arrival. In front of the southward prograding Pliocene Delta, there was a deepwater, southward-accreting submarine slope (Mud Hills Formation) and at the base of this slope, there were one or more sand-rich submarine fans (Wind Caves Formation). These fan lobes contain the first-arrival Colorado grains (C-suite sandstones).

Preservation of the Subaqueous Platform in Deguynos Formation:

The subaqueous platform is the key environment to differentiate a compound clinoform from a simple clinoform, because it alters the geometry of the deposits (figure 1.1c) and allows the formation and progradation of two separate clinoforms (figure 1.1a) (e.g. Helland-Hansen and Hampson 2009; Patruno et al. 2018; Peng et al., 2018). A general equilibrium between the subaqueous and shoreline clinoforms is needed to form and maintain the subaqueous platform (Swenson et al.,2005). This is achieved by a balance between the shallow marine tidal and wave processes on the shelf and the sediment discharged (figure 1.1b) by the River and tidal channels (Swenson et al., 2005). At the Yuha and Camel Head members, the subaqueous platform is preserved in the form of the topset of the subaqueous Delta. To understand the origin and preservation of platform deposits, it is necessary to examine the key sediment transport processes in this part of the double clinoform. In the case of both the Deguynos Formation and the modern Colorado Delta, the key roles are fulfilled by tidal channels (A6) and tidal bars (A5). Tidal channels, with the aid of River currents during floods, can bypass the subaqueous platform delivering

sediment right out to the platform edge (figures 1.6, 1.7). Otherwise, tidal bars migrate obliquely across the platform and accumulate sediment on the inclined Delta front (figure 1.15). Sediment accumulation during these activities causes the gradual aggradation of a sub-horizontal topset as well as transporting sand and mud sediment down onto the subaqueous Delta front. The eventual result is a thick flat-lying topset where the sand tends to decrease significantly out to the top of the subaqueous clinoform. The most fine-grained and heterolithic subaqueous Delta front sediments thickened to a maximum distally. This model is superficially like a textbook Delta, but the extensive subaqueous Delta removes the Delta-front rollover far (10s of km) from the shoreline (figure 1.23). Each sequence of topset channels or tidal bars becomes the topset coeval to a muddier Delta-front increment, and successive topset increments (each with coeval finer accreting Delta front) have a basinward rising trajectory as the subsiding subaqueous Delta builds forward. Each of these increments is capped by a "platform". This platform is a morphological surface that is repeated as the subaqueous Delta front progrades (figure 1.23).

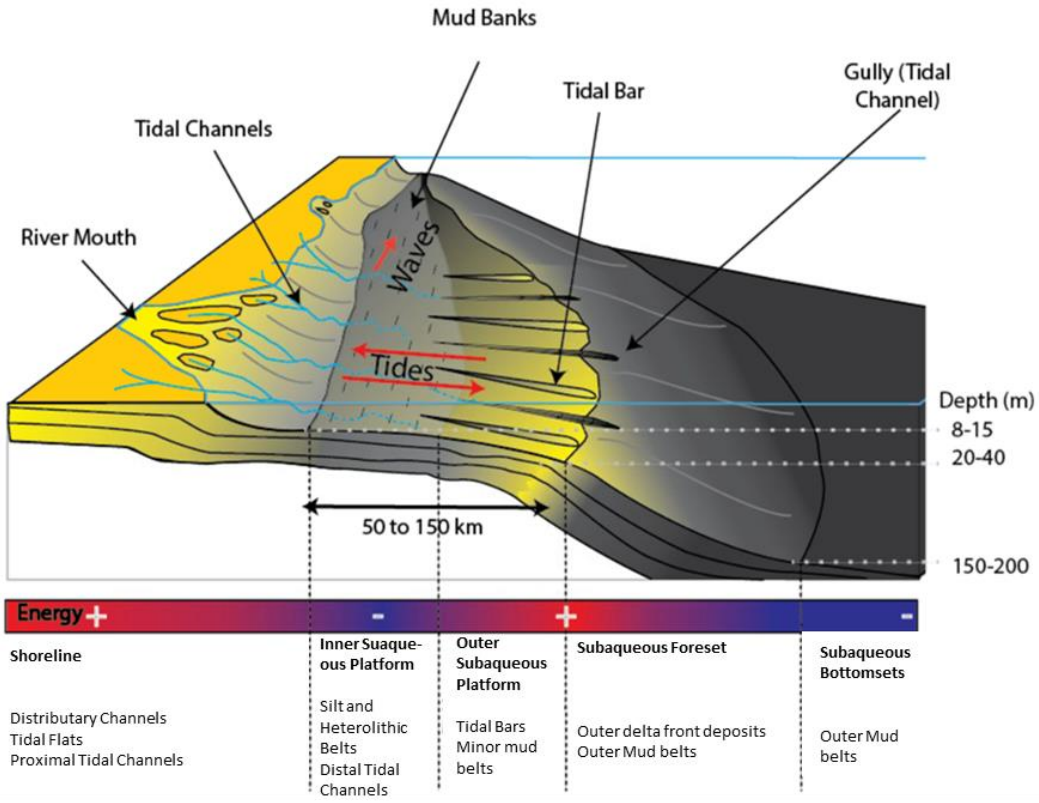

Figure 1.23. A 3D model of the compound clinoform morphology in a tidally dominated Delta, like the modern or ancient Colorado River Delta (see also Peng et al 2020). The figure shows the three components of the system (shoreline, subaqueous platform, and subaqueous Delta front) with their architectural elements. The distribution of energy of the system was based on the oceanographic sedimentation profile proposed by Fleming et al. (1933). In the lower part of the figure is added some characteristically deposits found in the Deguynos Formation that was interpreted as linked to the components of the compound clinoform.

Stratigraphic Cyclicity:

The implication of our interpretation of C3n.1r as the interval which fits with Yuha Member is that we can calculate the accumulation rates in table 3 for our unit and consider the possible origin of the cyclicity on the upper Deguynos Formation. To appreciate the

impact of eustatism in the cyclicity, we place the age equivalents of the Sequence and Sequence Sets into a plot with the relative sea-level curve of that period (figure 1.24). The intervals were placed using the thickness measured on the Notch and North Fork measure sections and the accommodation rate. From this plot, we learned that the R-T sequences are temporally too close to have been influenced significantly by changes in the sea level. However, the Sequence Sets position appears to be related to periods of relatively high sea level, which could suggest a higher accommodation rate and higher supply, due to an increase in precipitation linked to warmer weather.

Following the accommodation rate, the R-T sequences appear to have an approximate duration of 13+/-4 Kyr, a 5^{th} order time scale that can also correspond to an autogenic response such as Delta-lobe abandonment (caused by avulsion). Another evidence of a possible autogenic origin in the R-T sequences is the lateral changes in thickness for the same cycle (figure 1.21b). These changes would be related to avulsion, such as has been described for the Mekong River Delta in Nguyen et al. (2000).

For the sequence sets, the average timescale of the sequence sets is 66 Kyr, a 4^{th} order time scale which is close to the timespan of Milankovitch cycles, thus these sets may have a eustatic origin, especially as these deposits were of Pliocene age when the eustatic sea-level amplitudes were considerably high (Miller et al. 2005) and the comparison with the relative sea-level curve (figure 1.24).

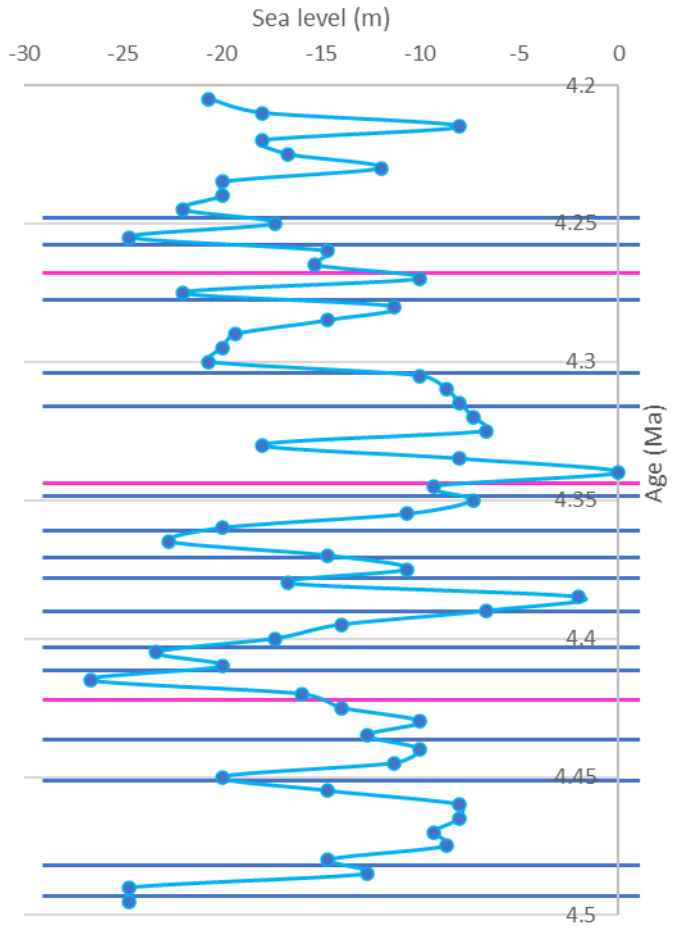

Figure 1.24. Relative Sea-level curve with the R-T sequences (blue) and Sequence Sets (pink). The position of the sequences was calculated using the calculated accommodation rate. The figure shows how the R-T Sequence is too close in time to be directly caused by a purely eustatic origin. However, most of the Sequence Sets happened during a relatively high sea level period (relative increase in accommodation space), supporting the eustatic origin hypothesis for these intervals.

Evolution of Yuha and Camel Head Members:

The sedimentation of the Yuha Member began ca. 4.49 Ma with progradation of the subaqueous foreset and subaqueous platform of the paleo-Colorado Delta into the Fish Creek Vallecito Basin (figure 1.25). During this period tidal bars were migrating across the platform toward the platform edge forming the coarsening upwards sequences (A5) distinctive of the lower and middle Yuha (sequence sets 1 and 2). At the edge of the platform, gullies were formed caused by the tidal currents. Hyperpycnal flows coming from the River mouth also moved through these tidal channels, leaving behind the characteristic rhythmites (A2) association, which usually preceded (were more distal to) the tidal bar deposits. Thick mudstone beds (A1) were deposited on the lower gentle slope of the subaqueous foreset and bottomset.

In the Upper Yuha and Lower Camel Head members (ca. 4.30 Ma) (sequence set 3), the shoreline clinoform prograded onto the subaqueous platform (figure 1.25). Tidal channel deposits (A6) became more frequent, while mud bank deposits (A3) were accumulated in the inner, low energy zone of the subaqueous platform.

Finally, in the upper Camel Head Member (ca 4.20 Ma) (sequence set 4), the shoreline clinoforms had completely prograded over the study area (figure 1.25). Distributary channels (A7), tidal channels (A6), and mudflat deposits (A4) are commonly found. The non-marine fluvial plain is related to the Arroyo Diablo Formation.

Although the 3 environments of the double clinoform were recognized in the Deguynos Formation., we do not see and would not expect to see a complete and continuous stack from subaqueous to subaerial clinoform environments in one sequence across the relatively short distance (2 km) of our outcrop “window” (Fig. 21b). If the conditions during the sedimentation of the Deguynos Formation. were similar to modern Colorado it would need 10s of km of the continuous outcrop to increase the chance of

outcrop capture/exposure of the complete double clinoform system in only one R-T sequence.

The Uniqueness of the Deguynos Formation:

Compound clinoforms has been described in other outcrops around the world (e.g. Sognefjord Formation, Jurassic offshore Norway, Patruno et al., 2015; Pliocene Paleo-Orinoco, Peng, et al., 2018; Triassic Shelf of Northern Pangea, Rossi, et al., 2019), in environments which had some mix between wave and tidal processes. However, Deguynos formation unique setting associated with the opening of the Gulf of California (Stock & Hodges, 1989b; Oskin et al., 2001; Lizarralde et al., 2007; Darin et al., 2016) allows it to be deposited in a tidal oceanographic setting forming tide-dominated environments with the marginal influence of wave-related processes. These conditions explain some of the particularities found on the deposits, such as the continuous cross-bedded coquina ridges interpreted as tidal bars (figure 1.15); the common cross-bedded sandstones with mud drapes (figure 1.11b); or the thick (10-30 m) mudstones beds in between of the ridges. Particularly, this last feature may have been also preserved due to the uncommonly high accommodation rate (1.84 m/ky) of the area during the lower Pliocene

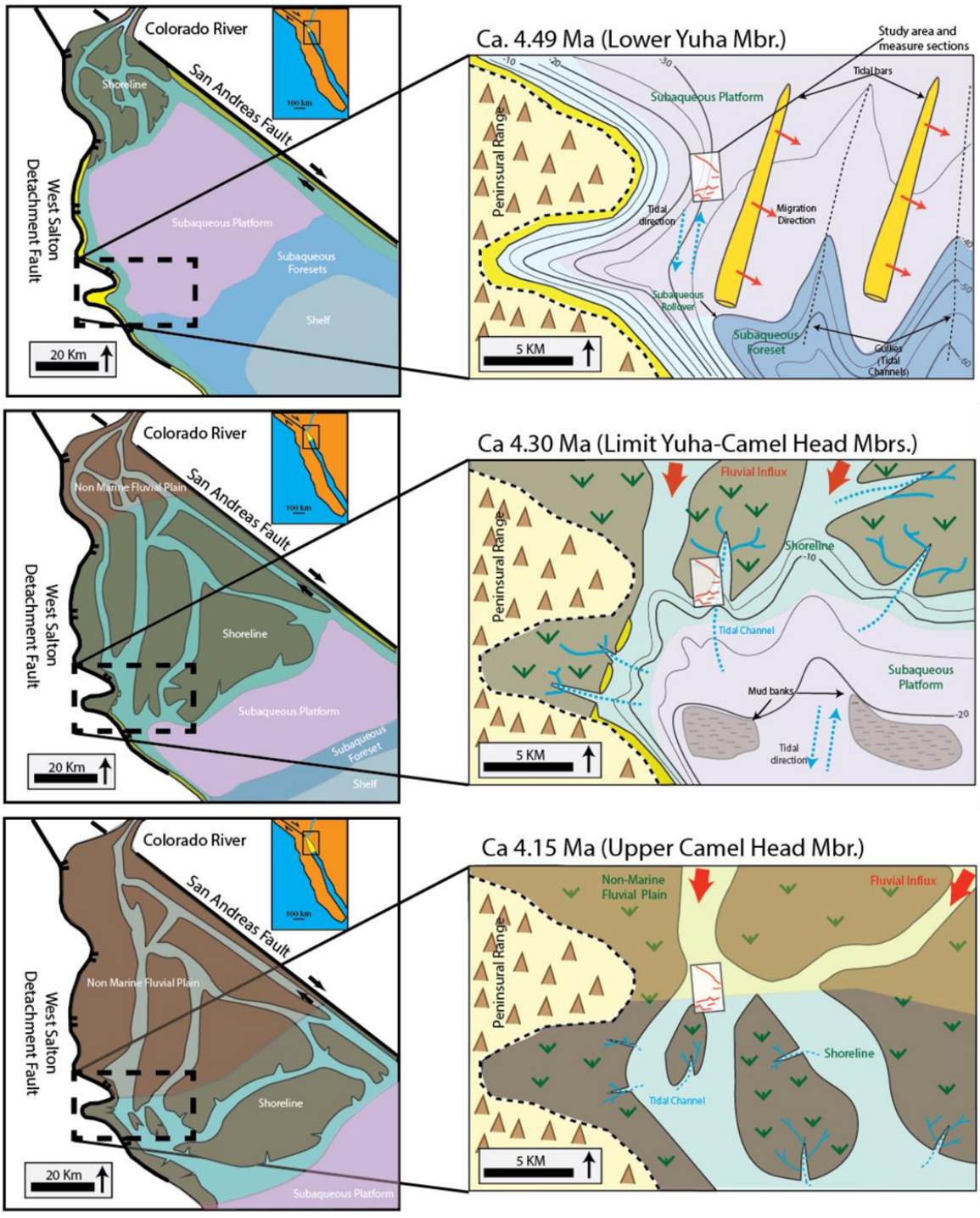

Figure 1.25. Paleogeographic reconstruction of the Salton Trough and surrounding regions at 4.49, 4.30, and 4.15 Ma.

The geometric reconstruction of the basin and the trace of the main faults (San Andreas and West Salton Detachment) were taken from Dorsey et al. (2011), Sharp (1967), and Janecke et al. (2010), and Cloos (2014). The area of study is represented in each figure by the dotted square. **a.** The 4.49 Ma reconstruction shows the environmental distribution during the sedimentation of the Lower Yuha. **b.** At 4.30 Ma (Upper Yuha/Lower Camel Head), the progradation of the Colorado River and Delta had driven the shoreline clinoforms into the study area. **c.** Ca 4.15 Ma, the Colorado purely fluvial deposits had entered the area of study (Upper Camel Head Member).

Conclusions:

- A compound clinoform has been recognized in the geomorphological/bathymetric profile of the modern Colorado Delta following the criteria proposed by Peng et al (2020). The shoreline, inner and outer subaqueous platform, and subaqueous foresets and bottomsets have been recognized using evidence such as bathymetry maps, morphology, gradient, and grain size. This morphology is a reflection of the balance of fluvial to basinal (mainly tidal) energy which existed before the construction of the dam projects along its catchment area.
- We based our interpretation of the Deguynos Formation on a hypothesis that it was analogous with the modern Colorado Delta. This interpretation rests on the evidence of the similar origin of the sediment facies and the dominance of tidal processes in both systems. Using this analogy, we interpreted the outcrops into three depositional environments from deep to shallow: subaqueous Delta foresets (A1-mud belts and A2-outer subaqueous Delta front), subaqueous platform (A5-tidal Bars, A6-tidal channels, and A3-heterolithic banks), and shoreline clinoform (A6-tidal channels, A7-Distributary channels, and A4-tidal flats).
- Twenty-two high-frequency regressive-transgressive (R-T) sequence and 4 sequence sets were described for Yuha and Camel Head Members. The stratigraphic sequences would be the 5th order time scale, related to autogenic shifting of Delta lobes with an average time of 13+/-4 Ky. The 4 sequence sets were explained as eustatic responses in the stratigraphy related to the Icehouse eustatic cycles which were becoming much higher amplitude in Pliocene times. The average timescale of the sequence sets is matching the scale of a 4th order cycle (66Kyr), which is in the timespan of Milankovitch cycles.

- The exceptional setting of the basin (strongly dominated by tidal processes and the uncommonly high accommodation rate) allowed to preserve the compound clinoform morphology formed during the progradation of ancient Colorado into the Fish Creek Vallecito basin of the Gulf of California during the early Pliocene.

Chapter 3

Modern Compound Clinoforms: Examples and Key variables

Introduction:

This chapter reviews the bathymetries of Deltas around the world, to better understand in which places and under which conditions we find compound clinoforms. Also, as the morphology of the subaerial part of the Delta is controlled by the dominance of tidal, wave, or fluvial processes (Galloway 1975; David and Hayes 1984; Hori et al 2002b), the morphology of the compound clinoform is heavily influenced by the prevalence of these processes (Peng et al 2020). In this review, we analyze the energy of the systems in which the compound clinoform is formed and how the components of the compound clinoform change with a differing mix of shallow marine processes and sediment influx. Finally, we are particularly interested in the subaqueous rollover depth, and the area of the subaqueous platform, and its relationship with the energy and sediment availability of each system.

Background:

River, Wave, and Tidal Dominated Deltas

Modern Deltas around the world show considerable variability in their morphology, prevalent lithology, dominant processes, and response to external forces. To understand this variability, Deltas are classified by the dominant process controlling sediment dispersal (Galloway, 1975). This classification has three endmembers (figure 2.1a): Sediment input (fluvial), waves, and tidal; with many examples exhibiting intermediate characteristics that can be classified as mixed energy (Goodbred and Saito, 2011). A variation of this classification was proposed by Davis and Hayes (1984) that better defined this intermediate zone, using the mean wave heigh versus mean tidal range, and is widely used for major Rivers with large sediment influx (figure 2.1b).

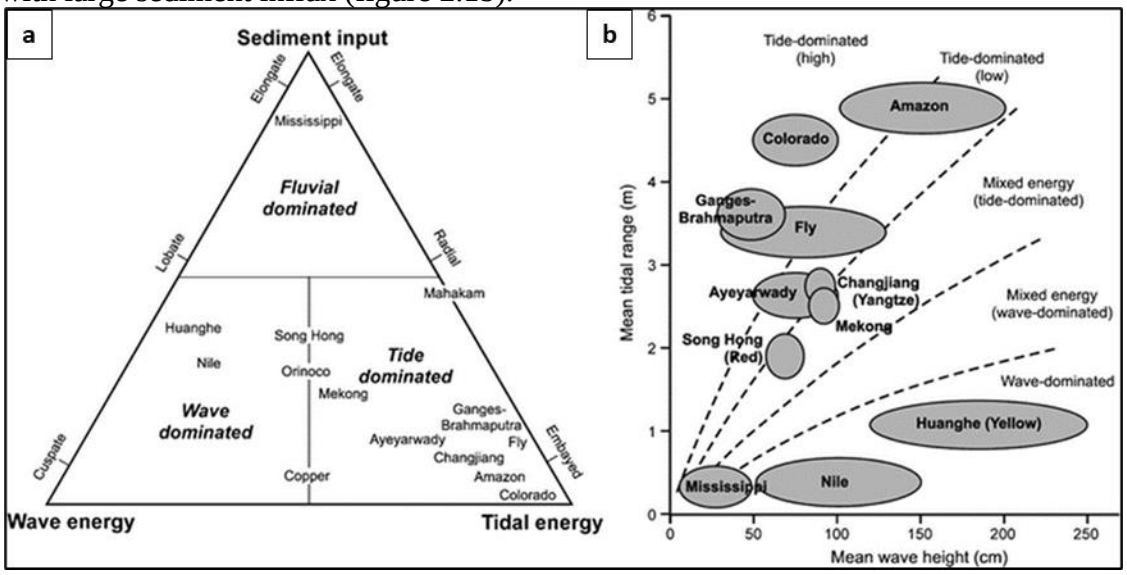

Figure 2.1. Classification of Deltas. (a) Classification of Deltas by the relative influence of River, wave, and tidal processes proposed by Galloway (1975). (b) The classification proposed by David and Hayes (1984) and modified by Hori et al (2002b), in which is used the mean wave height versus the tidal range to divide major large River Deltas into five morphological classes.

Compound Clinoform

Clinoforms, defined as inclined stratal surfaces (Rich 1951), occur over various spatial scales, ranging from Delta-front foresets (Steel & Olsen, 2002; Patruno et al., 2015a). The breaks at the top and bottom of these inclined stratal surfaces are called rollovers and separate low-gradient topsets and bottomsets from a steeper foreset zone (Sangree & Widmier, 1977; Pirmez et al., 1998; Adams & Schlager, 2000; Patruno et al., 2015). Modern Delta systems commonly exhibit compound clinoforms that consist of a shoreline (2-15m water depth) and subaqueous clinoforms (up to 200m water depth) with topset–foreset–bottomset morphology (figure 2.1.a) (Gilbert, 1885; Nittrouer et al., 1986; Kuehl et al., 1997; Pirmez et al., 1998; Ta et al., 2002; Walsh et al., 2004; Peng et al., 2018). These compound clinoforms are genetically and morphologically linked, and they are separated by a broad subaqueous topset platform (e.g., Cattaneo et al. 2003; Swenson et al. 2005; Helland-Hansen and Hampson 2009; Walsh and Nittrouer 2009; Patruno et al. 2015; Peng et al. 2018). In tidal-dominated Deltas, the shoreline clinoform comprises mainly the supratidal and intertidal portion of the Delta, including the lower coastal plain (e.g., Ta et al. 2002; Correggiari et al. 2005). The subaqueous platform is in the subtidal zone until the subaqueous rollover is reached, the limit between the platform and the subaqueous foreset. This foreset encompasses two parts: an upper part that is essentially the active Delta-front and a lower bottomset part that is contiguous with the shelf (figure 2.2a). Regarding the system bathymetry profile, the shoreline clinoform extension depends on the tidal range of the area, commonly occurring at water depths between 10-30 meters, whereas the subaqueous clinoform rollover lies at a variable distance (kilometers to tens of kilometers) offshore from the shoreline (Pirmez et al. 1998; Swenson et al. 2005) at water depths of 25 to 100 m (Patruno et al. 2015). The energy profile of the system is controlled by the position of the two clinoform rollovers. In the shoreline rollover, the fluvial influx

combines with the ebb-tidal currents to form a high-energy zone. Likewise, the subaqueous rollover energy profile is enhanced by the expected increase in current velocity when the current is moving across shallower depths (figure 2.2.b) (Fleming et al, 1939). As the gradient in the subaqueous platform tends to be very low, the system energy tends to generally decrease across the platform (figure 2.2.b), boosting the sedimentation of finer deposits at times (Peng et al., 2020), though there can also be higher energy zones of tidal scour and sediment bypass to the Delta front (Goodbred and Saito, 2006).

The interaction of fluvial influx with shallow marine processes controls the sediment dispersal and spatial separation of the subaerial and subaqueous clinoforms (Swenson et al. 2005; Walsh and Nittrouer 2009). Subaerial clinoforms are controlled by fluvial discharge, while subaqueous clinoforms are mainly affected by tides, waves, and other currents, including bottom-hugging sediment gravity flows (Pirmez et al. 1998; Driscoll and Karner 1999; Swenson et al. 2005; Rossi et al. 2016a; Peng et al., 2018). Swenson et al., (2004) proposed that to be able to preserve the compound clinoform, the system must be able to compensate the high sedimentary influx from the fluvial system with a similarly strong shallow marine process (figure 2.2.c).

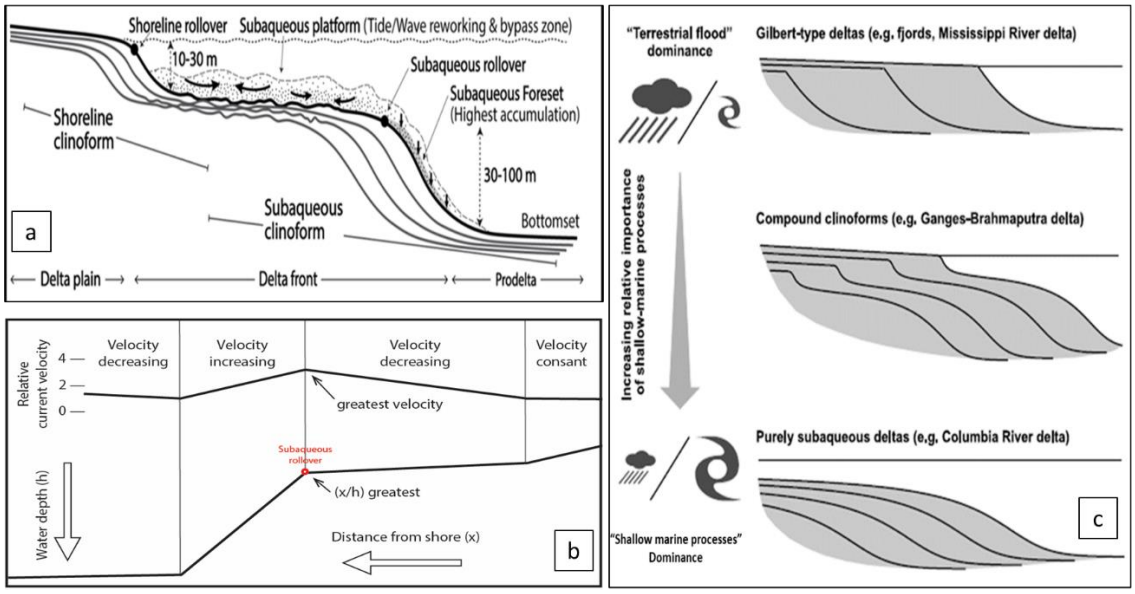

Figure 2.2. Compound Clinoforms. (a) Theoretical sketch of a compound-clinoform geometry showing the subaerial and subaqueous clinoforms (modified from Helland-Hansen and Hampson 2009; Patruno et al. 2015a; Peng et al., 2020) and the associated sub-environments. The subaqueous platform is represented as a bypass surface where the shallow marine processes reworked the sediments coming from the River mouth. Most of these sediments are finally deposited in the subaqueous foreset. (b) Distribution of maximum tidal current velocities over the continental shelf, where there is transport across the shelf. The point of expected greatest velocity coincides with the Subaqueous Rollover (modified from Fleming et al., 1939). (c) Phase diagram for a fluvioDeltaic clinoform showing the range of clinoform geometries to the dominant process; modified from Swenson et al., 2004.

Wave-dominated vs Tide-dominated Compound Clinoforms

Tide-dominated and wave-dominated Deltas that exhibit a compound clinoform exhibit different patterns that are visible on bathymetry data. tide-dominated Deltas show a shoreline clinoform in front of the River mouth, passing out onto a wide subaqueous platform (up to 150 km), then a shallow subaqueous rollover (10-30 m depth) passing down onto a gentle foreset slope (0.1-1.2°) (Patruno et al., 2015; Peng et al., 2020) with bottomsets down lapping the shelf (figure 2.3a). The compound-clinoform morphology

diminishes away from the depocenter in front of the River mouth (Peng et al., 2020). Elongate erosional features on the outer subaqueous platform and foreset (figure 2.3.a) are created by tidal currents parallel to sediment transport and physically linked with tidal distributary channels landwards (Rossi et al., 2016b). The compound clinoforms are well developed in modern tide-dominated Deltas situated in energetic marine environments, such as the Amazon (Kuehl et al. 1986; Nittrouer et al. 1986), the Ganges–Brahmaputra (Kuehl et al. 1997; Michels et al. 1998; Kuehl et al. 2005), the Yangtze (Hori et al. 2001; Liu et al. 2006; Liu et al. 2007), the Fly River Delta (Walsh et al. 2004) and the Orinoco River (Peng et al., 2018) Deltas.

In contrast to tide-dominated Delta, wave-dominated subaqueous Deltas have laterally extensive shore-parallel foresets with sediment accumulation aligned along bathymetric isobaths (figure 2.3b) (Peng et al., 2020). Sediment is dispersed alongshore from the River mouth and accumulated in the subaqueous clinoform with its subaqueous rollover located as deep as 60 m water depth (Peng et al., 2020). The subaqueous platform is relatively narrow (<30 km) perpendicular to the shoreline but will be wider if the cross-shelf component of waves is stronger (Pirmez et al., 1998; Swenson et al., 2005). This along-shore redistribution of sediment suggests that it takes a longer time for Deltas to reach the shelf edge, and there is likely to be less delivery to deep water. Compound clinoforms are well developed in modern wave-dominated Deltas such as the modern Adriatic shelf (Cattaneo et al., 2003; Pellegrini et al., 2015) or the shelf near the Magdalena River (figure 2.3b).

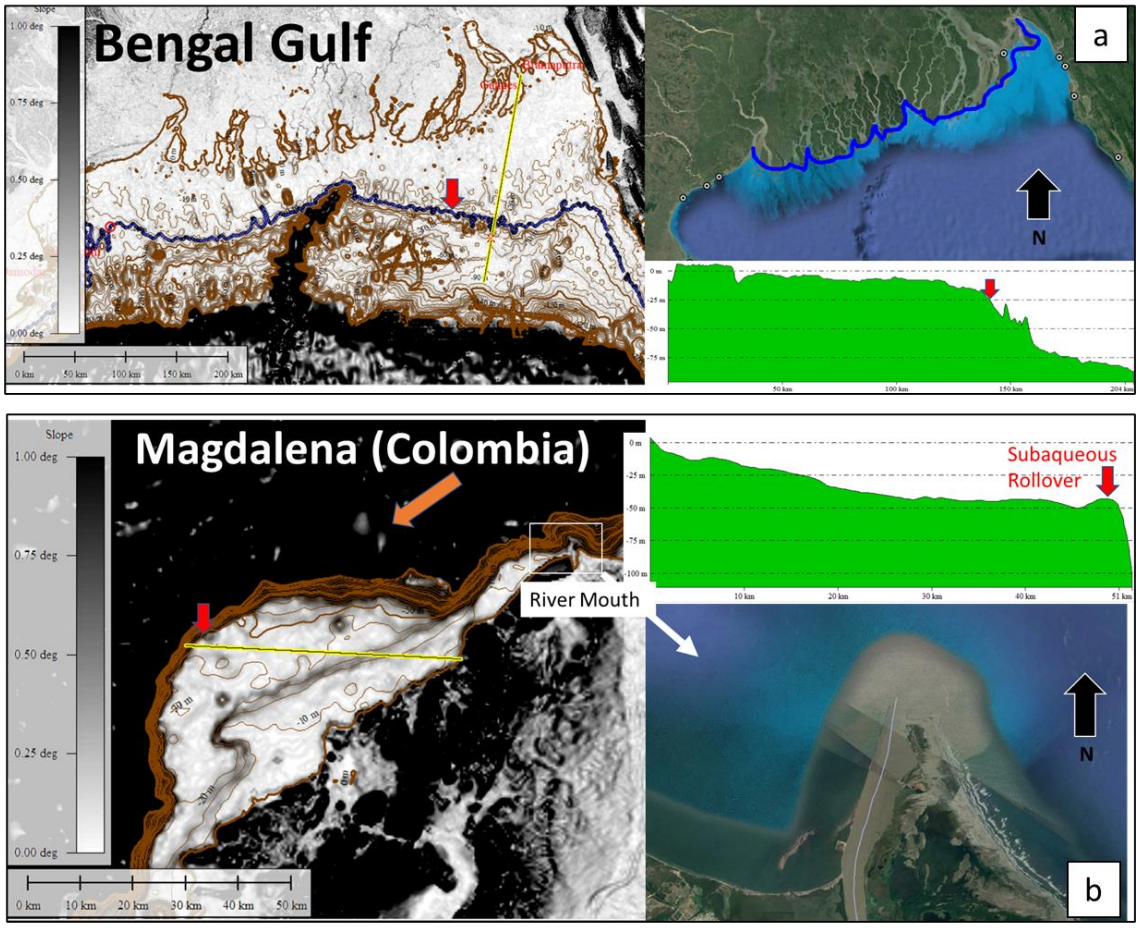

Figure 2.3. Examples of wave and tide-dominated compound clinoforms.(a) Bengal Gulf (Ganges-Brahmaputra system) bathymetry map (left, taken from GEBCO), the River mouth, and a profile of the subaqueous platform (right). tide-dominated Deltas show a shoreline clinoform in front of the River mouth, passing out onto a wide subaqueous platform (up to 150 km), then a shallow subaqueous rollover (10-30 m depth) passing down onto a gentle foreset slope (0.1-1.2). (b) Magdalena Delta (Colombia) bathymetry map (left, taken from GEBCO), the River mouth, and a profile of the subaqueous platform (right). Wave-dominated subaqueous Deltas have a relatively narrow subaqueous platform (<30 km), and deeper subaqueous rollovers. The sediment tends to accumulate laterally to the River mouth, in the predominant wave direction.

Hybrid Clinoform

Due to the differences in basinward progradation rates, shorelines (1000 to 100.000 m/Ky), subaqueous Delta (100 to 20000 m/Ky), shelf edge (1 to 100 m/Ky), and Continental Shelf Break (0,1 to 10 m/Ky) tend to merge at times forming shelf-edge Deltas or hybrid clinoforms (Patruno et al., 2015). Examples of Hybrid Clinoforms can be found on the Nile (Summerhayes et al., 1978), Niger (Short and Stauble, 1967; Damuth,1994), or the Mississippi Delta (Fisk et al., 1954). The cycle of cross-shelf Delta usually lasts less than 100ky (Muto and steel. 2001) and is controlled by relative sea change, rates of River-fed sediment supply, alongshore perpendicular shore currents, the bathymetry of the system (Patruno et al., 2018). It is important to note that most of the recent Delta scale clinoforms began prograding about 7ky before present with the waning of the rate of post-glacial eustatic sea-level rise (Patruno et al., 2018).

Methods:

To choose the subaqueous Delta bathymetries to analyze we first built a database by merging two existing datasets:

- The dataset from "River Discharge to the Coastal Ocean" by Milliman and Farnworth (2011), where we got modern and historic discharges and sediment influx coming from the River mouth into the system.
- The dataset from "A global Delta dataset and the environmental variables that predict Delta formation on marine coastlines" from Caldwell et al. (2018), where we got an estimation of the average tidal range and height of waves.

Secondly, with this dataset, we selected 138 River mouths around the world (figure 2.4), which have complete information about discharge, sediment flux, average wave heigh, and tidal range, and downloaded their bathymetry map from the "General Bathymetric Chart of the Ocean" (GEBCO) site to analyze looking for compound clinoforms morphologies. To correctly identify a compound clinoform, we need to recognize both rollovers (subaerial and subaqueous) and the subaqueous platform in between. After the morphological boundaries are mapped on the bathymetry, we measured the area of the subaqueous platform and the depth of the subaqueous rollover (figure 2.5).

If compound clinoform morphologies are not found, we try to understand the reason behind their absence, which could be related to the energy (lack or excess) of the system, latitude position, the River-derived sediment flux, and the morphology of the shelf (figure 2.6).

To analyze the energy of the shallow marine processes near the River mouth we used an equivalence between the average tidal range and the average wave height base on the plot proposed by Davis and Hayes (1984) (figure 2.1b). In this plot, the ratio of tidal range (m) is approximately 2.5 times the average wave height (figure 2.7). Knowing this

equivalence, we calculate a relatively shallow marine index which allows us to estimate the amount of energy available on the shelf to distribute and rework the sediments carried by the River (figure 2.7).

Figure 2.4. The location of the 138 River mouth bathymetry maps chosen to be analyzed in this study.

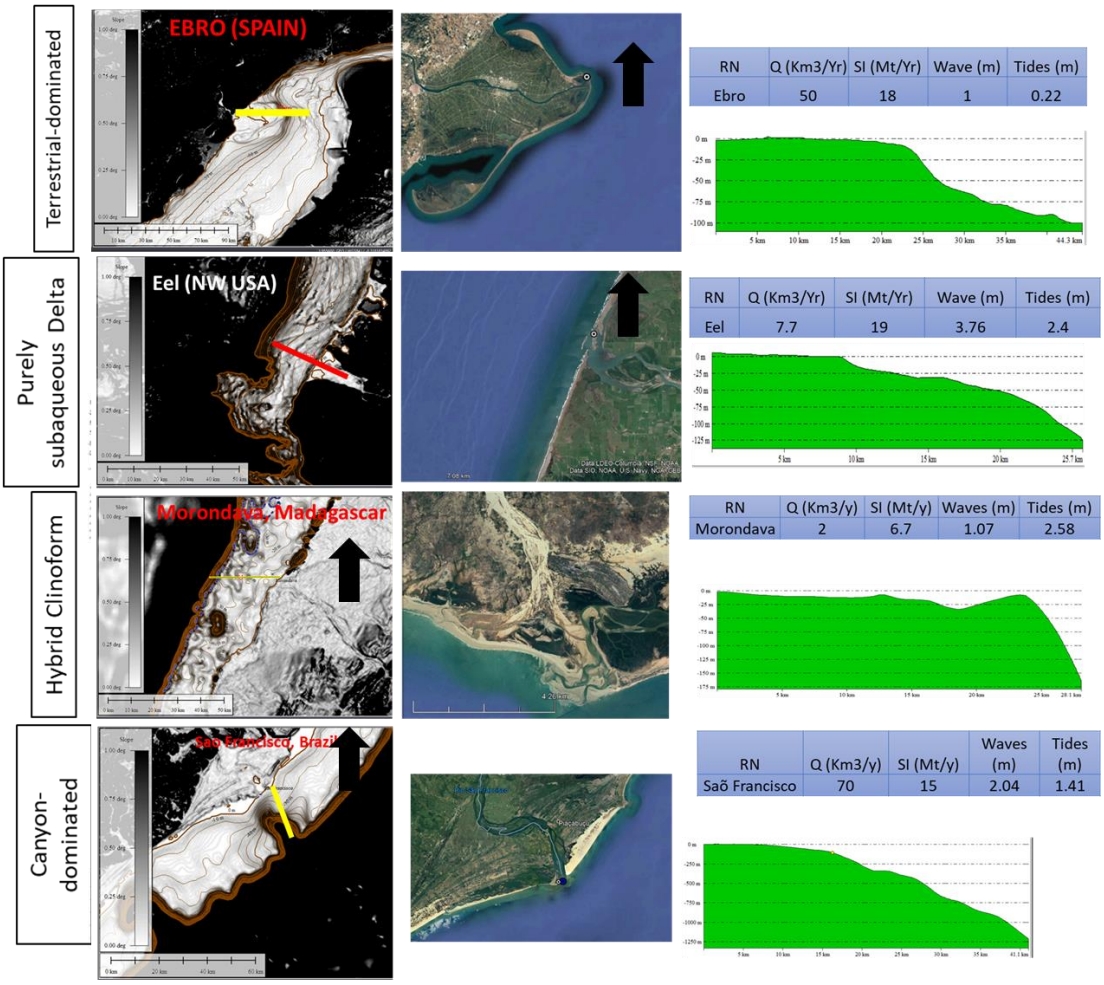

Figure 2.5. Examples of River mouths that don´t present compound clinoforms.In the figure are shown examples of Terrestrial-dominated, Purely Subaqueous Deltas, Hybrid Clinoform and Canyon dominated. The examples display the bathymetry map from GEBCO in a gradient map, a satellite image of the Delta (Google Earth Images), statistical data about the Discharge, Sediment Influx, average wave height, and tidal range, and a bathymetry profile of the shelf near the River mouth.

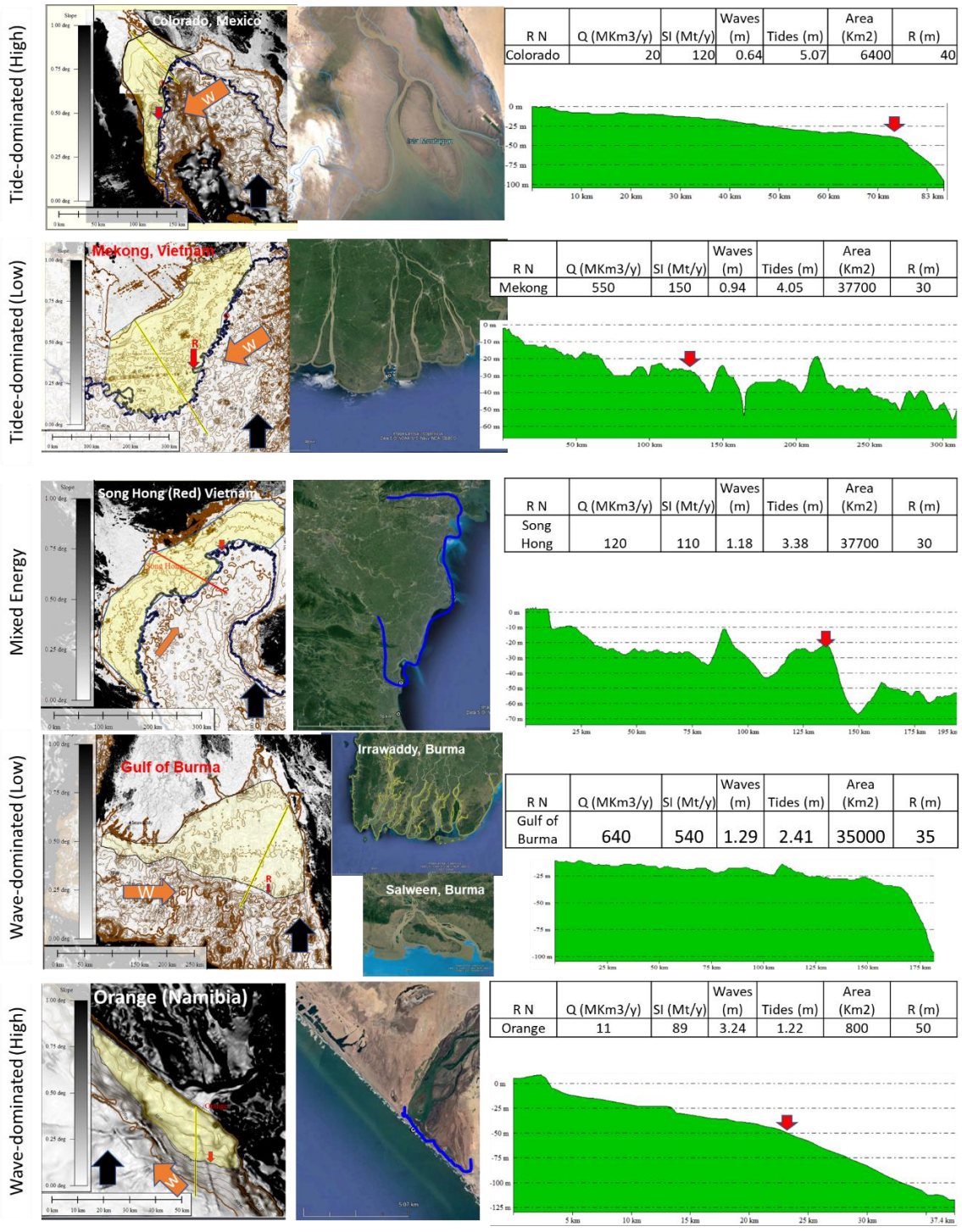

R N	Q (MKm3/y)	Sl (Mt/y)	Waves (m)	Tides (m)	Area (Km2)	R (m)
Colorado	20	120	0.64	5.07	6400	40
Mekong	550	150	0.94	4.05	37700	30
Song Hong	120	110	1.18	3.38	37700	30
Gulf of Burma	640	540	1.29	2.41	35000	35
Orange	11	89	3.24	1.22	800	50

Figure 2.6. Examples of River mouths that present compound clinoforms.

In the figure are shown examples of tide-dominated, mixed, and wave-dominated Deltas. The examples display the bathymetry map from GEBCO in

a gradient map, a satellite image of the Delta (Google Earth Images), statistical data about the Discharge, Sediment Influx, average wave height, and tidal range, and a bathymetry profile of the shelf near the River mouth.

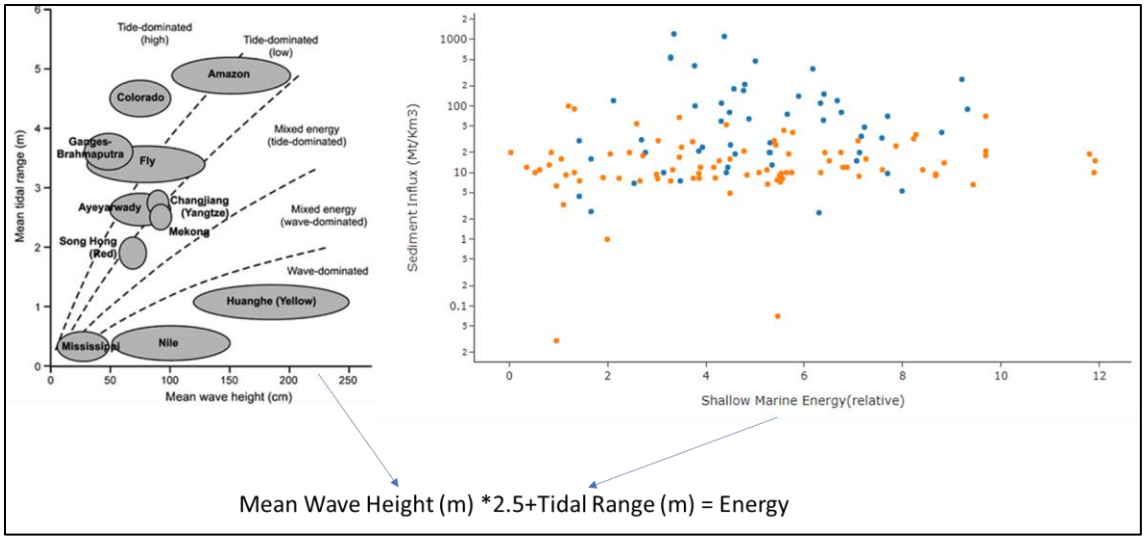

Figure 2.7. This figure explains how the shallow marine energy coefficient is calculated from an equivalence between tidal range and average wave height. This equivalence has been calculated using the plot proposed by Davis and Hayes (1984).

Results and Observations:

Occurrence of the Compound Clinoform on Modern Systems

From the analysis of the 138 River mouths, we found 54 compound clinoforms, 44 purely subaqueous systems, 21 terrestrial-dominated systems, 15 hybrid clinoforms, and 4 dominated by canyons which bypass most of the sediment toward the basin floor (figure 2.8). Also, we found that there are no compound clinoforms in high latitudes, being the Rhone (43° N), in the northern coast of the protected Mediterranean Sea, the system within the highest latitude (figure 2.8). The lack of compound clinoforms in high latitude system is probably related to the prevalence of ice during some or most parts of the year, which could inhibit the shallow marine processes to properly rework and distribute the sediment near the River mouth. In addition to this, we learned that compound clinoform morphology can be found in all the large Rivers with a sediment influx higher than 100 Mt/y (figure 2.8). The reason behind the ubiquity of the compound clinoform in these large Rivers could be related to the existence of a certain value of sediment supply from which it is not possible for the shallow marine processes, regardless of their energy, to not form a compound clinoform. The opposite effect happens when we run below 15 Mt/y of sediment influx (figure 2.9). Under this value, the compound clinoforms become rare, probably because the system doesn´t have enough sediment to form and preserve a subaqueous platform. Finally, we calculate the ratio between the sediment influx (Mt/y) and the discharge (Km^3/y), to evaluate if an increase in the concentration of sediment in the discharge could enhance the formation and preservation of a compound clinoform. We discover that this is the case (figure 2.10): as the sediment concentration in the total discharge increases, the efficiency of the fluvial influx to distribute the sediments on the shelf increase, boosting the chances to preserve a compound clinoform.

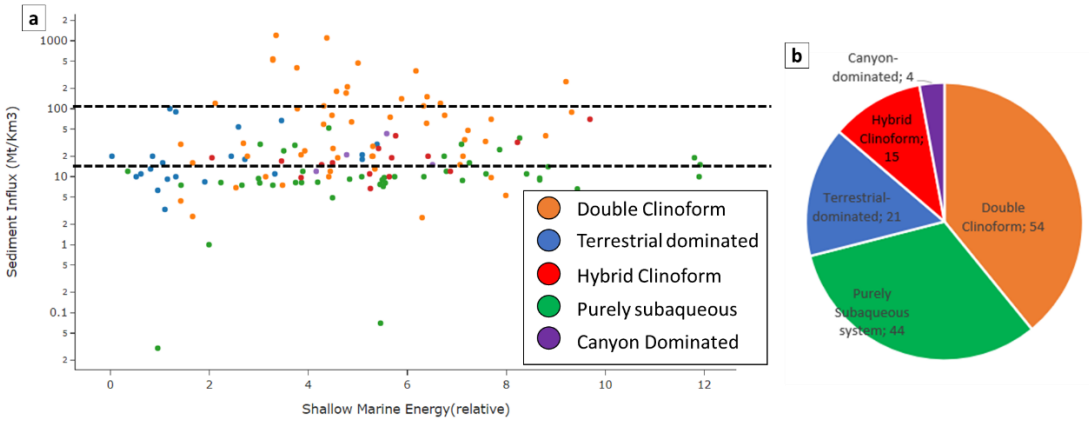

Figure 2.8. Classification of River mouths. (a) A plot of sediment influx versus shallow marine energy. In the plot, all the River mouths with values higher than 100 Mt/y show a compound clinoform. If the value falls below 15 Mt/y, the compound clinoforms become rare. (b) Pie chart of the 138 River mouths bathymetry analyzed.

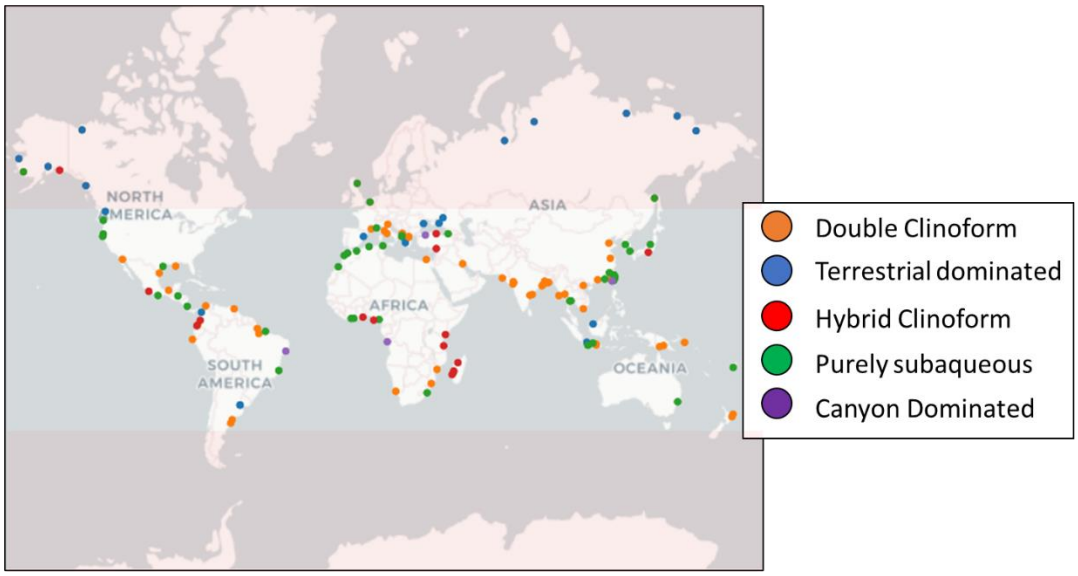

Figure 2.9. Classification of the subaqueous morphology regarding the presence of the compound clinoform or other clinoform morphology. In the cases where the compound clinoform is not present, we propose an explanation for the absence of the morphology. Moreover, it is important to note the lack of compound clinoforms at higher latitudes.

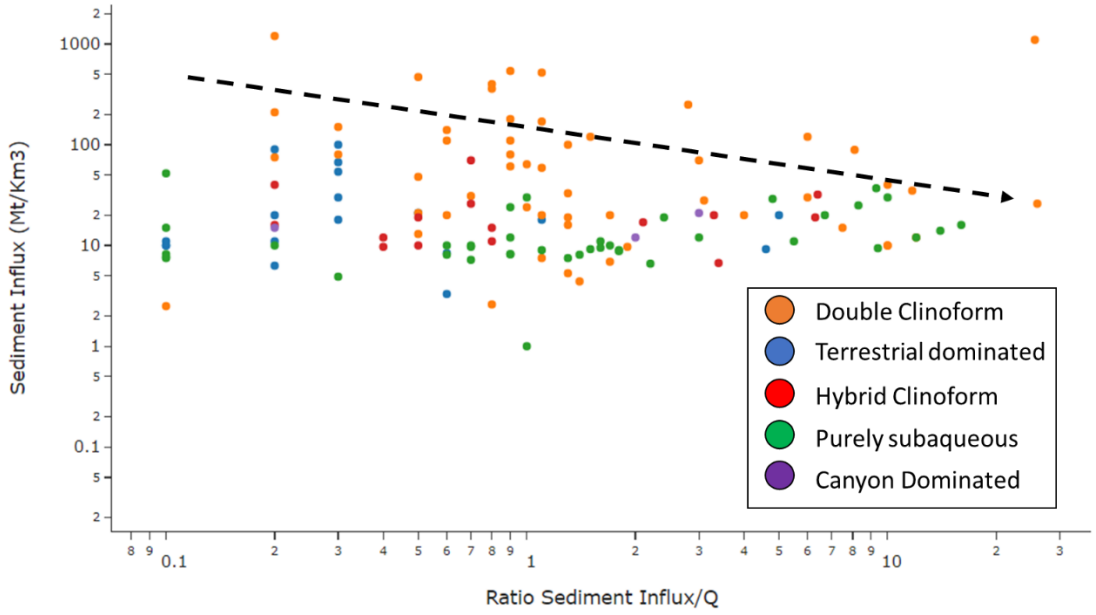

Figure 2.10. This plot is shown the relationship between the sediment influx (Mt/y) vs the ratio of sediment influx and Q (km^3/y). The plot shows that as the ratio of sediment influx/Q increases, we need less sediment influx to preserve a compound clinoform morphology.

Analysis of the Compound Clinoform Systems

From the 54 River mouths with compound clinoform systems, we combine the ones that share the same system reducing the number of locations to 39 (figure 2.11). To determine the averages of tidal ranges and waves of the River mouth within these systems, we calculate a weighted average using the sediment influx as the weighted factor. To classify these 39 systems, we use the plot proposed by Davis and Hayes (1984) and modified by Hori et al. (2002b). We determine that 7 systems are tide-dominated (high), 1 system is tide-dominated (low), 5 systems are mixed-energy, 6 systems are wave-dominated (low), and 20 systems are wave-dominated (high) (figure 2.11).

In these 39 systems we measure the area of the subaqueous platform and subaqueous rollover depth:

From the measurement of the area of the subaqueous platform, we determined that there is a direct relationship between the amount of River derived sediment influx discharged into the basin and the area of the subaqueous platform (figure 2.12.a). This relationship is not a surprise, since as we increase the amount of sediment flowing into the system, we will need more area to efficiently distribute it along the shelf. Also, we found that the tide-dominated systems tend to have a larger subaqueous platform in comparison with the wave-dominated systems (figure 2.12.a). This is aligned with the observations of Pirmez et al. (1998), Swenson et al. (2005), Patruno et al. (2015), and Peng et al. (2020), who stated that the tide-dominated systems tend to have a wide subaqueous platform (up to 150 km), while the subaqueous platform in the wave-dominated systems is relatively narrow (<30 km). If we compare the relative amount of energy of the shallow marine processes and the area of the subaqueous platform (figure 2.12.b), we found that the larger areas tend to be focused on the middle values of relative energy. The lower values in the extremes of the plot may be caused by too low or too high efficiency in the distribution of

sediment by the shallow marine processes; while the moderate values in the center are probably the most efficient value to maximize the area of distribution of the sediments in the subaqueous platform.

From the measurement of the depth of the subaqueous rollover we learned that wave-dominated systems tend to be deeper in comparison with the tide-dominated systems (figure 2.13.a), as was stated by Patruno et al. (2015), and Peng et al. (2020). Also, we found that, as the sediment influx in the system decrease and the energy of shallow marine processes gets stronger (figures 2.13.a,2.13b), we tend to find the subaqueous rollover on deeper positions. This observation matches the evidence presented by the lab experiments of Friedrichs and Wright (2004); and the observations in the Yellow River of Liu et al. (2013).

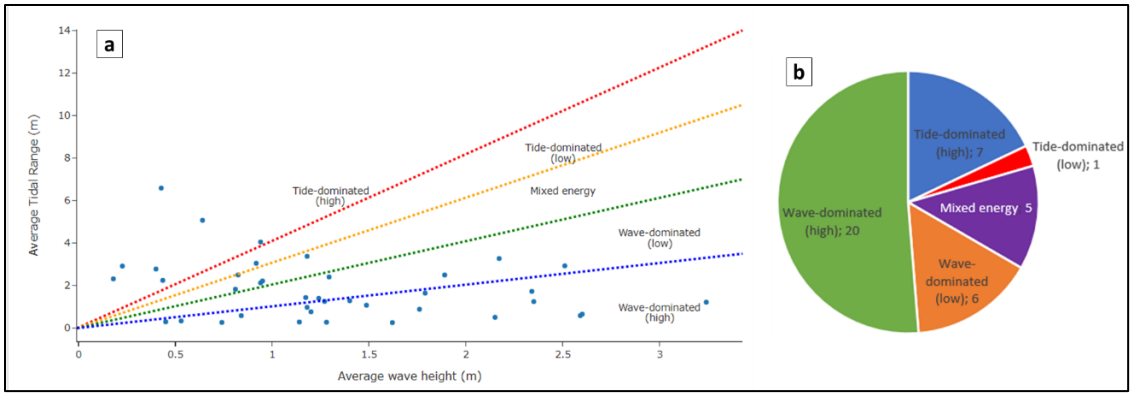

Figure 2.11. Classification of compound clinoforms. (a) This figure shows the River mouth with compound clinoforms in a plot of Average Tidal Range (m) vs Average Wave Height, following the plot proposed by Davis and Hayes (1984), and modified from Hori et al., (2002b). (b) Pie chart with the distribution of compound clinoform morphologies following the plot explained in (a).

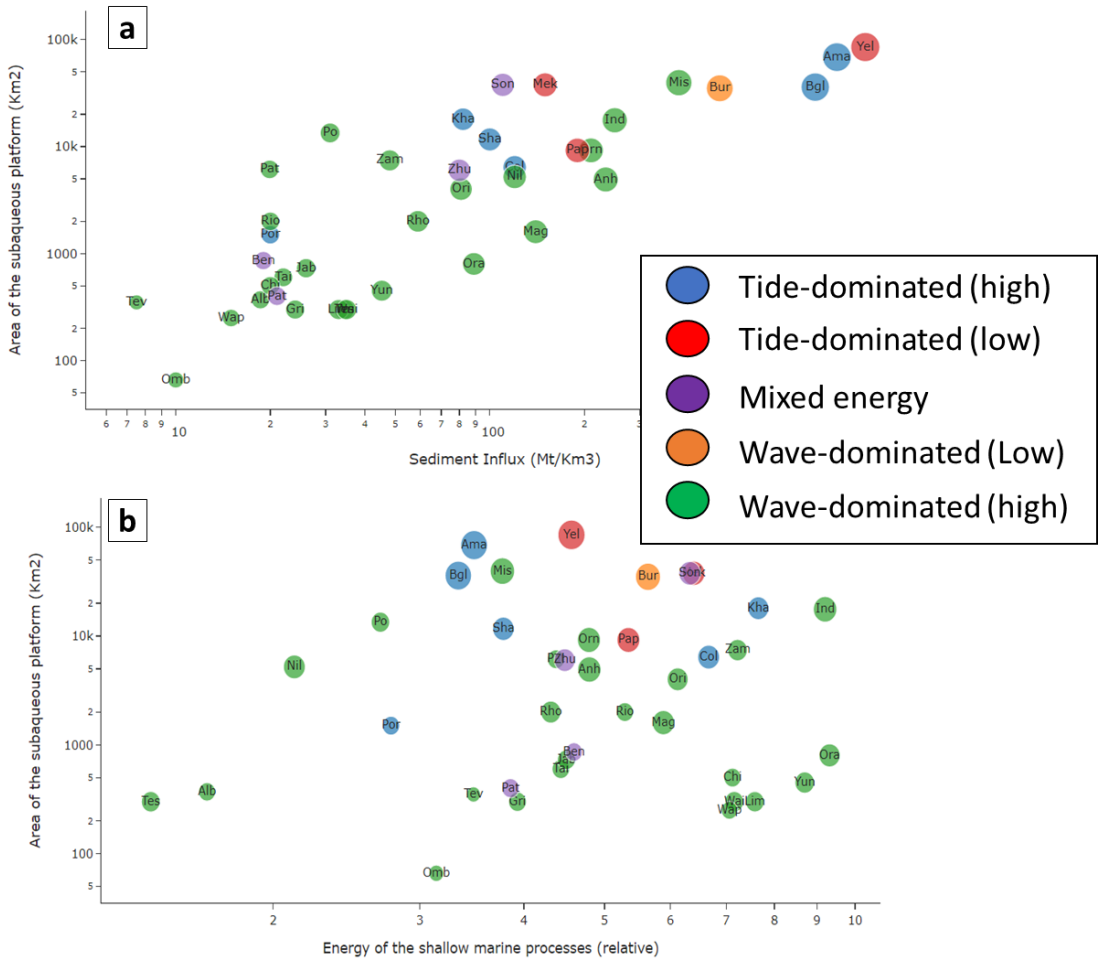

Figure 2.12. Area of Subaqueous Platform. (a) River mouth with compound clinoforms in a plot of area of the subaqueous platform (km^2) vs Sediment Influx (Mt/Km^3). The plot displays the direct relationship between these two variables. Also, the tide-dominated River mouths have larger measured areas in comparison with the wave-dominated River mouths. (b) River mouth with compound clinoforms in a plot of area of the subaqueous platform (km^2) vs relative energy of the shallow marine processes. The plot shows that the major values of the area are centered toward the middle values of energy.

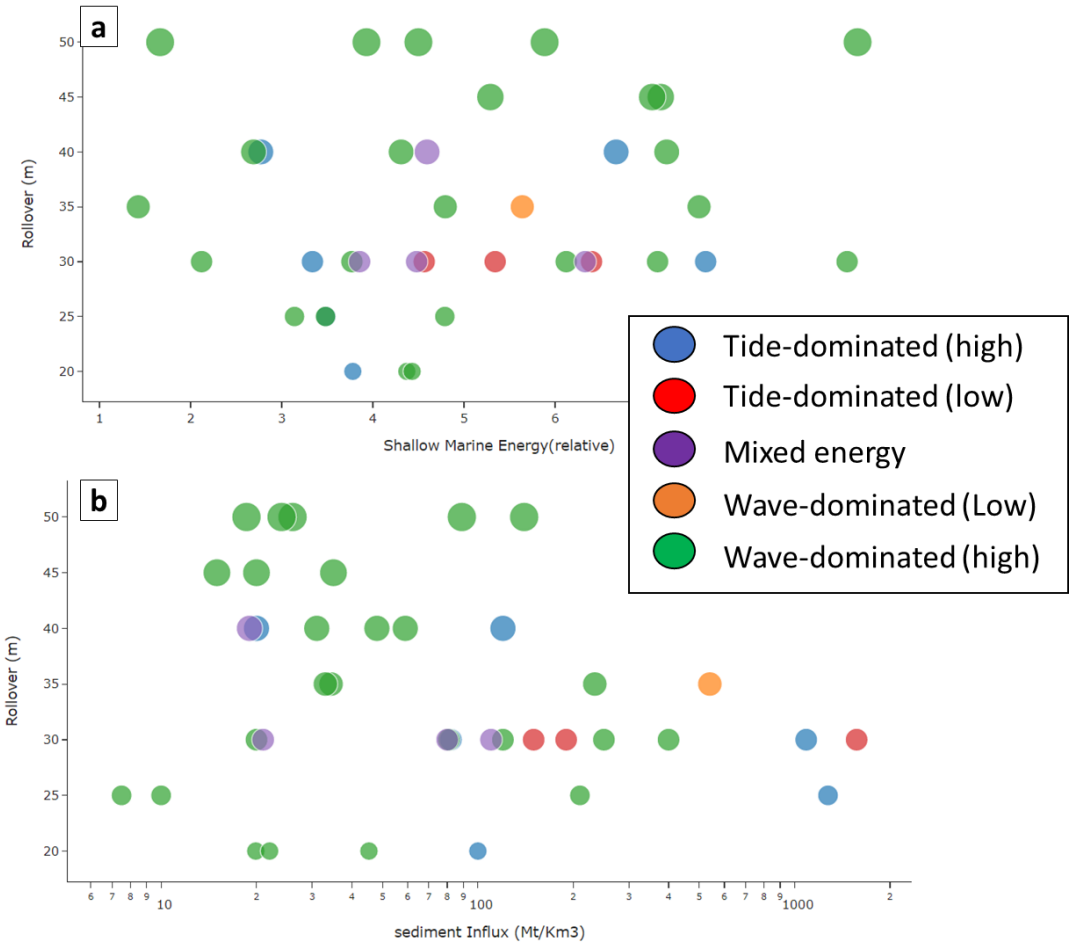

Figure 2.13. Subaqueous Rollover. (a) River mouth with compound clinoforms in a plot of the depth of the subaqueous rollover (m) vs sediment influx (Mt/y). The plot shows that the wave-dominated River mouth tends to have deeper rollovers and that as increase the sediment influx, the subaqueous rollover will be found in a shallower position. (b) River mouth with compound clinoforms in a plot of the depth of the subaqueous rollover (m) vs sediment influx (Mt/y). The plot shows that an increment in the energy of the system tends to increase the depth of the subaqueous rollover.

Preliminary Conclusions and Future Work:

- We examined 138 bathymetry maps near River mouth around the world, finding 54 compound clinoform morphologies encompassed within 39 systems.
- The sediment influx appears to be the most important factor in the preservation of the compound clinoform morphology. All the River mouths with a sediment influx higher than 100 Mt/Yr have a compound clinoform. In contrast, in River mouths with less than 15 Mt/Yr, the compound clinoforms become rare. Also, if we increase the ratio of sediment to water discharge, compound clinoforms become more common.
- Compound clinoforms are absent at higher latitudes, probably because of the prevalence of ice during the major part of the year hinter the energy of the shallow marine processes.
- We classified the 39 systems with compound clinoform using the plot proposed by Davis and Hayes (1984) and modified by Hori et al. (2002b), in which the systems are divided into the tide and wave-dominated, and mixed, following the averages values of tidal ranges and wave height.
- In these systems we measured the subaqueous platform area, finding a direct relationship with the sediment influx. Also, when we compared the areas with the energy of the shallow marine processes, the higher values of the area tend to align in the center of the plot, implying the existence of an optimum value of energy to enhance the progradation and expansion of the platform. The contrast of dimension between the wave (narrow) and tidal (wide) dominated systems tend were aligned with the stated by Pirmez et al. (1998), Swenson et al. (2005), Patruno et al. (2015), and Peng et al. (2020).

- We also measured the depth of the subaqueous rollover in these systems, finding that wave-dominated systems tend to be deeper in comparison with the tide-dominated systems and that as the sediment influx in the system decreases and the energy of shallow marine processes gets stronger, we tend to find the subaqueous rollover on deeper positions. Both observations have been reported in the laboratory by Friedrichs and Wright (2004), and on the Holocene Yellow River by Liu et al. (2013).

As future work, we want to develop strategies to apply these modern observations to the rock record. This is usually problematic because the compound clinoforms geometries observed in the modern may look different on the outcrop: the upper shoreline clinoform might be removed through erosion or rework as the Delta as a whole progrades forward; and the lower muddy subaqueous clinoform might change its geometry, attenuating its relief and architecture, due to compaction. Two possible strategies to achieve this goal could be:

- To look at the distribution of the grain size at the subaqueous platform to try to understand better the circulation and dissemination of sediment and their variation system to system.
- To analyze the roughness in the bathymetry maps, as a proxy of the relationship between accommodation rate and sediment supply. We expect to find more rough surfaces in environments where either the sediment supply is not enough to keep the subaqueous clinoform prograding, so the shallow marine processes are cannibalizing the subaqueous platform, or the accommodation is so low that most of the sediments pour into the Delta are bypass toward the subaqueous clinoform. This approach may have possible implications on better understanding bypass,

erosional surfaces, accommodation, and changes in base level in compound clinoform systems.

Appendix

Paleocurrents measured in Deguynos Formation:

Sample	Latitude	Longitude	Direction (°)	Orientation	Detail
D8	32.9842972	-116.151156	15	NNE	Entrecruzada
D8	32.9842972	-116.151156	20	NNE	Entrecruzada
A3	32.9795	-116.154139	21	NNE	Herringbone
E8	32.9987194	-116.165397	50	NE	Flaser
D7	32.9840833	-116.150942	85	E	Entrecruzada
D9	32.9945361	-116.161461	85	E	Entrecruzada
D8	32.9842972	-116.151156	95	E	Entrecruzada
E8	32.9993444	-116.164864	100	E	Ripple
D6	32.9874139	-116.150811	116	ESE	Entrecruzada
E5	32.9982917	-116.166031	120	ESE	Entrecruzada
E3	32.9979972	-116.162078	125	SE	Acreation
D5	32.9870028	-116.151583	130	SE	Entrecruzada
D3	32.9867806	-116.152122	134	SE	Entrecruzada
C1	32.9814417	-116.155394	135	SE	Entrecruzada
D8	32.9842972	-116.151156	137	SE	Entrecruzada
A6	32.98	-116.154583	140	SE	Herringbone
E3	32.9979972	-116.162078	140	SE	Entrecruzada
D8	32.9842972	-116.151156	142	SE	Entrecruzada
D6	32.9874139	-116.150811	145	SE	Entrecruzada
E1	32.9953472	-116.162428	145	SE	Entrecruzada
D7	32.9840833	-116.150942	147	SSE	Entrecruzada
B1	32.9806667	-116.153139	149	SSE	Entrecruzada
D6	32.9874139	-116.150811	150	SSE	Entrecruzada
E1	32.9953472	-116.162428	150	SSE	Entrecruzada
E3	32.9979972	-116.162078	150	SSE	Entrecruzada
C2	32.9814444	-116.129194	153	SSE	Entrecruzada
E1	32.9953472	-116.162428	155	SSE	Entrecruzada
E3	32.9979972	-116.162078	155	SSE	Entrecruzada
E6	32.9985361	-116.166217	155	SSE	Entrecruzada
C2	32.9814444	-116.129694	160	SSE	Entrecruzada
D2	32.9864528	-116.152853	160	SSE	Acreation
D3	32.9867806	-116.152122	160	SSE	Entrecruzada
D6	32.9874139	-116.150811	160	SSE	Entrecruzada

E1	32.9953472	-116.162428	160	SSE	Entrecruzada
E3	32.9979972	-116.162078	160	SSE	Entrecruzada
E7	32.9985833	-116.161703	160	SSE	Ripple
D5	32.9870028	-116.151583	165	SSE	Entrecruzada
B9	32.9814111	-116.158942	168	SSE	Ripple
E1	32.9953472	-116.162428	170	S	Entrecruzada
E1	32.9953472	-116.162428	170	S	Entrecruzada
E6	32.9985361	-116.166217	170	S	Entrecruzada
E7	32.9985833	-116.161703	170	S	Entrecruzada
C3	32.9815667	-116.158817	172	S	Ripple
D5	32.9870028	-116.151583	172	S	Entrecruzada
E3	32.9979972	-116.162078	175	S	Entrecruzada
D4	32.9868139	-116.151894	176	S	Entrecruzada
B5	32.9809278	-116.151367	177	S	Entrecruzada
E2	32.9961444	-116.162669	180	S	Entrecruzada
E2	32.9961444	-116.162669	180	S	Entrecruzada
D4	32.9868139	-116.151894	181	S	Entrecruzada
E3	32.9979972	-116.162078	182	S	Entrecruzada
B7	32.9813611	-116.128833	183	S	Entrecruzada
C6	32.9818611	-116.129361	184	S	Entrecruzada
E3	32.9979972	-116.162078	184	S	Entrecruzada
E1	32.9953472	-116.162428	185	S	Entrecruzada
C4	32.9816389	-116.1295	186	S	Entrecruzada
B3	32.9808056	-116.128694	187	S	Entrecruzada
A9	32.9803333	-116.129194	188	S	Entrecruzada
C7	32.9817778	-116.129444	189	S	Entrecruzada
D4	32.9868139	-116.151894	190	S	Entrecruzada
D4	32.9868139	-116.151894	190	S	Entrecruzada
E3	32.9979972	-116.162078	190	S	Entrecruzada
D4	32.9868139	-116.151894	194	SSW	Entrecruzada
A3	32.9795	-116.154139	195	SSW	Herringbone
C8	32.9818056	-116.129472	200	SSW	Entrecruzada
D8	32.9842972	-116.151156	200	SSW	Entrecruzada
E2	32.9961444	-116.162669	200	SSW	Entrecruzada
E5	32.9982917	-116.166031	200	SSW	Entrecruzada
B2	32.9807222	-116.152333	205	SSW	Entrecruzada
C9	32.9821667	-116.129111	205	SSW	Entrecruzada
A1	32.9782806	-116.163375	210	SSW	Entrecruzada
A8	32.9803056	-116.158722	210	SSW	Ripples
E1	32.9953472	-116.162428	210	SSW	Entrecruzada

B4	32.9810833	-116.128639	212	SSW	Entrecruzada
D7	32.9840833	-116.150942	212	SSW	Entrecruzada
C5	32.9818333	-116.129	213	SSW	Entrecruzada
E1	32.9953472	-116.162428	215	SW	Entrecruzada
E9	32.9829833	-116.151017	215	SW	Entrecruzada
D6	32.9874139	-116.150811	220	SW	Entrecruzada
B8	32.9815278	-116.129	221	SW	Herringbone
A1	32.9782806	-116.163375	222	SW	Entrecruzada
E4	32.9971889	-116.163131	222	SW	Ripple
D3	32.9867806	-116.152122	230	SW	Entrecruzada
D2	32.9864528	-116.152853	232	SW	Acreation
A2	32.9787167	-116.163764	240	WSW	Entrecruzada
E1	32.9953472	-116.162428	240	WSW	Entrecruzada
E1	32.9953472	-116.162428	250	WSW	Entrecruzada
E8	32.9989444	-116.164392	250	WSW	Ripple
A1	32.9782806	-116.163375	255	WSW	Entrecruzada
E7	32.9985833	-116.161703	270	W	Ripple
D9	32.9945361	-116.161461	280	W	Ripple
D9	32.9945361	-116.161461	280	W	Entrecruzada
A4	32.9797222	-116.160556	297	WNW	Entrecruzada
E7	32.9985833	-116.161703	300	WNW	Entrecruzada
B8	32.9815278	-116.129	312	NW	Herringbone
A5	32.9799444	-116.153056	313	NW	Ripple
D8	32.9842972	-116.151156	315	NW	Entrecruzada
A6	32.98	-116.154583	316	NW	Herringbone
B6	32.9810722	-116.151172	320	NW	Entrecruzada
D1	32.9864361	-116.152653	330	NNW	Acreation
E1	32.9953472	-116.162428	340	NNW	Entrecruzada
A7	32.9801389	-116.158833	345	NNW	Entrecruzada
D6	32.9874139	-116.150811	356	N	Entrecruzada
E8	32.9987194	-116.165397	358	N	Ripple

References

Adams, E.W. and Schlager, W. (2000) Basic types of submarine slope curvature. J. Sed. Res., 70, 814–828.

Allison, Mead & Lee, Michael & Aller, Robert. (2000). Origin of Amazon mudbanks along the northeast coast of South America. Marine Geology. 163. 10.1016/S0025-3227(99)00120-6.

Alvarez, L. G., Suárez-Vidal, F., Mendoza-Borunda, R., & González-Escobar, M. (2009). Bathymetry and active geological structures in the Upper Gulf of California. Boletín de la Sociedad Geológica Mexicana, 61(1), 129-141.

Andrews, E. D. (1991), Sediment transport in the Colorado River basin: in Colorado River Ecology and Dam Management, Committee to Review the Glen Canyon Environmental Studies, Water Science and Technology Board, Commission on Geosciences, Environment, and Resources, National Academy of Sciences Press, p. 54–74.

Atwater, T. (1970), Implications of plate tectonics for the Cenozoic tectonic evolution of western North America: Geological Society of America Bulletin, v. 81, p. 3513-3536.

Axen, G.J., and Fletcher, J.M. (1998), Late Miocene– Pleistocene extensional faulting, northern Gulf of California, Mexico and Salton Trough, California: International Geology Review, v. 40, p. 217–244, DOI: 10.1080/00206819809465207.

Birgenheier, L.P., Horton, B., McCauley, A.D., Johnson, C.L. and Kennedy, A. (2017) A depositional model for offshore deposits of the lower Blue Gate Member, Mancos Shale, Uinta Basin, Utah, USA. Sedimentology, 64, 1402–1438

Caldwell, R. L., Edmonds, D. A., Baumgardner, S., Paola, C., Roy, S., and Nienhuis, J. H. (2019), A global Delta dataset and the environmental variables that predict

Delta formation on marine coastlines, Earth Surf. Dynam., 7, 773–787, https://doi.org/10.5194/esurf-7-773-2019, 2019.

Canet C., Prol-Ledesma R.M., Dando P.R., Vázquez-Figueroa V., Shumilin E., Birosta E., Sánchez A., Robinson C.J., Camprubí A. & Tauler E. (2010). Discovery of massive seafloor gas seepage along the Wagner Fault, northern Gulf of California. Sedimentary Geology, 228: 292-303.

Carbajal, N., Montaño, Y. (2001), Comparison between predicted and observed physical features of sandbanks: Estuarine, Coastal, and Shelf Science, 52, 435-443.

Carriquiry, J.D., Sánchez, A. (1999), Sedimentation in the Colorado River Delta and Upper Gulf of California after nearly a century of discharge loss: Marine Geology, 158, 125-145.

Cattaneo, A., Correggiari, A., Langone, L. and Trincardi, F. (2003) The late-Holocene Gargano subaqueous Delta, Adriatic shelf: sediment pathways and supply fluctuations. Mar. Geol., 193, 61 –91.

Choi, K., Dalrymple, R.W., Chun, S.S. and Kim, S.-P. (2004) Sedimentology of modern, inclined heterolithic stratification (IHS) in the macrotidal Han River Delta, Korea. J. Sed. Res., 74, 677–689.

Cloos, M. E. (2014) Detrital zircon U-Pb and (U-Th)/He geo-thermochronometry and submarine turbidite fan development)t in the Mio-Pliocene Gulf of California, Fish Creek-Vallecito Basin, southern California [M.S.]: The University of Texas at Austin.

Coleman, I.M., Wright, L.D. (1975), Modern River Deltas: Variability of Processes and Sand Bodies, in Broussard, M.L. (ed.) Deltas: Models for Exploration: Houston, Tex., Houston.

Colorado River Basin Map [USGS], pubs.usgs.gov/media/images/colorado-River-basin-map.html.

Correggiari, A., Cattaneo, A. and Trincardi, F. (2005) The modern Po Delta system: lobe switching and asymmetric proDelta growth. Mar. Geol., 222–223, 49 –74.

Curtis, W. F., J. K. Culbertson & E. B. Chase (1973). Fluvial Sediment Discharge to the Oceans from the Conterminous United States, US Geol. Surv. Circular, 17 pp.

Dalrymple, R.W. (2010) Tidal depositional systems. In: Facies Models 4 (Eds N.P. James and R.W. Dalrymple), Geological Association of Canada, 4, 201–231.

Dalrymple, R. W., Zaitlin, B. A., & Boyd, R. (1992). Estuarine facies models; conceptual basis and stratigraphic implications. Journal of Sedimentary Research, 62(6), 1130-1146.Fan, 2012

Dalrymple, R.W. and Choi, K. (2007) Morphologic and facies trends through the fluvial–marine transition in tide-dominated depositional systems: a schematic framework for environmental and sequence-stratigraphic interpretation. Earth Sci. Rev., 81, 135–174.

Damuth, J.E. (1994). Neogene gravity tectonics and depositional processes on the deep Niger Delta continental margin. Mar. Pet. Geol. 11 (3), 320–346.

Darin, M. H., Bennett, S. E. K., Dorsey, R. J., Oskin, M. E., & Iriondo, A. (2016). Late Miocene extension in coastal Sonora, México: Implications for the evolution of dextral shear in the proto-Gulf of California oblique rift. Tectonophysics, 693, 378–408. https://doi.org/10.1016/j.tecto.2016.04.038

Davis RA, Hayes MO (1984) What is a wave-dominated coast? Mar Geol 60:313–329

DeMets, C. (1995). A reappraisal of seafloor spreading lineations in the Gulf of California: Implications for the transfer of Baja California to the Pacific plate and estimates of Pacific-North America motion. Geophysical Research Letters, 22(24), 3545-3548.

Dibblee, T.W., Jr. (1954), Geology of the Imperial Valley region, California, in Jahns, R.H., ed., Geology of Southern California: California Division of Mines Bulletin 170, p. 21–28.

Dibblee, T.W., Jr. (1984), Stratigraphy and tectonics of the San Felipe Hills, Borrego Badlands, Superstition Hills, and vicinity, in Rigsby, C.A., ed., The Imperial Basin— Tectonics, Sedimentation, and Thermal Aspects: Los Angeles, California, Pacifi c Section, Society of Economic Paleontologists and Mineralogists, p. 31–44.

Dorsey, R.J. (2006), Stratigraphy, tectonics, and basin evolution in the Anza-Borrego Desert region, in Jefferson, G.T., and Lindsay, L.E., eds., Fossil Treasures of Anza-Borrego Desert: San Diego, California, Sunbelt Publications, p. 89–104.

Dorsey, R. J., Fluette, A., McDougall, K., Housen, B. A., Janecke, S. U., Axen, G. J., & Shirvell, C. R. (2007). Chronology of Miocene–Pliocene deposits at Split Mountain Gorge, southern California: A record of regional tectonics and Colorado River evolution. Geology, 35(1), 57-60.

Dorsey, R. J., Housen, B. A., Janecke, S. U., Fanning, C. M., & Spears, A. L. (2011). Stratigraphic record of basin development within the San Andreas fault system: Late Cenozoic Fish Creek–Vallecito basin, southern California. Bulletin, 123(5-6), 771-793.

Driscoll, N.W. and Karner, G.D. (1999) Three-dimensional quantitative modeling of clinoform development. Mar. Geol., 154, 383–398.

Fan, D. (2012) Open-coast tidal flats. In: Principles of Tidal Sedimentology (Eds R.A. Davis Jr and R.W. Dalrymple), pp. 187–229. Springer, Netherlands, Dordrecht

Fisk, H.N., McFarlan, E., Kolb, C.R., Wilbert, L.J. (1954). The sedimentary framework of the modern Mississippi Delta. J. Sediment. Res. 24 (2).

Fletcher, J.M., Grove, M., Kimbrough, D., Lovera, O., and Gehrels, G.E. (2007) Ridge-trench interactions and the Neogene tectonic evolution of the Magdalena shelf and the southern Gulf of California: Insights from detrital zircon U-Pb ages from the Magdalena fan and adjacent areas: Geological Society of America Bulletin, v. 119, p. 1313–1336.

Friedrichs, C.T., Wright, L.D. (2004). Gravity-driven sediment transport on the continental shelf: implications for equilibrium profiles near River mouths. Coastal Engineering 51, 795–811.

Galloway WE (1975) Process framework for describing the morphologic and stratigraphic evolution of Deltaic depositional systems. In: Broussard ML (ed) Deltas: models for exploration. Houston Geological Society, Houston, pp 87–98

Geehan, G.W. (1978), Nearshore sand bars in the Gulf of California: San Diego, California, U.S.A., University of California, Ph.D. Thesis, 198 pp.

General Bathymetric Chart of the Ocean (GEBCO), https://www.gebco.net/

Gibson, L., Malinconico, L., Downs, T., and Johnson, N. (1984), Structural implications of gravity data from the Vallecito-Fish Creek basin, western Imperial Valley, California, in Rigsby, C. A., ed., The Imperial Basin- Tectonics, Sedimentation, and Thermal Aspects: Pacific Section SEPM, Volume 40, p. 15-29.

Gilbert, G.K. (1885) The topographic feature of lakeshores. U.S. Geol. Surv. Annu. Rep., 5, 104–108.

Goodbred, Steven & Saito, Yoshiki. (2011). Tide-Dominated Deltas. 10.1007/978-94-007-0123-6_7.

Gorsline, D.S. (1967), Sedimentologic studies of the Colorado Delta: Report USC Geology 67-1, University of Southern California, Los Angeles, California, 80 p.

Hampson, G.J. and Premwichein, K. (2017) Sedimentologic character of ancient muddy subaqueous-Deltaic clinoforms: down cliff clay member, Bridport Sand Formation, Wessex Basin, UK. J. Sed. Res., 87, 951–966.

Hanna, G.D. (1926), Paleontology of Coyote Mountain, Imperial County, California: Proceeding of the California Academy of Sciences, fourth series, v. 14, p. 427–503.

Helland-Hansen, W. and Hampson, G.J. (2009) Trajectory analysis: concepts and applications. Basin Res., 21, 454– 483.

Hermoso-Salazar, M., Frontana, S., Solís-Weiss, V., Prol Ledesma, R. M., Estradas, M. (2013). The occurrence of Sipuncula in the Wagner and Consag Basins, Northern Gulf of California. Cahiers de Biologie Marine. 54.

Hori, K., Saito, Y., Zhao, Q., Cheng, X., Wang, P., Sato, Y., Li, C. (2001). Sedimentary facies and Holocene progradation rates of the Changjiang (Yangtze) Delta, China. Geomorphology 41, 233–248.

Hori K, Saito Y, Zhao Q, Wang P (2002a) Evolution of the coastal depositional systems of the Changjiang (Yangtze) River in response to late Pleistocene– Holocene sea-level changes. J Sediment Res 72:884–897

Hori, K., Saito, Y., Zhao, Q., Wang, P., (2002b). Architecture and evolution of the tide-dominated Changjiang (Yangtze) River Delta, China. Sedimentary Geology 146, 249–264.

Huthnance, J.M. (1982), On one mechanism forming linear sandbanks: Estuarine and Coastal Marine Science, 14, 79-99.

Janecke, S.U., Markowski, D., Thornock, S.J., Evans, J.P., Steely, A.N., and Bykerk-Kauffman, A. (2016), The strange geometries of strike-slip faults: Insights from

southern California's active faults: Geological Society of America Abstracts with Programs, v. 48, no. 7, https://doi.org/10.1130/ abs/2016AM-286960.

Jefferson, G.T., and Lindsay, L.E., eds. (2006), Fossil Treasures of Anza-Borrego Desert: San Diego, California, Sunbelt Publications, 394 p.

Liu, J., Kong, X., Saito, Y., Liu, J. P., Yang, Z., & Wen, C. (2013). Subaqueous Deltaic formation of the Old Yellow River (AD 1128–1855) on the western South Yellow Sea. Marine Geology, 344, 19-33.

Johnson, N.M., Officer, C.B., Opdyke, N.D., Woodard, G.D., Zeitler, P.K., and Lindsay, E.H. (1983), Rates of late Cenozoic tectonism in the Vallecito–Fish Creek basin, western Imperial Valley: California Geology, v. 11, p. 664–667.

Kerr, D.R. (1982), Early Neogene Continental Sedimentation, Western Salton Trough, California [M.S. thesis]: San Diego, California, San Diego State University, 138 p.

Kuehl, S.A., Nittrouer, C.A. and DeMaster, D.J. (1986) Nature of sediment accumulation on the Amazon continental shelf. Cont. Shelf Res., 6, 209–225.

Kuehl, S.A., Levy, B.M., Moore, W.S., Allison, M.A. (1997). Subaqueous Delta of the Ganges–Brahmaputra River system. Marine Geology 144, 81–96.

Kuehl, S.A., Allison, M.A., Goodbred, S.L. and Kudrass, H. (2005) The Ganges-Brahmaputra Delta. In: River Deltas – Concepts, Models and Examples (Eds L. Giosan and J.P. Bhattacharya), SEPM Spec. Publ., 83, 413–434. Hori et al. 2001

Lavın, M. F., Godınez, V. M., & Alvarez, L. G. (1998). Inverse-estuarine features of the Upper Gulf of California. Estuarine, Coastal and Shelf Science, 47(6), 769-795.

Liu, J. P., Li, A. C., Xu, K. H., Velozzi, D. M., Yang, Z. S., Milliman, J.D. and DeMaster, D.J. (2006) Sedimentary features of the Yangtze River-derived along-shelf clinoform deposit in the EastChinaSea.Cont.ShelfRes.,26,2141–2156.

Liu, J.P., Xu, K.H., Li, A.C., Milliman, J.D., Velozzi, D.M., Xiao, S.B. and Yang, Z.S. (2007) Flux and fate of Yangtze River sediment delivered to the East China Sea. Geomorphology, 85, 208–224.

Lizarralde, D., Axen, G. J., Brown, H. E., Fletcher, J. M., González-Fernández, A., Harding, A. J., Holbrook, W. S., Kent, G. M., Paramo, P., Sutherland, F., & Umhoefer, P. J. (2007). Variation in styles of rifting in the Gulf of California. Nature, 448(7152), 466–469.

Lizarralde, D., Axen, G. J., Brown, H. E., Fletcher, J. M., González-Fernández, A., Harding, A. J., Umhoefer, P. J. (2007). Variation in styles of rifting in the Gulf of California. Nature, 448(7152), 466-469.

Longhitano, S.G., Mellere, D., Steel, R.J. and Ainsworth, R.B. (2012) Tidal depositional systems in the rock record: a review and new insights. Sed. Geol., 279, 2–22.

Macquaker, J.H.S., Bentley, S.J. and Bohacs, K.M. (2010) Wave-enhanced sediment-gravity flows and mud dispersal across continental shelves: reappraising sediment transport processes operating in ancient mudstone successions. Geology, 38, 947–950.

Mellere, D., & Steel, R. J. (1996). Tidal sedimentation in Inner Hebrides half grabens, Scotland: the Mid-Jurassic Bearreraig Sandstone Formation. Geological Society, London, Special Publications, 117(1), 49-79.

Michels, K.H., Kudrass, H.R., H€ubscher, C., Suckow, A. and Wiedicke, M. (1998) The submarine Delta of the Ganges Brahmaputra: cyclone-dominated sedimentation patterns. Mar. Geol., 149, 133–154.

Miller, K. G., Kominz, M. A., Browning, J. V., Wright, J. D., Mountain, G. S., Katz, M. E., ... & Pekar, S. F. (2005). The Phanerozoic record of global sea-level change. science, 310(5752), 1293-1298. Milliman, J., & Farnsworth, K. (2011). River Discharge to

the Coastal Ocean: A Global Synthesis. Cambridge: Cambridge University Press. doi:10.1017/CBO9780511781247

Miller, K.G., G.S. Mountain, J.D. Wright, and J.V. Browning. 2011. A 180-million-year record of sea level and ice volume variations from continental margin and deep-sea isotopic records. Oceanography 24(2):40–53, https://doi.org/10.5670/oceanog.2011.26.

Nguyen, Van & Thi Kim Oanh, Ta & Tateishi, Masaaki. (2000). Late Holocene depositional environments and coastal evolution of the Mekong River Delta, Southern Vietnam. Journal of Asian Earth Sciences. 18. 427-439. 10.1016/S1367-9120(99)00076-0.

Nittrouer, C.A., Kuehl, S.A., DeMaster, D.J. and Kowsmann, R.O. (1986) The Deltaic nature of Amazon shelf sedimentation. GSA Bull., 97, 444–458.

Olariu, C., Steel, R. J., Dalrymple, R. W., & Gingras, M. K. (2012). Tidal dunes versus tidal bars: The sedimentological and architectural characteristics of compound dunes in a tidal seaway, the lower Baronia Sandstone (Lower Eocene), Ager Basin, Spain. Sedimentary Geology, 279, 134-155.

Olariu, C., Steel, R. J., Olariu, M. I., & Choi, K. (2015). Facies and architecture of unusual fluvial–tidal channels with inclined heterolithic strata: Campanian Neslen Formation, Utah, USA. In Developments in Sedimentology (Vol. 68, pp. 353-394). Elsevier.

Opdyke, N.D., Lindsay, E.H., Johnson, N.M., and Downs, T. (1977), The paleomagnetism and magnetic polarity stratigraphy of the mammal-bearing section of Anza Borrego State Park, California: Quaternary Research, v. 7, p. 316–329, DOI: 10.1016/0033-5894(77)90024-2.

Oskin, M., Stock, J., & Martín-Barajas, A. (2001). Rapid localization of Pacific-North America plate motion in the Gulf of California. Geology, 29(5), 459–462. https://doi.org/10.1130/0091-7613(2001)029<0459:RLOPNA>2.0.CO;2

Patruno, S., Hampson, G.J., Jackson, C.A.L., and Dreyer, T., (2015), Clinoform geometry, geomorphology, facies character and stratigraphic architecture of a sand-rich subaqueous Delta: Jurassic Sognefjord Formation, offshore Norway: Sedimentology, v. 62, p. 350– 388.

Patruno, S., & Helland-Hansen, W. (2018). Clinoforms and clinoform systems: Review and dynamic classification scheme for shorelines, subaqueous Deltas, shelf edges, and continental margins. Earth-Science Reviews, 185, 202-233.

Pellegrini, C., Maselli, V., Cattaneo, A., Piva, A., Ceregato, A., Trincardi, F. (2015). Anatomy of a compound Delta from the post-glacial transgressive record in the Adriatic Sea. Mar. Geol. 362, 43–59.

Peng, Y., Steel, R. J., Rossi, V. M., & Olariu, C. (2018). Mixed-energy process interactions read from a compound-clinoform Delta (paleo–Orinoco Delta, Trinidad): preservation of River and tide signals by mud-induced wave damping. Journal of Sedimentary Research, 88(1), 75-90.

Peng, Y., Olariu, C., & Steel, R. J. (2020). Recognizing tide-and wave-dominated compound Deltaic clinothems in the rock record. Geology.

Peryam, T. C. (2012), Sedimentation, climate change, and tectonics: Dynamic stratigraphy of the Pliocene-Pleistocene Palm Spring Group, Fish Creek-Vallecito Basin, California [Ph.D.]: University of Oregon, 190 p.

Pirmez, C., Pratson, L.F. and Steckler, M.S. (1998) Clinoform development by advection-diffusion of suspended sediment: modeling and comparison to natural systems. J. Geophys. Res., 103, 24141–24157.

Reineck, H.-E. and Wunderlich, F. (1968) Classification and origin of flaser and lenticular bedding. Sedimentology, 11, 99–104.

Remeika, P. (1995), Basin tectonics, stratigraphy, and depositional environments of the western Salton Trough detachment, in Remeika, P., and Sturz, Anne, ed., Paleontology and Geology of the Western Salton Trough Detachment, Anza Borrego Desert State Park, California: San Diego Association of Geologists Field Trip Guidebook I: San Diego, California, p. 3-54.

Rich, J.L. (1951) Three critical environments of deposition and criteria for recognition of rocks deposited in each of them. GSA Bull., 62,1 –20.

Rossi, V.M. and Steel, R.J. (2016a) The role of tidal, wave, and River currents in the evolution of mixed-energy Deltas: an example from the Lajas Formation (Argentina). Sedimentology, 63, 824–864.

Rossi, V.M., Kim, W., Lopez, J.L., Edmonds, D., Geleynse, N., Olariu, C., Steel, R.J., Hiatt, M., and Passalacqua, P. (2016b), Impact of tidal currents on Delta-channel deepening, stratigraphic architecture, and sediment bypass beyond the shoreline: Geology, v. 44, p. 927–930.

Rossi, V. M., Paterson, N. W., Helland-Hansen, W., Klausen, T. G., & Eide, C. H. (2019). Mud-rich Delta-scale compound clinoforms in the Triassic shelf of northern Pangea (Havert Formation, south-western Barents Sea). Sedimentology, 66(6), 2234-2267.

Saha, S., Burley, S., Banerjee, S., Ghosh, A., Saraswati, P. (2016). The morphology and evolution of tidal sand bodies in the macrotidal Gulf of Khambhat, Western India. Marine and Petroleum Geology. 77. 714-30. 10.1016/j.marpetgeo.2016.03.028

Sangree, J.B. and Widmier, J.M. (1977) Seismic stratigraphy and global changes in sea level, 9, Seismic interpretation of depositional facies. In: Seismic Stratigraphy: Applications to Hydrocarbon Exploration (Ed. C.E. Payton), pp. 165–184. American Association of Petroleum Geologists, Tulsa, Oklahoma.

Sharp, R.V. (1967), San Jacinto fault zone in the Peninsular Ranges of southern California: Geological Society of America Bulletin, v. 78, p. 705–729.

Short, K.C., Stauble, A.J. (1967). Outline of the geology of Niger Delta. AAPG Bull. 51 (5), 761–779.

Steel, R.J. and Olsen, T. (2002) Clinoforms, clinoform trajectory, and deepwater sands. In: Sequence Stratigraphic Models for Exploration and Production: Evolving Methodology, Emerging Models and Application Histories (Eds J.M. Armentrout and N.C. Rosen), GCS-SEPM Spec. Publ., Gulf Coast Section, 367–381.

Stock, J. M., and Hodges, V. K. (1989a). America was partitioned into separate regimes of strike-slip. Tectonics, 8(1), 99–115.

Stock, J.M., and Hodges, V.K. (1989b), Pre-Pliocene extension around the Gulf of California and the transfer of Baja California to the Pacific plate: Tectonics, v. 8, p. 99–115.

Stride, A.H., Belderson, R.H., Kenyon, N.H., Johnson, M.A., 1982. Offshore tidal deposits: sand sheet and sand bank facies. In: Stride, A.H. (Ed.), Offshore Tidal Sands: Processes and Deposits. Chapman & Hall, London, pp. 95–125.

Stupples, P. (2002) Tidal cycles preserved in late Holocene tidal rhythmites, the Wainway Channel, Romney Marsh, southeast England. Mar. Geol., 182, 231–246.

Summerhayes, C.P., Sestini, G., Misdorp, R., Marks, N. (1978). Nile Delta: nature and evolution of continental shelf sediments. Mar. Geol. 27 (1–2), 43–65.

Sutherland, F.H., Kent, G.M., Harding, A.J., Umhoefer, P.J., Driscoll, N.W., Lizarralde, D., Fletcher, J.M., Axen, G.J., Holbrook, W.S., González-Fernández, A., and Lonsdale, P. (2012), Middle Miocene to early Pliocene oblique extension in the southern Gulf of California: Geosphere, v. 8, p. 752–770.

Swenson, J.B., Paola, C., Pratson, L., Voller, V.R. and Murray, A.B. (2005) Fluvial and marine controls on combined subaerial and subaqueous Delta progradation: morphodynamic modeling of compound-clinoform development. J. Geophys. Res., 110,1 –16.

Sydow, J.C., Finneran, J., Bowman, A.P. (2003). Stacked shelf-edge Delta reservoirs of the Columbus Basin, Trinidad, West Indies. In: Roberts, H.H., Rosen, N.C., Fillon, R.H., Anderson, J.B. (Eds.), Shelf Margin Deltas and Linked Down-Slope Petroleum Systems: Global Significance and Future Exploration Potential, Proceedings of the 23rd Annual GCSSEPM Foundation Bob F. Perkins Research Conference, Houston, TX, pp. 441–465.

Ta, T.K.O., Nguyen, V.L., Tateishi, M., Kobayashi, I., Tanabe, S. and Saito, Y. (2002) Holocene Delta evolution and sediment discharge of the Mekong River, southern Vietnam. Quatern. Sci. Rev., 21, 16 –17.

Terwindt, J.H.J. (1988) Palaeo-tidal reconstructions of inshore tidal depositional environments. In: TideInfluenced Sedimentary Environments and Facies (Eds P.L. de Boer, A. Van Gelder, and S.D. Nio), pp. 233–263. Reidel, Dordrecht.

Thompson, R.W. (1968), Tidal flat sedimentation on the Colorado River Delta, Northwestern Gulf of California: Geological Society of America, Memoir 107, 133 p.

Thomsen, L., Gust, G. (2000). Sediment erosion thresholds and characteristics of resuspended aggregates on the western European continental margin. Deep-Sea Research Part I: Oceanographic Research Papers 47, 1881–1887.

Vakarelov, B.K., Ainsworth, R.B., and Maceachern, J.A. (2012), Recognition of wave-dominated, tide-influenced shoreline systems in the rock record: variations from a microtidal shoreline model: Sedimentary Geology, v. 279, p. 23–41.

van Cappelle, M., Ravnas, R., Hampson, G.J. and Johnson, H.D. (2017) Depositional evolution of a progradational to aggradational, mixed-influenced Deltaic succession: Jurassic Tofte and Ile formations, southern Halten Terrace, offshore Norway. Mar. Petrol. Geol., 80, 1–22.

Van den Berg, J.H., Boersma, J.R. and Van Gelder, A. (2007) Diagnostic sedimentary structures of the fluvial-tidal transition zone–Evidence from deposits of the Rhine and Meuse. Neth. J. Geosci./Geol. Mijnbouw, 86, 287–306.

Walsh, J.P., Nittrouer, C.A., Palinkas, C.M., Ogston, A.S., Sternberg, R.W., Brunskill, G.J. (2004). Clinoform mechanics in the Gulf of Papua, New Guinea. Continental Shelf Research 24, 2487–2510.

Walsh, J.P., and Nittrouer, C.A. (2009) Understanding finegrained River sediment dispersal on continental margins. Mar. Geol., 263, 34 –45.

Waresak, S. E. (2016) Cyclically-Forced Hyperpycnites of the Ancient Colorado River Proximal ProDelta [M.S.]: Loma Linda University.

Willis, B. J. (2005). Deposits of tide-influenced River Deltas.

Winker, C.D. (1987), Neogene stratigraphy of the Fish Creek–Vallecito section, southern California: Implications for the early history of the northern Gulf of California and Colorado Delta [Ph.D. thesis]: Tucson, University of Arizona, 494 p.

Winker, C.D., and Kidwell, S.M. (1986), Paleocurrent evidence for lateral displacement of the Pliocene Colorado River Delta by the San Andreas fault system, southeastern: California Geology, v. 14, p. 788–791.

Winker, C.D., and Kidwell, S.M. (1996), Stratigraphy of a marine rift basin: Neogene of the western Salton Trough, California, in Abbott, P.L., and Cooper, J.D., eds., Field Conference Guidebook and Volume for the American Association of Petroleum

Geologists Annual Convention: American Association of Petroleum Geologists: Bakersfi eld, California, p. 295–336.

Woodard, G.D. (1963), The Cenozoic Succession of the West Colorado Desert, San Diego and Imperial Counties, Southern California [Ph.D. thesis]: Berkeley, University of California, 494 p.

Woodard, G.D. (1974), Redefinition of Cenozoic stratigraphic column in Split Mountain Gorge, Imperial Valley, California: The American Association of Petroleum Geologists Bulletin, v. 58, p. 521–539.

Yang, B.C., Dalrymple, R.W. and Chun, S.S. (2005) Sedimentation on a wave-dominated, open-coast tidal flat, south-western Korea: summer tidal flat – winter shoreface. Sedimentology, 52, 235–252.

Vita

Fernando Rey was born in Buenos Aires, Argentina in 1986. In November 2011, he graduated from the University of Buenos Aires, Argentina with a Bachelor of Science in Geology. He attended the University of Texas at Austin in August of 2019 to pursue a Master of Sciences in Geological Sciences.

Permanent email address: Fernando.rey@utexas.edu

This thesis was typed by the author.